UNIVERSITÀ DEGLI STUDI DI NAPOLI "FEDERICO II"

Controlled release of bacteriophage from PLGA microparticles included in fully implantable bicompartmental polymeric microneedles to induce the innate and adaptive immune system response

Ph.D. Thesis in Industrial Products and Process Engineering

Cycle 33

Supervisors

Dr. Raffaele Vecchione

Prof. Paolo Antonio Netti

PhD Candidate

Rezvan Jamaledin

Coordinator

Prof. Andrea Danna

2018-2021

Table of Contents

List of Figures

List of abbreviations

ABC	Ammonium bicarbonate
APC	Antigen presenting cell
BGNs	Bioactive glass nanoparticles
BM-DCs	Bone marrow-derived dendritic cells
CD	Circular dichroism
CpG	Cytosine triphosphate deoxynucleotide guanine triphosphate deoxynucleotide
DAB	Droplet-born air blowing
DC	Dendritic cell
DCM	Dichloromethane
DMSO	Dimethyl sulfoxide
ELISA	Enzyme-linked immunosorbent assay
FDM	Fused deposition modeling
FITC	Fluorescein isothiocyanate
GOx	Glucose oxidase
HA	Hyaluronic acid
HRSV	Human respiratory syncytial virus
IL	Interleukin
IPTG	Isopropyl-beta–d-thiogalactopyranoside
LCs	Langerhans cells
MN	Microneedle

MP	Microparticle
NOA	Norland Optical Adhesive
PBA	Phenylboronic acid
PBS	Phosphate-buffered saline
PDI	Polydispersity index
PDMS	Poly(dimethylsiloxane)
PEG	Polyethylene glycol
PLGA	Poly(lactic-co-glycolic acid)
PMMA	poly(methyl methacrylate)
PVA	Poly(vinyl alcohol)
PVP	Poly(vinylpyrrolidone)
TFF	Transverse failure force
TLR	Tool like receptor
TPP	two-photon polymerization
$W_1/O/W_2$	Water-oil-water

Chapter 1

Introduction

Controlled release of bacteriophage from PLGA microparticles included in fully implantable bicompartmental polymeric microneedles to induce the innate and adaptive immune system response

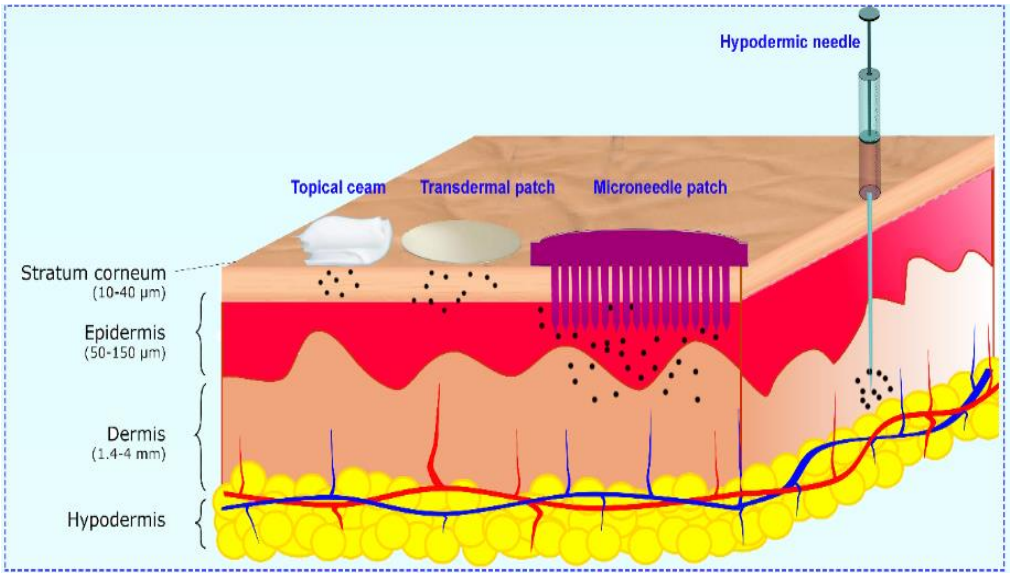

Part of this chapter is based on these review papers:

"Progress in Microneedle-Mediated Protein Delivery" R. Jamaledin, C. Di Natale, V. Onesto, Z. B. Taraghdari, E. N. Zare, P. Makvandi, R. Vecchione, P. A. Netti, *J. Clin. Med.* **2020**, *9*, 542.

"Advances in Antimicrobial Microneedle Patches for Combating Infections" R. Jamaledin, Cynthia K.Y. Yiu, E. N. Zare, Li-Na Niu, R. Vecchione, G. Chen, Z. Gu, F. R. Tay, and P. Makvandi, Adv. Mat. **2020,** 32, 2002129.

"Engineered Microneedle Patches for Controlled Release of Active Compounds: Recent Advances in Release Profile Tuning" R. Jamaledin, P. Makvandi, C. K. Y. Yiu, T. Agarwal, R. Vecchione, W. Sun, T. Kumar Maiti, F.R. Tay, and P. A. Netti, Adv. Ther. **2020,** 3, 202000171.

"Stimuli-responsive transdermal microneedle patches" P. Makvandi, R. Jamaledin, G. Chen, Z B. Taraghdari, E. N. Zare, C. Di Natale, V. Onesto, Vecchione, J. Lee, F. R. Tay, P. Netti, V. Mattoli, A. Jaklenec, Z. Gu, R. Langer, Mater. Today, **2021,**

Abstract

The increasing demand for patient-compliance therapies in recent years has led to the development of intradermal and transdermal drug/vaccine delivery, which has several superiorities as compared to conventional methods. This research project endeavored to successfully encapsulate filamentous bacteriophage (Fd) into a Poly(lactic-co-glycolic acid)-based microparticulate system (PLGA MPs). The release profile of these microparticles suggests that they could be used to successfully induce immune and adaptive system. It was the first time that filamentous bacteriophages have been encapsulated in PLGA. The present study also devised a microneedle (MNs) system. A multi compartment microneedles (MNs) system was validated for a number of actives encapsulation (ex. laccase, collagenase) during the PhD activity and upon this optimization the system has been coupled with pillars as a strong mechanical pedestal to increase insertion ability. At the moment, *in vivo* intradermal delivery from MPs and MNs encapsulated bacteriophages are under investigation. Aside from the development of bacteriophage delivery systems, novel work in the application of fd-bacteriophage was completed with extremely successful results.

1. Introduction

Vaccines are pharmacological formulations incorporating the disease-causing agents to stimulate an immune response when introduced into a human body, without causing the disease itself. They represent one of the most useful inventions in medicine with consequent successful drastic mortality reduction and population growth [1]. However, these strongest weapons still suffer from several problems which restrict their maximum potential. There are several logistical challenges such as difficulties in storage, repeated hypodermic injection, and administration by trained personnel.

To overcome these hurdles, microneedles have been proposed as sub-millimetric microcones that can be inserted into the skin with no pain and they can release the encapsulated drug upon dissolution and degradation of the polymeric matrix. They cause less discomfort, tissue damage, or inflammation for patients as compared to conventional syringes, and could be appealing for patients. The use of MNs also eliminates trypanophobia (needle phobia) that is related to the use of hypodermic syringes for delivery of parenteral medications.

Potential benefits of intradermal delivery for vaccine delivery have been evaluated by research groups, as the skin layer that lies under the stratum corneum is highly populated by a densely connected network of dendritic cells (DCs) which are the most professional antigen-presenting cell (APC). DCs capture, process, and present antigens to T cells. The strategic targeting of the epidermis and dermis is a manually difficult technique that the aid of healthcare professional is needed [2–4].

A vaccine is administered into the body to mimic infection and triggering the body to produce antibodies against the pathogens. Edward Jenner for the first time explored the vaccine concept, and ever since then, it has become a necessary entity of human healthcare. However, the huge amount of studies on vaccines show that administration of vaccines in solid forms have several advantages over liquid dosage forms, as they generate stronger immune responses, thereby leading to a dose-sparing effect. Additionally, being these systems used needle-free, this will also minimize the disease spreading from needle-stick injury and enhance patient compliance, as it would be painless. The vaccines approved for human use in today's pharmaceutical industry are primarily categorized into several types, such as live (attenuated), inactivated vaccines, subunit vaccines [5], viral vector [6], and the more recently DNA-based vaccine [7,8]. Live attenuated could theoretically revert to its original pathogenic form. Inactivated form can be prepared with

heat and/ or chemicals. They need the administration of multiple doses or immune response-boosting adjuvants. Adjuvants are substances incorporated into the vaccines that allow them to work efficiently by enhancing the immune response, decreasing the quantity of vaccine needed to gain protective immunity, or lowering the number of doses required. In general, there are some types of adjuvants such as Aluminum salts, Cytosine triphosphate deoxynucleotide guanine triphosphate deoxynucleotide (CpG), and Tool like receptor (TLR) [9]. Subunit vaccines contain only fragmented portions of the pathogen such as an individual protein as the antigen since they cannot revert to a virulent form so they are much safer than live vaccines. In contrast, they are typically weakly immunogenic so they need the co-presence of an adjuvant apt to intensify the immune response [5]. Viral vector vaccines use a modified version of a different virus (the vector e.g. adenoviruses, retroviruses or lentiviruses) to deliver important instructions to the immune cells [6,10]. DNA vaccines inject genetically engineered plasmid incorporating the DNA sequence encoding the antigen of interest, so the cells directly produce the antigen, thus causing a protective immunological response [11,12].

In this project, we have used bacteriophage to deliver vaccine model (OVA peptide) both *in vitro* and *in vivo*. Bacteriophages have been utilized for more than a century as therapeutic agents against bacterial infections, without causing any side effects in human. *Escherichia coli* filamentous bacteriophages (M13, f1, and fd) have attracted great interest of immunologists as an outstanding antigen carrier and vaccine delivery tool with a wide variety of applications in the development of vaccines. The application of fd bacteriophage as a vaccine delivery system relies on a modification of bacteriophage surface utilizing phage display technology **(Figure 1.1)** [13]. Fd bacteriophage is engineered to express multiple copies of exogenous peptides (or polypeptides) chemically bonded to viral capsid proteins [14]. The genome of fd bacteriophage is intrinsically rich in CpG

motifs, which can be recognized by TLRs. After activation of TLRs, signaling stimulates the creation of inflammatory signal mediators such as cytokines and can extend acquired immune responses without using any kind of exogenous adjuvant [15].

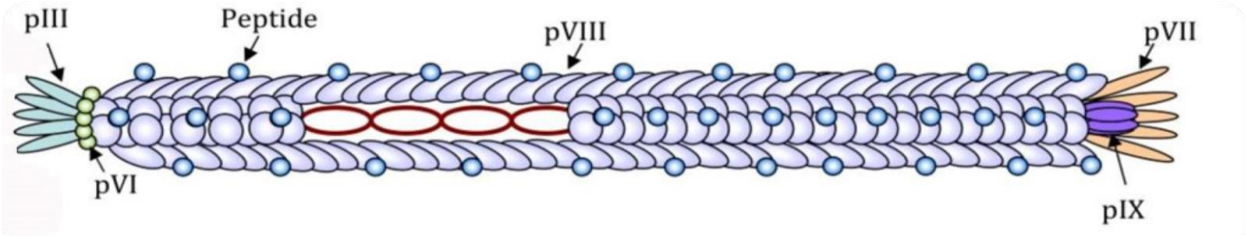

Figure 1.1 Schematic representation of a Fd bacteriophage nanostructure designed for the expression of a short antigenic peptide as a fusion with N-terminus of the pVIII protein. The circular single-strand DNA rich in CpG motifs can be recognized by pattern recognition receptor, which can act as an adjuvant. Reprinted with permission from [15].

There are some pre-clinical studies of fd bacteriophages to deliver peptide-based cancer vaccines. For instance, expressing melanoma epitope MAGE-A1$_{161–169}$ on the major coat protein pVIII of the filamentous phage using B16.F10 tumors in C57BL/6J mice demonstrated prevention and suppression of tumor growth. Immunization primed cytotoxic T lymphocytes and elicited $CD4^+$ responses and NK cells activity [16]. Representing protein of the human respiratory syncytial virus (HRSV) to protect immunized BALB/c mice against infection by HRSV induced a strong anti-HRSV immune response and conferred complete protection of mice against RSV infection [17]. Immunization with double hybrid filamentous bacteriophages co-expressing a tumor peptide from MAGE-A10 or MAGE-A3 together with a Th peptide of viral origin protected humanized HHD transgenic mice from tumor growth. In addition, human anti-MAGE-A3271–279-specific T cell clones isolated from bacteriophage-stimulated T cell lines exhibited high avidity for the MAGE-

A3 epitope and were able to kill human MAGE tumor cell lines expressing MAGE-A3271–279 peptide-HLA complex on the surface [14].

The main aim of vaccination is to stimulate a robust immune response and preserve the immune responses for a longer time [18]. Some antigens are incapable of initiating a powerful and long-lasting immune response, which can be due to the lack of a suitable delivery system. Hence, the emergence of an optimal delivery vehicle is of great interest for new vaccine formulations [19]. In this project for the first time, we encapsulated filamentous bacteriophage in a biodegradable porous Poly(lactic-co-glycolic acid) PLGA microparticles, which can adjust the release of bacteriophages, thereby promoting stimulation of the immune system over time and enhancing the immunogenicity of the phage-based vaccine.

In our first published work, we designed an innovative and fast stamp-based method for fabricating bi-compartmental polymeric MNs with adjustable drug release properties. In this system not only the MPs but also the hydrophilic polyvinylpyrrolidone (PVP) tip, can successfully encapsulate labile molecules such as laccase and leading to a bi-compartmental system [20]. In our second published work, the PVP tip that is highly sensitive to the humidity and storage condition has been replaced with a solution of PVP–hyaluronic acid (PVP–HA) that is also less fragile allowing strong dehydration which is vital for maintaining the structure of sensitive enzyme such as collagenase from ambient humidity [21].

However, numerous studies demonstrated that due to the elasticity of the skin, polymeric MNs may be unable to totally penetrate the skin, leading to random and inconsistent delivery of therapeutic agents. In the last few decades, outstanding efforts have been made to ameliorate the insertion capability and efficacy of MNs. In some cases, the mechanical fracture force showed that MNs possess sufficient mechanical strength to puncture the skin without breakage, but they are

unable to insert into the skin completely. The delivery efficacy of MNs is related to several different parameters, such as insertion force and elasticity of the skin. For the skin with high elasticity, MNs tend to push the skin instead of puncturing and creating holes to translocate the drug cargo. Fabricating MNs over micro-pillars makes it easier to distribute the force over each MN, and accomplish a uniform and complete insertion of the whole patch into the skin [22–25]. Pedestal-based MNs have an extra length to overcome the elasticity properties of the skin and provide additional mechanical strength to have a complete penetration/insertion. Taking this into account, in our third work regarding microneedles, we designed MNs over poly(methyl methacrylate) PMMA pillars to ameliorate the skin insertion ability.

In this study, we used filamentous bacteriophage expressing the ovalbumin antigen determinant as the vaccine model. Then, we encapsulated them into PLGA microparticles with porous structure via two different methods which allow the integrity of the structure and controllable release over time. Additionally, mathematical modeling successfully predicts and tune the release profile of bacteriophage. Afterward, MPs were incorporated into fully implantable polymeric MNs to induce immune system responses.

2. Control of Protein/Vaccine Delivery

Polymeric microparticles (MPs) are attracting huge attention not only in drug delivery settings but also in other fields such as biosensing and tissue engineering. Their progress is essentially related to the several superiorities of this kind of microstructure including relatively simple protocols and the potential ability of industrial scale up. As a drug delivery system, MPs possess several benefits such as the use of different administration routes or the opportunity of entrapping different molecules including proteins/vaccines and nucleic acids. In the case of vaccine delivery, the release of antigens can be pulsatile to imitate current prime-boost paradigms, or continuous to

mimic a naturally developing infection [3]. Additionally, the main goal of vaccination is achieved through extended antigen exposure from a single shot delivery [3]. In light of this, many biodegradable polymers can be applied to create MPs as alginate, dextran, chitosan, gelatin, and PLGA. These polymers are popular in common usage because their degradation products are non-toxic metabolites and are also easily excreted from the body. PLGA microparticles are gaining attention due to the possibility to achieve a controlled drug release by governing its bio-degradation, which is dictated by the polymer chemistry such as glycoside units content, initial MW, stereochemistry, or end-group functionalization. Another essential factor is the fabrication technique. There are many methods that can be applied for the preparation of MPs. Depending on the fabrication technique, MPs show specific size, polydispersity index (PDI), and morphological properties. These characteristics are vital to ensure stability, encapsulation, and an adequate release of the drug. For these reasons, fabrication techniques are chosen in accordance with the drugs and their specific application. For hydrophilic molecules and highly unstable molecules like proteins, the gold method is represented by the double emulsion solvent evaporation technique, because this method can protect proteins from degradation conversely, lipophilic molecules can be encapsulated by means of single emulsion techniques. All these characteristics combined with the PLGA degradation, make PLGA MPs a very promising vehicle as a drug delivery system.

The single emulsion method is one of the most common methods used to encapsulate hydrophobic molecules such as steroids [26]. This simplest emulsion contains droplets of one liquid dispersed in another liquid (continuous phase), for example, oil-in-water (O/W) and water-in-oil (W/O) emulsions. The double emulsion technique is the main method to encapsulate water-soluble molecules such as proteins, peptides, and vaccines. The double emulsion has a simple process, low-cost instrumentation, and good control of the process parameters. A water-in-oil (W_1/O)

primary emulsion, or so-called ‘inner’ emulsion, is prepared during the first emulsification step, and afterward dispersed into a continuous water phase (W_2) [26] **Figure 1.2**.

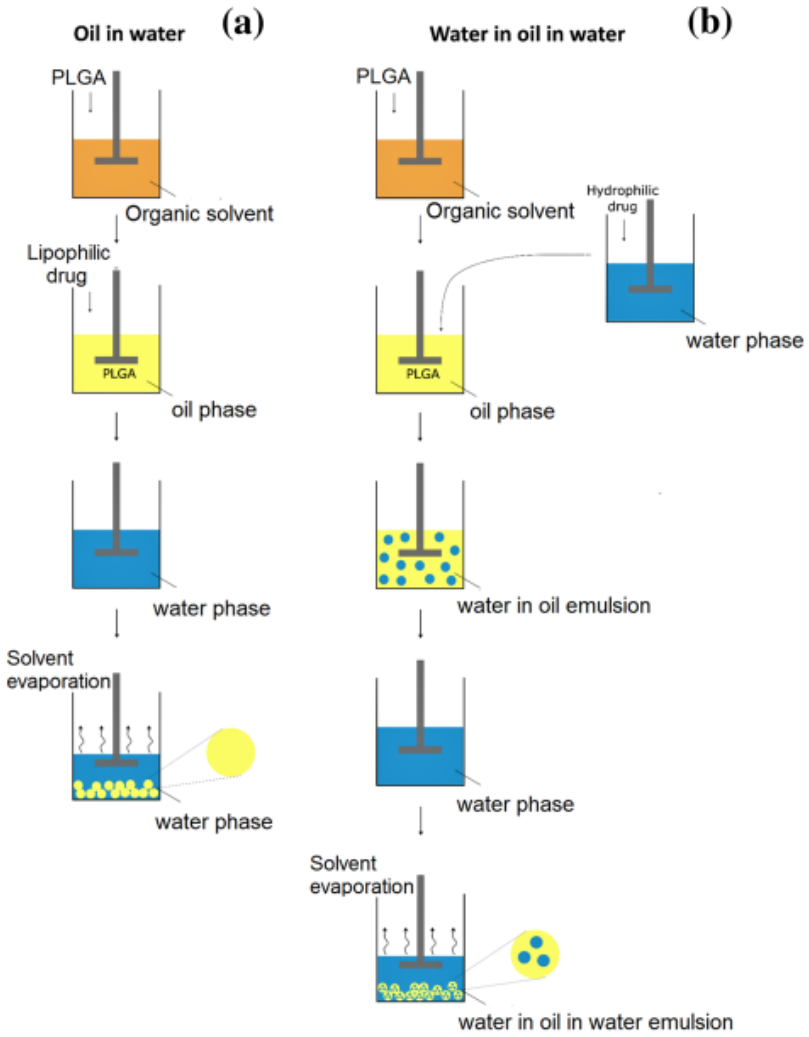

Figure 1.2 Schematic representation of emulsion solvent evaporation techniques for PLGA MPs production: (a) O/W single emulsion method and (b) W/O/W double emulsion.

3. Microneedles-mediated Protein/Vaccine Delivery

MN patches that consist of sub-millimetric needles have been developed as promising vehicles for puncturing the outermost layer of the skin and translocating therapeutic agents to the epidermis and dermis without touching blood vessels and pain-sensing neuron [19,27]. Because these

miniaturized needles are typically only 100 to 1000 μm in length, they can puncture the stratum corneum with limited interaction with the nerve endings in the dermis. These characteristics lead to less pain, tissue damage, and skin inflammation for patients compared with injection methods, and could be desirable for patients with chronic diseases [28]. The use of MNs also eliminates needle phobia that is associated with the use of hypodermic syringes for the delivery of medications. Since the skin is a very immune-competent organ and easily accessible, intradermal delivery is an attractive route of vaccine administration. The viable epidermis and dermis are highly populated by APCs such as Langerhans cells (LCs) and DDCs. Additionally, the emergence of MNs for vaccine delivery in the pharmaceutical industry will eliminate the requirement of costly cold-chain distribution to poor countries. Another fundamental superiority of MNs is their dose-sparing quality, in which the direct targeting of the rich network of immunogenic APCs generates higher immune responses for MNs over the conventional intramuscular route. Numerous research attempts are being performed to qualitatively compare the effectiveness of immune responses stimulated via MN vaccination as compared to conventional delivery routes [3].

4. Fabrication Methods of Microneedles

4.1. Mold-Based Methods

Micro-molding is the most frequently used method for the manufacturing of MNs. It includes the creation of a positive master from the template structures from which a negative structure can be attained. Then, after the creation of the mold, MNs can be created on it. There are different methods for fabricating master for instances photolithography using deep X-ray lithography of Lithographie Galvanoformung Abformung [29,30] and ultraviolet (UV) lithography [31], laser ablation [32],

micro milling and micro grinding [33], additive manufacturing [34], laser percussion drilling, and deep reactive ion etching (DRIE) [35]. The fabricated positive master can be re-used frequently to make some other molds, and each mold can be used many times for the preparation of MN after proper cleaning.

There are various types of micro-molding methods including hot embossing, injection, and drop-casting (**Figure 1.3a**). In hot embossing, the mold needs to be firstly heated to a temperature upper than the glass transition temperature (Tg) of the polymer, allowing the pressed polymer flow to fill the mold microholes. The mold is then cooled down to a temperature below the Tg. Microinjection molding involves the injection of the melted polymer, forcing it into the mold and afterward cooling step and solidifying the polymer. This is carried out by using an injection molding machine which consists of two units: a clamping unit and an injection unit. Injection molding results are highly related to the process parameters such as temperature, clamping force, injection rate, pressure, and decompression velocity [36]. Applying high temperatures makes this process unable for the direct encapsulation of labile molecules such as peptide and protein. In drop-casting method, a polymer solution is poured into the microcavities, and afterward, the vacuum and/or centrifugation steps are carried out to fill the holes. Long dehydration times may affect the activity of the labile molecules, in addition to being economically high-priced. Spray coating as an alternative may be applied to deposit polymer solutions into microcavities in a quicker and securer way for the proteins. Finally, the solution in the mold is left to become completely dried. The dehydration step could be replaced by photopolymerization if a photocrosslinkable material is used to accelerate the process and make it faster and, thus, less expensive. However, the UV radiation can compromise the integrity of the active compound embedded within the polymer matrix as well

as the photoinitiator residuals within the final products, which can introduce danger in terms of toxic materials.

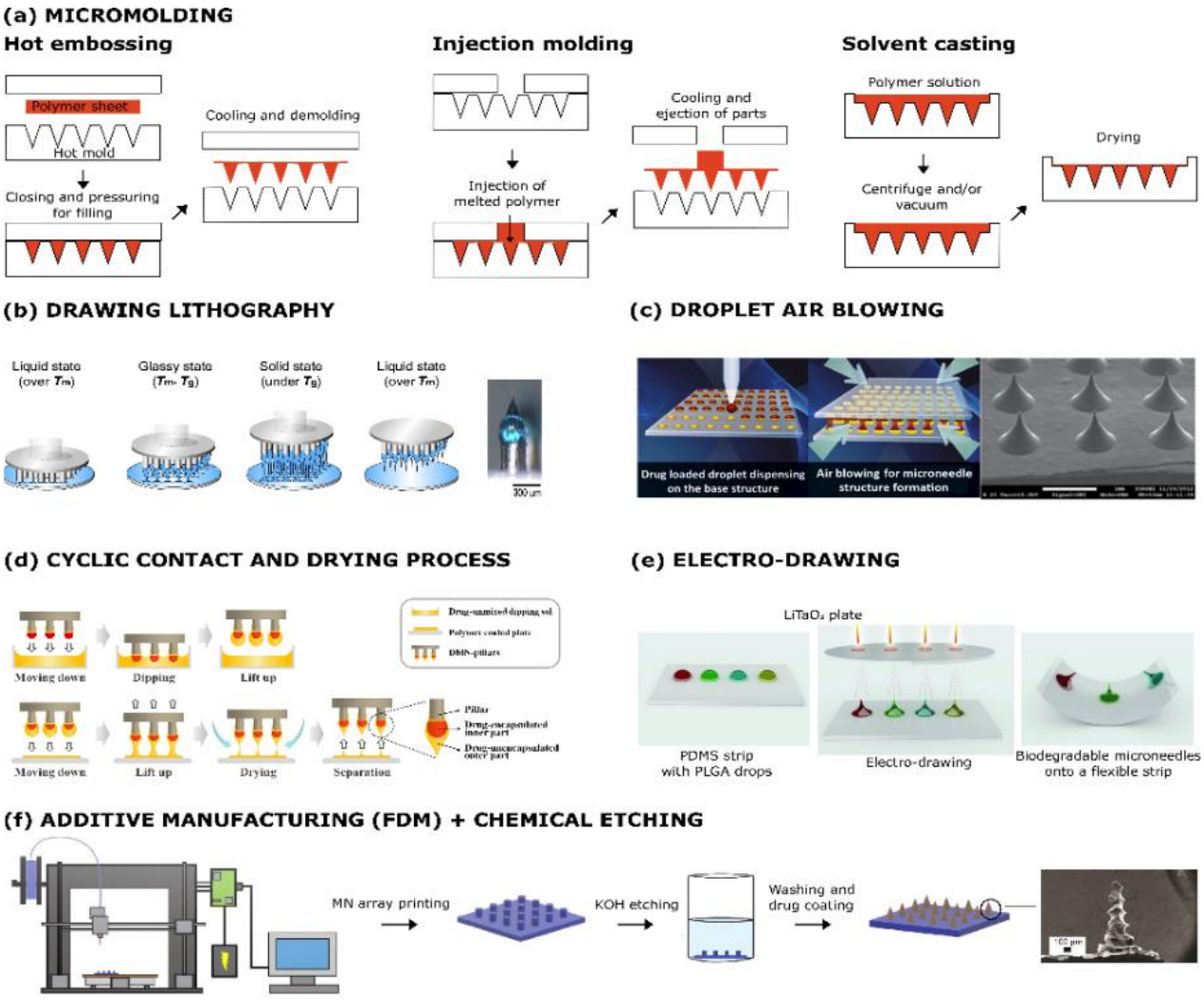

Figure 1.3. Fabrication methods of Microneedles. (a) Micromolding: The microneedles can be fabricated by hot embossing, injection molding, or solvent casting. (b) Drawing lithography: After melting the polymer, polymer dispense on a fixed plate, and elongated by pillars in the upper-moving plate. (c) Droplet air blowing: Two plates, with polymer drops within, are in contact and then moved. When the final shape is achieved, the polymer is hardened through air blowing. (d)

Cyclic contact and drying: Pillars are repeatedly contacted with a drug-polymer solution, lifted, and dried with air blowing. (e) Electro-drawing: A thermal stimulus is applied to a pyroelectric crystal, generating an electric field that causes the microneedle drawing process. (f) Fused deposition modeling (FDM) of biodegradable polymer MNs: FDM is followed by KOH etching process to improve feature size. Fused deposition modeling FDM. Reprinted with modification from [37].

4.2. Mold-Free Methods

Another MN fabrication strategy based on drawing lithography has been suggested as a mold-less and therefore a less expensive method as compared to the molding procedure [38]. This strategy relies on the elastic behavior of the polymeric material in its glass transition point. Melted polymer is dispensed on a fixed plate and elongated by drawing pillars in the upper-moving plate, creating a three-dimensional structure of the MN (**Figure 1.3b**). Even though this strategy is free of master manufacturing processes or replica molding, the restrictions arise from the high process temperatures. Additionally, the reproducibility of the features is less than the mold-based techniques. The drawing lithography technique has been reincarnated by the droplet-born air blowing (DAB) method (**Figure 1.3c**)[39]. In this method, droplets of a polymeric solution are deposited in an array configuration on two sheets. The sheets are in contact with each other and then moved at an adjustable speed. When the desirable gap between the sheets is achieved, the elongated polymer is solidified via air blowing, and the final MNs are gained. The droplet-born air blowing technique has recently been joined with a cyclic contact and drying process on pillars (CCDP process) (**Figure 1.3d**) to create dissolvable MN patches, characterized by the possibility of the rapid separation of MNs from their base. In spite of the fact that the DAB technique is free from high process temperature and UV, the process is still influenced by the problem attributed to

the driving interaction with the contact plate. Moreover, this method seems to be inappropriate for a consistent drug distribution within the MNs, together with the non-ideal radius of curvature of their tips.

The lack of multi-step sequences, based on the molding method, is one of the particular characteristics of a novel strategy for the fabrication of biodegradable polymeric MNs which was developed by Vecchione et al. (**Figure 1.3e**). This method is based on the pyroelectric effect of a dielectric crystal (lithium tantalate, $LiTaO_3$); under a thermal stimulus applied to the crystal, an electric field is provided, which leads to the polymer drawing. During the shaping process, the fast evaporation of the organic solvent solidifies the cones. In this technique, high process temperature and UV radiation are avoided.

Among stamp-less technologies, additive manufacturing, or 3D printing, is a promising field in MN structure fabrication. Design of MNs with Computer-Aided Design (CAD) software allows the design of MNs with the desired density, height, size, and geometry, which can be printed with high reproducibility through the consecutive deposition of layers. Additive manufacturing involves several strategies to fabricate MNs. Micro-stereolithographic 3D printing was applied to fabricate MN arrays, after having integrated the active agent into the polymeric matrix before photopolymerization. Stereolithography has even recently been utilized to print different shape e.g. pyramidal and conical-shaped polymeric MNs for transdermal drug delivery.

Additive manufacturing is usually joined with other technologies. As an example, fused deposition modeling was recently proposed to prepare biodegradable polymeric MNs (**Figure 1.3f**) and was joined with a chemical etching protocol to ameliorate the feature size of the printed MN tips. A more fascinating method is based on the use of two-photon polymerization (TPP) 3D printing to fabricate a refillable drug reservoir equipped with hollow MNs in microelectromechanical devices.

This structure allows MNs to interface with larger delivery loads. Equally interestingly, stereolithography 3D printing was employed to fabricate—in a single step—hollow MNs interfaced with microfluidic structures within a single device to obtain higher fluid management capabilities for transdermal drug delivery.

Additive manufacturing is an outstanding strategy to manufacture MNs and MN integrated devices. However, some restrictions need to be overcome. It is generally a slow method especially in case of high-resolution 3D printing. Then, there is low availability of 3D printable biomaterials with particular features and viscosities at different temperatures or photo-sensitivities that are biocompatible and which have the desired biodegradation rate in the case of drug-containing materials. In addition, the material needs to have a good mechanical behavior to allow MNs to successfully perforate the skin. In general, the sensitivity of the protein has to be considered: the structure of proteins can denature when exposed to UV radiation and high temperatures.

5. Materials of MNs

Different materials for instances silicon, metal, silica glass, ceramics, and polymers have been exploited to fabricate MNs. The initial study concerning silicon MNs to increase drug delivery through the skin was published in 1998 [40]. The use of silicon possesses some restrictions related to its intrinsic fragility (some silicon MNs could fracture after insertion into the skin, causing the onset of silicon-based granulomas) and high production costs. Some biocompatible metals e.g. stainless steel, palladium, and titanium have also been applied. They show excellent mechanical characteristics, expressing Young's moduli of 180, 117, and 110 GPa, respectively. These values are comparable with silicon for which the range is between 50 and 180 GPa. The first reported metal to fabricate MNs was stainless steel. Silica glass is another alternative, which is intrinsically physiologically inert. Since silica glass is delicate and not absorbable, like silicon, it can be utilized

exclusively for experimental purposes, not for commercial usage [41]. Some types of ceramics, such as alumina (Al_2O_3), calcium sulfate dihydrate, calcium phosphate dehydrate, and Ormocer can be used to fabricate MNs. Some sugars such as maltose, sucrose, and trehalose can be applied as a matrix of MNs. They possess high biocompatibility and safety for drug delivery applications. Other carbohydrates e.g. hyaluronic acids (HA), with molecular weights higher than the previous sugars, e.g. maltose, can be used in the matrix of MNs or as particles incorporated in MN structure. Proteins, polysaccharides, and synthetic polymers showed great biocompatibility and degradability. The most commonly used matrix materials include poly-L-lactic acid (PLA)[42], polymethylmethacrylate (PMMA)[43], poly(lactic-co-glycolic) acid (PLGA)[20], poly(vinylpyrrolidone) (PVP)[44], and poly(vinyl alcohol) (PVA) (**Figure 1.4**). Synthetic polymers such as poly(methyl vinyl ether-*alt*-maleic anhydride) (Gantrez AN-139) or poly(methyl vinyl ether-*alt*-maleic acid) (Gantrez S-97®) have also been employed [45].

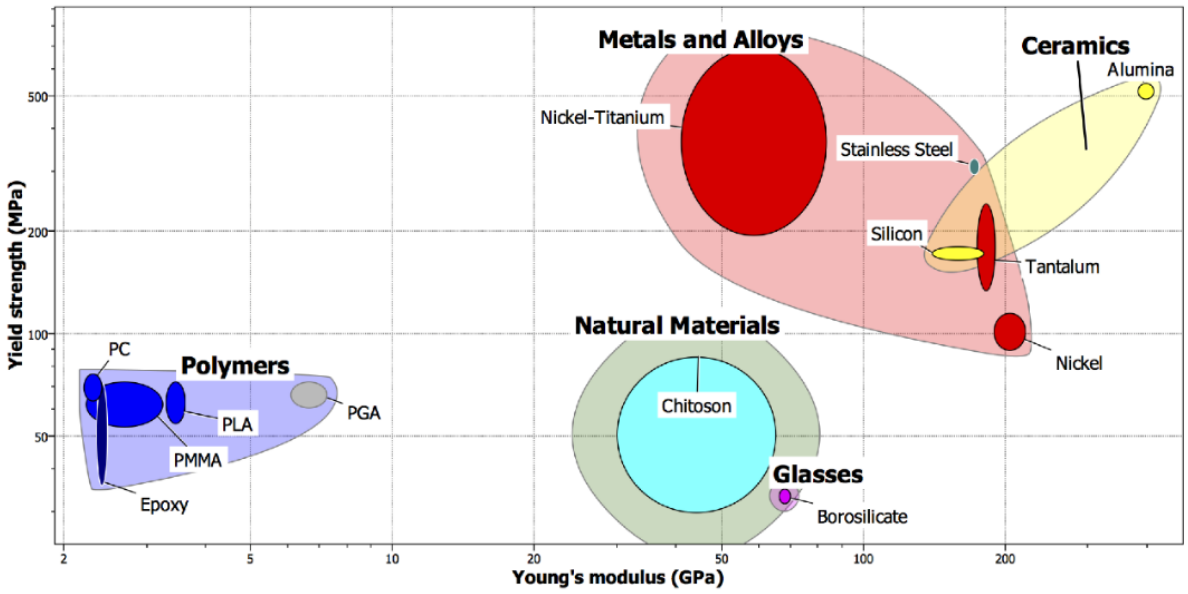

Figure 1.4. Yield strength vs. Young's modulus of different materials used for the fabrication of microneedles. Reprinted with permission from [46].

6. Mechanical aspect of Microneedles

The human skin plays a crucial role in protecting and enclosing our bodies against the invasion of external toxic materials. The surface area of human skin in adults is between 1.5 and 2.0 m^2, whereas skin thickness differs among the different parts of the body and between different genders and ages. For instance, the thickness of the forearm skin in men and women is 1.3 mm and 1.26 mm, respectively. Generally, there are three layers of the skin: the epidermis, dermis, and hypodermis. The epidermis acts as a barrier that protects humans from infectious diseases and adjusts the amount of water released from the body. The dermis is the second layer of the skin which lies beneath the epidermis and above the hypodermis and is categorized into the papillary region and reticular dermis. The subcutaneous layer is the deepest and thickest layer of skin and it contains fibroblasts, fat cells, connective tissue, larger nerves or blood vessels, and macrophages. The subcutaneous thickness varies in various areas of male and female bodies.

Therefore, based on human skin features, tests to evaluate the mechanical properties of MNs in human skin are necessary [47]. Having an optimal strength is necessary to avoid MN fracture due to bending, buckling, and baseplate fracturing. In general, there is no specific test to prove the sufficient mechanical performance of MNs for *in vivo* skin insertion. Consequently, MNs' mechanical characterization involves a series of tests including axial and transverse loadings [48].

The axial fracture forces test is commonly applied to evaluate the MN mechanical strength. The maximum force applied definitely before falling down is considered to be the force of needle failure. Axial compression tests involve a force applied in parallel to the MNs axis. They typically require the employment of a mechanical test station that reports both displacement and force while the MNs are pushed against a hard, metallic surface at a distinct MN row.

The transverse failure force (TFF) and shear strength tests are necessary to evaluate a comprehensive profile of MN behavior during their applications. In this test, a mechanical station is typically employed where a transverse force is applied at a distinct MN row until the breakage of the MNs. A sudden fall in force corresponds to MN failure. TFF testing of a MN row in an array includes dividing the force applied for the failure of all MNs within the row by the number of MN to calculate the transverse failure force per each MN. A restriction of this test is the difficult alignment of the probe with a distinct length on the MN because of the tiny-scale of MNs.

A lot of sophisticated techniques have been explored to increase drug delivery after MN insertion. As an example, the *in vitro* delivery of high molecular weight fluorescein isothiocyanate (FITC)-dextran derivatives, combining the effect of MN pre-treatment and iontophoresis (ITP) has been investigated by Wu et al. Results exhibited that a significant intensification in FITC-dextran penetration was observed when MNs and ITP were combined. Unfortunately, this method is invasive and may cause poor patients´ compliance [49]. Better results were gained by a novel dissolving microneedle (DMN) called the "Troy microneedle". Kim et al. demonstrated that the traditional patch-based DMNs failed because of inadequate skin insertion and rapid separation of MNs due to their strong bond with the supporting material. On the contrary, the Troy MNs, created by cyclic contact and drying on the pillar (CCDP), is able to generate complete and fast delivery of the encapsulated drugs. In particular, *in vivo* skin penetration studies showed that the development of MNs on pillars produces an instant separation without waiting for the dissolution of the polymer matrix. This feature allows the complete delivery of the drug into the skin, counteracting the viscoelasticity of the skin. Although the Troy MNs goes beyond the limits of the low penetration efficacy of the patch-based DMNs, other studies have yet to be implemented to achieve optimal insertion ability. Additionally, some other factors must be examined in the field

of MN penetration. For example, penetration is mainly obtained by using sharp-tipped needles with a sufficient length to counteract the bending of the skin's compliant surface that occur before penetration. The depth of MN insertion increases with increased applied velocity and applied force. Needle reliability during insertion has been mainly obtained by minimizing the required insertion force by using cone-shaped needles and by maximizing the mechanical strength through increasing the Young's modulus. To evaluate whether polymer MNs are strong enough to insert into the skin without fracturing, it is essential to determine the force needed to cause needle fracture by axial loading measures as a function of the needle length, base diameter, and Young's modulus. The fracture force plunged with an increasing needle length. On the other hand, the fracture force rises with an increasing base diameter. The fracture force in polymer MNs goes up with an increasing Young's modulus, due to the employment of polymers with higher mechanical strength which have greater failure forces.

7. Different Type of MNs for Protein/Vaccine Delivery

MNs can be divided into five categories: solid MNs and hollow, coated, dissolvable, degradable, and hydrogel-forming systems. Some responsive polymeric materials were exploited into MNs to obtain an on-demand drug release during the last decade. Solid MNs as the first generation of MNs are typically manufactured with silicon or metals. Based on the release profile, there are some configurations of MNs that exist for either burst release or prolonged release.

For example, sustained release can be performed by embedding the drug in polymeric particles and swellable structures, while instant release profile can be achieved utilizing dissolvable matrices. Additionally, MNs, as intelligent drug delivery tools, are responsive to internal and external stimuli and have been prepared to possess a smart drug delivery. In the following part a

list of possible MNs based solutions for the encapsulation and delivery of protein/peptide is provided, since our final aim of the project is encapsulating a peptide-based vaccine.

7.1. Hollow MNs

Hollow MNs were firstly designed to inject liquids [50] and suspensions for drug infusion into the skin through the needle bore. Metal, Silicon, or glass can be utilized for the fabrication of hollow MNs with tunable bore diameters. A study using ovalbumin (OVA)-loaded PLGA nanoparticles (NPs) delivered by hollow MNs exhibited a greater amount of antibody and interferon-γ compared with intramuscular NP injection and soluble antigen delivered by the same tool [51].

In another study, several types of NPs including PLGA, liposomes, mesoporous silica, and gelatin NPs delivered by hollow MNs were applied to encapsulate OVA and adjuvant to determine the effectiveness and characteristics of different types of NPs. PLGA NPs, considerably, cationic liposomes, generated the greatest immune responses, which may be due to the strong interaction between the antigen/adjuvant and the polymeric NPs. Gelatin and mesoporous silica showed a faster release, arising from the poor electrostatic interaction among the antigen/adjuvant on the surface of the particles [52]. Using the same liposome composition and the co-encapsulation of diphtheria toxoid and adjuvant, it was shown that cationic liposome is capable of initiating strong immune responses. The strong interaction between a positive liposome and the negatively-charged cell membrane leads to the prolonged release of the antigen and adjuvant [53]. Hollow MNs possess intense mechanical strength to avoid breakage into the dermis and to ensure that the needle bores are not blocked during intradermal drug delivery. In spite of the fact that some sophisticated manufacturing techniques have been explored during recent years, hollow MNs still show some restrictions. First of all, there is a possibility to have allergic reactions in the case of metal MNs and require trained personnel and a complex pump-based setup for their injection. However, some

studies suggest their applications in the dermatological field as well as in clinical applications for local and systemic delivery of drugs, vaccines, and cells.

7.2. Coated MNs

In this type of MN patches, therapeutic agents adhere directly onto the external part of solid or polymeric MNs. Since the coating layer decreases the sharpness and mechanical strength of the MNs, the loaded drug on the MN surface is restricted to a low amount. As a result, coated MNs are only applicable for some particular applications in which a low dose should be applied [54]. The study on human growth hormone-coated on metal MNs exhibited a bioavailability similar to the subcutaneous injections. In another study, interferon-alpha coated on polymeric MNs stimulated an antitumor effect in cancerous mice, similar to that of subcutaneous injections. Coated MNs for delivery of parathyroid hormone exhibited a sharp peak in plasma, quicker than subcutaneous injections, with high-temperature stability for more than 24 months. In a study, delivery of immune polyelectrolyte multilayers coated on MNs has been accomplished to deliver human melanoma antigens and as a potent toll-like receptor adjuvant. In particular, the layer-by-layer deposition of vaccine components, consisting of tumor peptides and adjuvants, on MNs triggered the tumor-specific T cell response and led to recall responses (**Figure 1.5**). The H1N1 influenza vaccine was coated on stainless steel MNs to initiate an immune response in young mice, demonstrating that microneedles generated higher amount of antibodies than of intramuscular injection.

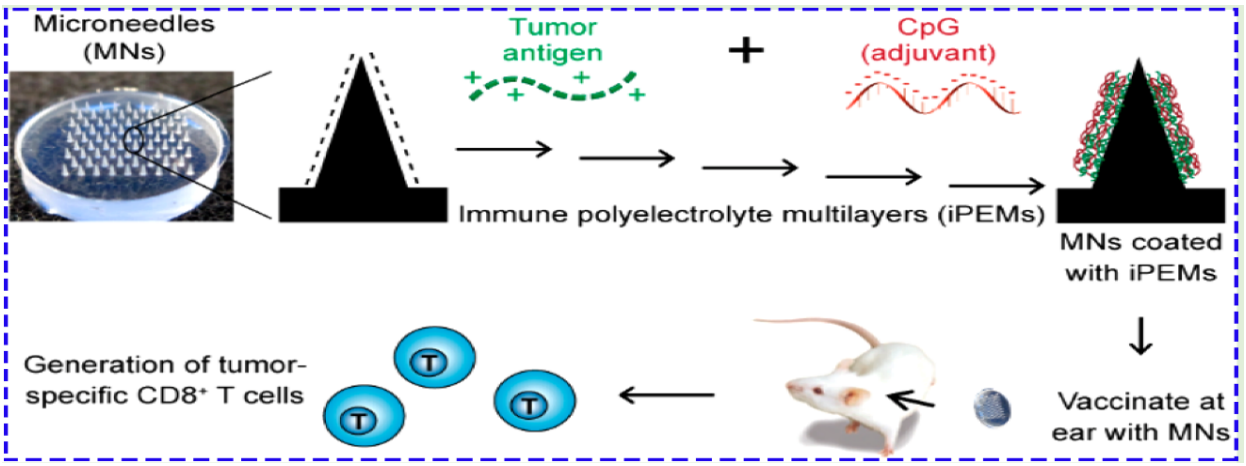

Figure 1.5. Schematic reorientation of immune polyelectrolyte multilayers on microneedle arrays to enhance cancer vaccination. Immune polyelectrolyte multilayers: iPEM, cytosine triphosphate deoxynucleotide guanine triphosphate deoxynucleotide: CpG. Reprinted with permission from [55].

7.3. Dissolvable MNs

Dissolvable polymeric MNs were emerged to entrap therapeutic agents within a water-soluble matrix, and they become fully dissolved after inserting into the skin, leaving no biohazardous sharp waste [56]. Prausnitz et al. explored dissolvable polymeric patches using PVP as a water-soluble matrix to encapsulate the influenza vaccine. In order to assess the stability of antigen, mice were immunized intramuscularly with an inactivated influenza virus or via MN patches incorporating the same amount of virus. Results exhibited that a single administration with dissolving MNs developed a stronger immune response as compared to that of intramuscular injections (**Figure 1.6**).

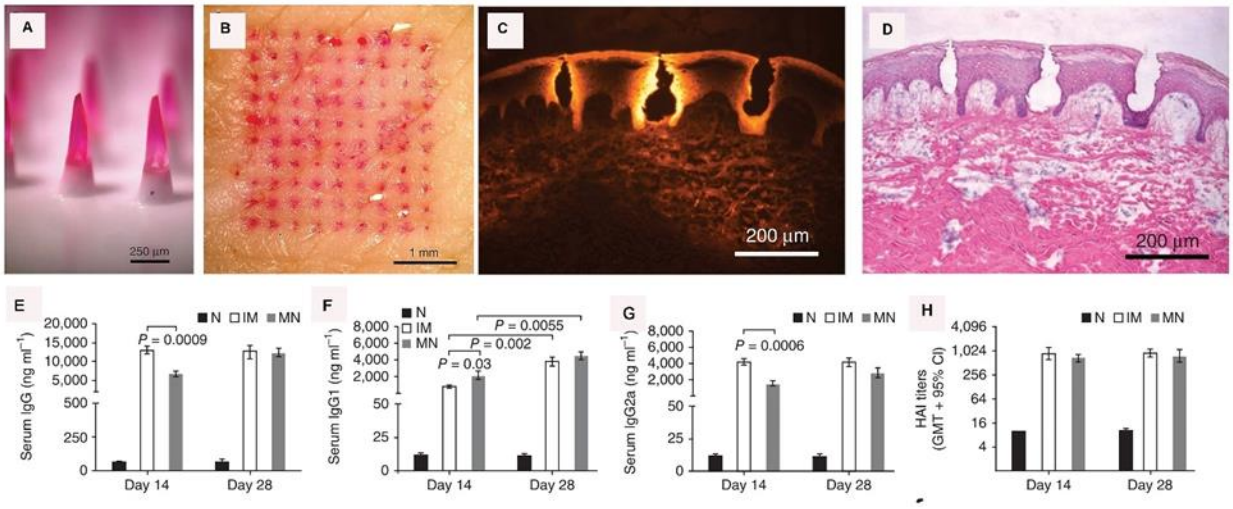

Figure 1.6. A, Dissolving microneedles. B, Top view of porcine skin. C, Fluorescence micrograph of pigskin histological section after insertion. D, Brightfield micrograph of the same skin section with H&E staining. E, Immunoglobulin G (IgG) titers. F, IgG1 titers. G, IgG2a titers. H, hemagglutination inhibition titers. Reprinted with modification from [57]. Naïve group: N microneedle: MN, intramuscular: IM.

For the first time, acceptability of inactivated influenza vaccine delivered by dissolvable MN patches for influenza vaccination in clinical trial was carried out by the Georgia Institute of Technology and the Emory University Hope Clinic. The seroconversion percentages were significantly higher at day 28 after MN patch vaccination compared with placebo and were similar to intramuscular injection. Clinical trial demonstrated that dissolvable MN patches were well tolerated and generated robust antibody responses with no adverse events [58].

In addition, for influenza vaccination, carbohydrates such as carboxymethyl cellulose and trehalose have been applied to prepare dissolvable MN patches. MNs composed of HA as a polymeric matrix have been employed for tetanus, diphtheria, influenza, and malaria [59]. Ling et al. created a dissolvable MN patch with a starch/gelatin matrix, providing sufficient mechanical

strength for delivery of insulin, which was able to have a fast delivery into the skin for diabetic patients.

In the direction of fast release, HA-MNs were loaded with an amyloid-β 42-amino acid peptide antigen to create a vaccine for Alzheimer's disease. The results demonstrated a robust immune response after MN insertion. However, dissolvable MNs are not the optimal system when sustained drug delivery is desirable.

7.4. Degradable MNs

To achieve pulsatile release which is the final goal of vaccination, biodegradable polymer particles were embedded in MN patches [28]. These drug delivery vehicles release their payload by simple diffusion and hydrolysis of the polymer. PLGA has been among the most attractive biocompatible and biodegradable polymers used to load drug/therapeutic agents [60]. Embedding labile molecules like peptides and proteins in MPs and NPs has great superiority, particularly if compared to soluble antigen formulations [61]. Encapsulating antigens in particles can maintain the antigen stability from enzymatic degradation and enhance the uptake by APCs in a targeted and prolonged manner while reducing the entry of encapsulated antigens to the systemic circulation [61]. Furthermore, the encapsulated form of antigens are more effectively cross-presented via MHCI molecules to CD8+ T cells than soluble antigens. This leads to the simultaneous stimulation of both CD4+ as well as robust CD8+ T cell responses. In a study, OVA-loaded NPs were fabricated by the double emulsion technique and subsequently incorporated into the MN patches. The results exhibited a potent CD8+ cytotoxic T cell and CD4+ Th1 immune responses against the encapsulated antigen. In order to tune the payload release, degradable and dissolvable MNs were explored by Vecchione et al. In this configuration (**Figure 1.7**), not only the MPs but also the hydrophilic tip, are capable of entrapping bioactive molecules, developing a bi-compartmental

system. In this method, firstly, a water soluble polymer such as PVP or HA is deposited on the mold, after drying, polymeric MPs are incorporated into the microcavities [28].

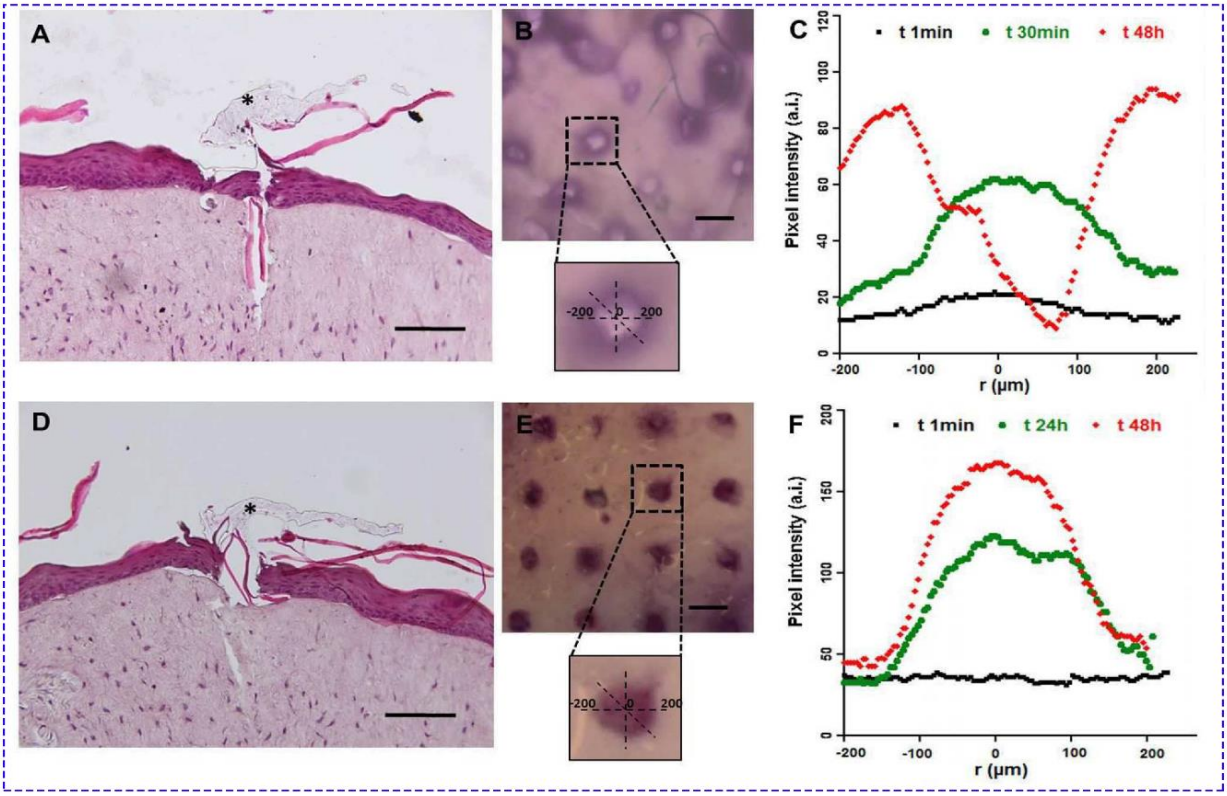

Figure 1.7. Histological result of MNs after insertion into a full-thickness human skin model. The pictures in A, B, and C refer to the embedding enzyme into the dissolvable tip; D, E, and F refer to enzyme-encapsulated microparticles. A D Histological images after 48 h; black asterisks indicate the polyvinyl pyrrolidone (PVP) polymer remained after removing the patch (scale bar = 100 µm). B E Stereomicroscopic images of Endo-Human Skin Equivalent (Endo-HSE) (histological) 48 h after indentation (scale bar = 500 µm). The inserts of the stereomicroscopic images are the schematic representation of the methods used to calculate the diffusive radius reported in the x-axis of the successive graphs. C,F: The graphs plot, at three-time points, the pixel

intensity as it corresponds to the concentration of the substrate oxidation product diffusing into the extracellular matrix vs. the radius of the diffusion pattern. Reprinted with permission from [28].

Great attempt has been carried out to solve the denaturation of protein structures over the fabrication process. In this direction, OVA, as an antigen model, was encapsulated into PLGA particles by the self-healing method [3]. This method guarantees the integrity of the OVA structure, since MPs are incubated with the antigen solution, avoiding the antigen from exposure to the mechanical stresses during the fabrication process.

In the other study, prolonged delivery has been achieved utilizing the PLGA MPs/poly(acrylic acid) composite MN patches. Implanting the MPs or solid polymer MNs in the tissue leads to robust cellular immunity and similar creation of serum antibodies as compared to traditional syringe-based vaccination [62].

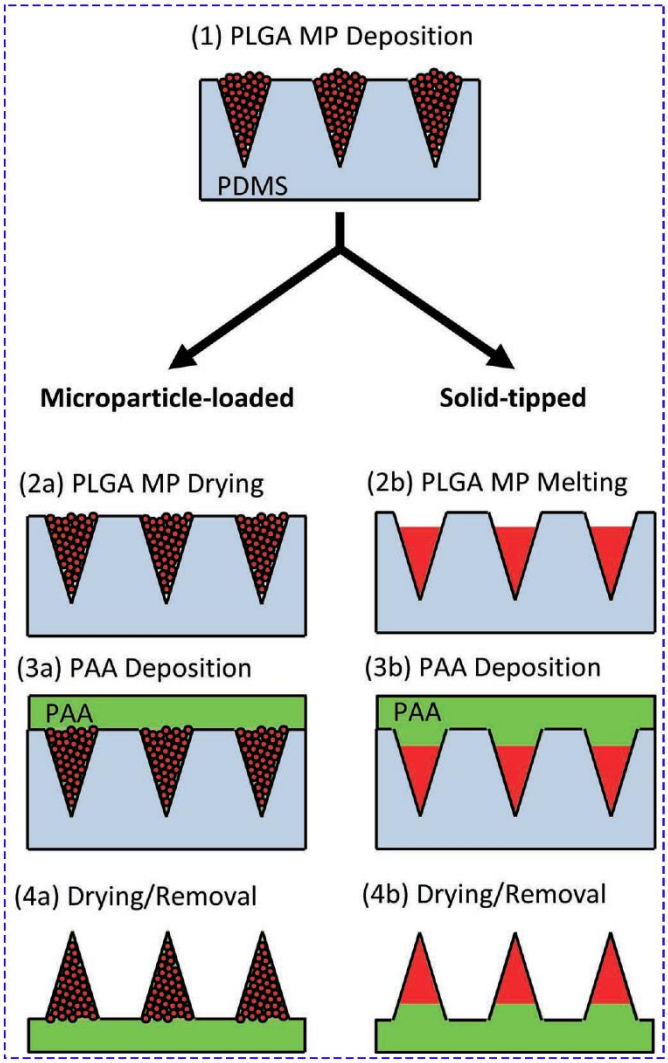

Figure 1.8. Schematic representation of composite microparticle and bulk poly(lactic-co-glycolic) acid (PLGA) tip MN fabrication. The PDMS stamp were first filled with PLGA microparticles (1). PLGA microparticles were then either dried in microcavities (2a) or fused at an elevated temperature to create a solid tip (2b). Poly(acrylic acid) solution was then centrifuged onto the filled stamps to create a matrix (3a) or pedestal (3b) for instant dissolution in vivo. After drying, MNs were extracted from the stamps (4a, 4b). Poly(lactic-co-glycolic) acid: PLGA, microparticle: MP, Polydimethylsiloxane: PDMS, Poly(acrylic acid): PAA. Reprinted with permission from [62].

In the context of the long-term delivery of the vaccine, MNs consist of a silk tip supported on a poly(acrylic acid) PAA base has been designed. PAA bases dissolve instantly to deliver the antigen while also implanting silk hydrogel depots for long-term cutaneous release within 1–2 weeks. Microneedle patches containing OVA loaded in the silk needle tips or OVA in the PAA pedestals allow for bolus and prolonged release **(Figure 1.8)** [63]. The use of a complex system such as the degradable particle within MNs is justified in the case of need for an engineered release profile.

7.5. Hydrogel-forming MNs

Hydrogel-forming MNs, also known as cross-linked hydrogels, are solid systems that can rapidly swell after the uptake of interstitial fluid into their three-dimensional matrix, after which they release the encapsulated materials, and are pulled out intact from the skin [64]. These swellable MNs dated back to 2012 and contained poly(methyl vinyl ether/maleic acid), cross-linked with poly (ethylene glycol) (PEG) to deliver bovine serum albumin (BSA). As another alternative, PVA also can give rise to a swellable system with a unique phase-transition property during temperature change [65]. Unlike chemical cross-linking, phase-transition MN patches (**Figure 1.9**) can provide microcrystalline domains as a junction by a freeze-thaw method. The microcrystalline cross-linking can embed protein drugs such as insulin, free of hazardous cross-linking agents, which typically is needed for chemical and ionic cross-linking. The applications of cross-linkable MNs are not just restricted to drug delivery but can also be used to extract interstitial fluid for further analysis. Designing bullet-shaped double-layered MN patches with water-swellable tips allows adherence to the skin owing to the formation of a desirable structure for interlocking with tissues [66]. Insulin-loaded swellable MNs showed prolonged release, thereby a progressive drop in blood glucose levels [66]. Delivery of the anticancer drug bevacizumab with dissolving and hydrogel-forming MNs has been compared. The results exhibit the better performance of the hydrogel-

forming MNs as compared with the dissolving MNs. The maximum concentration of bevacizumab in the serum was obtained 1 day after removing the hydrogel from the skin, proposing that the controlled delivery via this system stem from the fact that bevacizumab enters the microcirculation through the skin [67].

Some restrictions concerning swellable MNs are related to the need to keep the patch on the skin for all release timeframes. Additionally, great attention has to be given to the choice of cross-linkage reaction, which needs to be biocompatible.

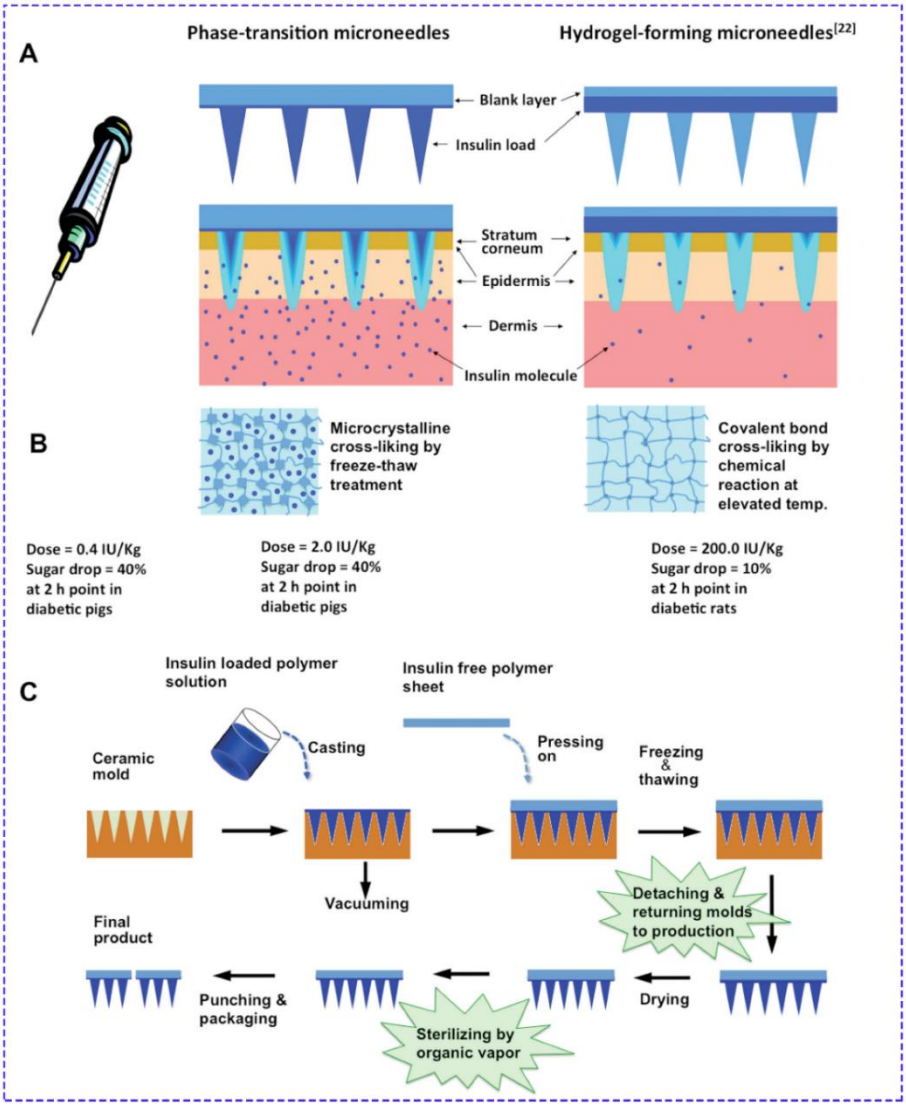

Figure 1.9. The fabrication method of phase transition patches. A, The MNs absorb the interstitial fluid from the dermis layer to convert from a hard, glassy state to a hydrogel state to allow the release of preloaded insulin to the fluid in the dermis layer. B, The microneedle matrix of phase-transition microneedles is cross-linked through microcrystalline domains as the cross-linking junctions via a freeze-thaw treatment to avoid dissolution, while that of hydrogel-forming is cross-linked through covalent bonds as the cross-linking junctions by means of chemical reaction. Hence, insulin can be trapped in the needle tips of PTM to achieve a relative bioavailability of 20%, while insulin has to be loaded at the back of the microneedle array of hydrogel-forming microneedles (HFMs), leading to the bioavailability of less than 1% due to the extended diffusion pathway. C, The PTM patch may be fabricated using a scalable process comprising a sequence of simple unit operations involving the circulation of the molds in the production line and sterilization of the final product by steaming in oxirane vapor. Phase-transition microneedles: PT, hydrogel-forming microneedles: HFMs. Reprinted with permission from [68].

7.6. Responsive MNs

Responsive materials have the exceptional properties that release drugs and bioactive molecules as a response to physiological signals as internal stimuli (e.g., pH, reactive oxygen species, glucose and enzymes) and/or physical signals as external stimuli (e.g., temperature, electric field, light, and mechanical stress). One of the most vital proteins that need to be released with respect to physiological conditions is insulin. The insulin source should be able to release the therapeutic in high blood glucose level, imitating physiological dynamical insulin secretion to avoid dangerous situations like hyper/hypoglycemia [69]. Different glucose-responsive materials have been incorporated into the MN matrix [70] or in particles embedded in MNs [71]. As an example, non-degradable MNs were designed from hydrogel containing phenylboronic acid (PBA) as a glucose-

sensitive agent. The results demonstrated that not only the release of insulin is dependent on BGLs, but they also showed stability and shape preservation after 7 days in an aqueous solution, which exhibited their capability for sustained and on-demand insulin release [72].

In another study, Juiang et. al. designed polymeric MNs loaded with insulin-containing glucose-responsive mesoporous bioactive glass nanoparticles (BGNs). The silica NPs were coated by a pH-responsive material and glucose oxidase (GOx), which made them link BGLs. As the pH changed, subsequently giving the ability of glucose level sensing. Due to the high concentration of glucose, this system can sense pH alteration through the pH-responsive material and leads to insulin release [73]. Applying another strategy, insulin-loaded mesoporous bioactive glasses (MBGs) containing GOx were capped by ZnO quantum dots (ZnO QDs) .Since ZnO QDs are dissolvable at a low pH, they can act as pH-sensitive agents **(Figure 1.10)**. In vivo studies demonstrated the achievement of prolonged and moderate blood glucose control by the glucose-responsive MNs, while blood glucose level dropped immediately after subcutaneous injections [74].

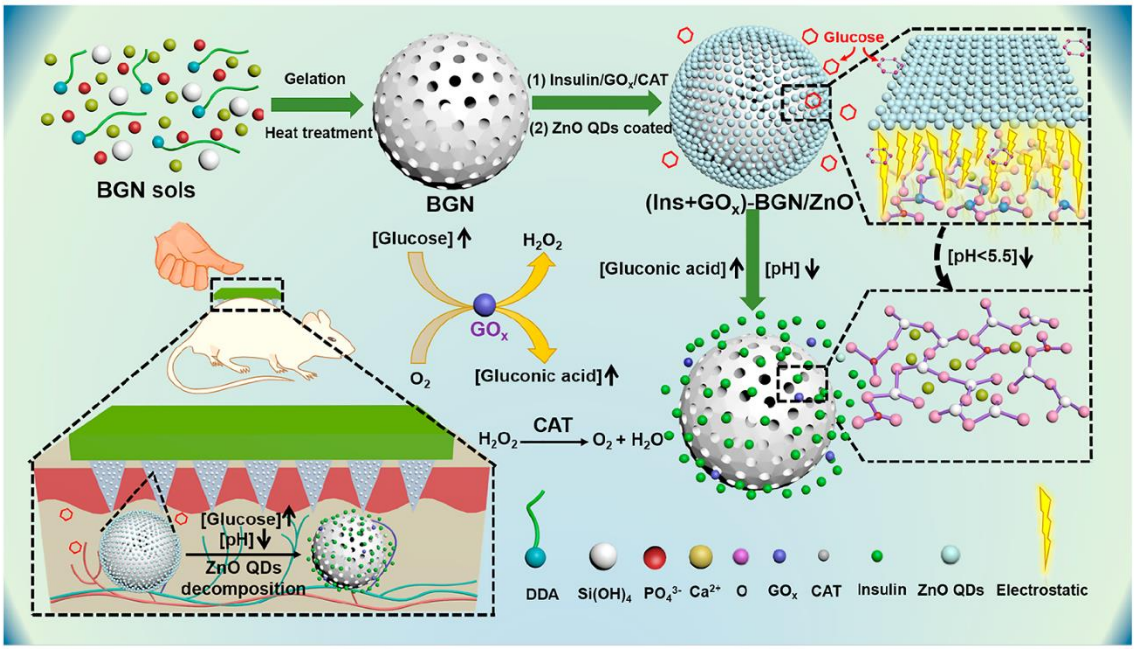

Figure 1.10. Bioactive glass nanoparticles (BGN) can be fabricated by BGN soles through gelation under high temperatures. These BGNs were filled with GOx/catalase (CAT) inside their pores, and then the NPs were coated by ZnO quantum dots (QDs). As BGLs increase, the pH reduces to a value lower than 5.5 as a result of the reaction occurring by GOx. ZnO QDs are dissolved under the low pH, which disintegrates the BGN, and therefore, insulin is free to be released from the disassembled particle. The CAT enzyme is responsible for decreasing the harm caused by H_2O_2 on the surrounding tissue. Bioactive glass nanoparticles: BGN, catalase: CAT, quantum dots: QDs. Reprinted with permission from [74].

Control of glucose level can also be achieved by live (cell-based) and synthetic glucose-responsive systems. As an example, glucose-responsive MNs based on cross-linked HA with β-cells embedded in microgels on the tip of MNs. High glucose levels can efficiently diffuse and activate the release of β-cells on the tips of MNs. The amplified signal exhibited efficient glucose control for almost 8 h compared with other treatments lacking the live/synthetic part or even with one of

the enzymes involved [75]. The responsive system could be extended in the field of vaccine as potential strategy to promote a sustained release of protein-based vaccines.

There are some factors to be taken into account for protein delivery. For instances, the sterilization methods should be carefully chosen to avoid losing the integrity of the product and increasing the manufacturing costs. Aseptic manufacturing could be expensive, and heat or microwave heating could damage the MNs or their cargo. Alternatively, GMP productions would be needed to skip sterilization. Regarding storage, since MNs are quite sensitive to temperature and mechanical stress, it is essential to preserve the MNs in a humidity-free state, e.g., in a desiccator. However, stability studies of long-term patches are needed. In this regard, Hiraishi et al. [76] in a study observed that environmental humidity has an effect on the mechanical strength of the microneedle patches. The mechanical failure force test indicated that by raising the level of humidity, the needle strength dropped. Wet conditions are also not appropriate for maintaining the stability of proteins; indeed, the presence of an uncontrolled atmosphere can lead to protein unfolding, aggregation, or chemical degradation [77].

References

[1] H. Suh, J. Shin, Y.-C. Kim, Clin. Exp. Vaccine Res. 3 (2014) 42–49.

[2] R. Donnelly, D. Douroumis, Drug Deliv Transl Res 5 (2015) 311–312.

[3] J.M. Mazzara, L.J. Ochyl, J.K.Y. Hong, J.J. Moon, M.R. Prausnitz, S.P. Schwendeman, Bioeng. Transl. Med. 4 (2019) 116–128.

[4] K.T.M. Tran, T.D. Gavitt, N.J. Farrell, E.J. Curry, A.B. Mara, A. Patel, L. Brown, S. Kilpatrick, R. Piotrowska, N. Mishra, Nat. Biomed. Eng. (2020) 1–10.

[5] S. Bobbala, S. Hook, Pharm. Res. 33 (2016) 2078–2097.

[6] I. Jones, P. Roy, Lancet (2021).

[7] K. Modjarrad, C.C. Roberts, K.T. Mills, A.R. Castellano, K. Paolino, K. Muthumani, E.L. Reuschel, M.L. Robb, T. Racine, M. Oh, Lancet Infect. Dis. 19 (2019) 1013–1022.

[8] T.R.F. Smith, A. Patel, S. Ramos, D. Elwood, X. Zhu, J. Yan, E.N. Gary, S.N. Walker, K. Schultheis, M. Purwar, Nat. Commun. 11 (2020) 1–13.

[9] S. Shi, H. Zhu, X. Xia, Z. Liang, X. Ma, B. Sun, Vaccine 37 (2019) 3167–3178.

[10] M.D. Knoll, C. Wonodi, Lancet 397 (2021) 72–74.

[11] Z. Cui, Adv. Genet. 54 (2005) 257–289.

[12] E.H. Livingston, JAMA 325 (2021) 898.

[13] R. Sartorius, D. Russo, L. D'Apice, P. De Berardinis, in: Innov. Vaccinol., Springer, 2012, pp. 123–134.

[14] R. Sartorius, P. Pisu, L. D'Apice, L. Pizzella, C. Romano, G. Cortese, A. Giorgini, A. Santoni, F. Velotti, P. De Berardinis, J. Immunol. 180 (2008) 3719–3728.

[15] R. Sartorius, L. D'Apice, A. Prisco, P. De Berardinis, Pharmaceutics 11 (2019) 437.

[16] J. Fang, G. Wang, Q. Yang, J. Song, Y. Wang, L. Wang, Vaccine 23 (2005) 4860–4866.

[17] N. Bastien, M. Trudel, C. Simard, Virology 234 (1997) 118–122.

[18] L.J. Cruz, P.J. Tacken, R. Fokkink, B. Joosten, M.C. Stuart, F. Albericio, R. Torensma, C.G. Figdor, J. Control. Release 144 (2010) 118–126.

[19] R. Jamaledin, C. Di Natale, V. Onesto, Z.B. Taraghdari, E.N. Zare, P. Makvandi, R. Vecchione, P.A. Netti, J. Clin. Med. 9 (2020) 542.

[20] M. Battisti, R. Vecchione, C. Casale, F.A. Pennacchio, V. Lettera, R. Jamaledin, M. Profeta, C. Di Natale, G. Imparato, F. Urciuolo, P.A. Netti, Front. Bioeng. Biotechnol. 7 (2019).

[21] C. Di Natale, D. De Rosa, M. Profeta, R. Jamaledin, A. Attanasio, E. Lagreca, P.L. Scognamiglio, P.A. Netti, R. Vecchione, J. Mater. Chem. B 9 (2021) 392–403.

[22] S. Lee, S. Fakhraei Lahiji, J. Jang, M. Jang, H. Jung, Pharmaceutics 11 (2019) 402.

[23] M.C. Chen, K.Y. Lai, M.H. Ling, C.W. Lin, Acta Biomater. (2018).

[24] M.-C. Chen, S.-F. Huang, K.-Y. Lai, M.-H. Ling, Biomaterials 34 (2013) 3077–3086.

[25] H. Jun, M.H. Ahn, I.J. Choi, S.K. Baek, J.H. Park, S.O. Choi, RSC Adv. 8 (2018) 17786–17796.

[26] K. Sahil, M. Akanksha, S. Premjeet, A. Bilandi, B. Kapoor, Int. J. Res. Pharm. Chem 1 (2011) 1184–1198.

[27] R. Jamaledin, P. Makvandi, C.K.Y. Yiu, T. Agarwal, R. Vecchione, W. Sun, T.K. Maiti, F.R. Tay, P.A. Netti, Adv. Ther. (n.d.) 2000171.

[28] M. Battisti, R. Vecchione, C. Casale, F.A. Pennacchio, V. Lettera, R. Jamaledin, M. Profeta, C. Di Natale, G. Imparato, F. Urciuolo, Front. Bioeng. Biotechnol. 7 (2019).

[29] X. He, J. Sun, J. Zhuang, H. Xu, Y. Liu, D. Wu, Dose-Response 17 (2019) 1559325819878585.

[30] H. Juster, B. van der Aar, H. de Brouwer, Polym. Eng. Sci. 59 (2019) 877–890.

[31] S.P. Sullivan, N. Murthy, M.R. Prausnitz, Adv. Mater. 20 (2008) 933–938.

[32] H.R. Nejad, A. Sadeqi, G. Kiaee, S. Sonkusale, Microsystems Nanoeng. 4 (2018) 1–7.

[33] Y.K. Demir, Z. Akan, O. Kerimoglu, PLoS One 8 (2013) e77289.

[34] K.J. Krieger, N. Bertollo, M. Dangol, J.T. Sheridan, M.M. Lowery, E.D. O'Cearbhaill, Microsystems Nanoeng. 5 (2019) 1–14.

[35] T.E. Andersen, A.J. Andersen, R.S. Petersen, L.H. Nielsen, S.S. Keller, Microelectron. Eng. 195 (2018) 57–61.

[36] A. Ono, H. Azukizawa, S. Ito, Y. Nakamura, H. Asada, Y.-S. Quan, F. Kamiyama, I. Katayama, S. Hirobe, N. Okada, Int. J. Pharm. 532 (2017) 374–383.

[37] R. Jamaledin, C. Di Natale, V. Onesto, Z.B. Taraghdari, E.N. Zare, P. Makvandi, R. Vecchione, P.A. Netti, J. Clin. Med. 9 (2020) 542.

[38] K. Lee, J.D. Kim, C.Y. Lee, S. Her, H. Jung, Biomaterials 32 (2011) 7705–7710.

[39] J.D. Kim, M. Kim, H. Yang, K. Lee, H. Jung, J. Control. Release 170 (2013) 430–436.

[40] S. Henry, D. V McAllister, M.G. Allen, M.R. Prausnitz, J. Pharm. Sci. 87 (1998) 922–925.

[41] M.W. Zhu, H.W. Li, X.L. Chen, Y.F. Tang, M.H. Lu, Y.F. Chen, J. Micromechanics Microengineering 19 (2009) 115010.

[42] S. Aoyagi, H. Izumi, Y. Isono, M. Fukuda, H. Ogawa, Sensors Actuators A Phys. 139 (2007) 293–302.

[43] F. Perennes, B. Marmiroli, M. Matteucci, M. Tormen, L. Vaccari, E. Di Fabrizio, J. Micromechanics Microengineering 16 (2006) 473.

[44] S. Yang, Y. Feng, L. Zhang, N. Chen, W. Yuan, T. Jin, Int. J. Nanomedicine 7 (2012) 1415.

[45] R.F. Donnelly, R. Majithiya, T.R.R. Singh, D.I.J. Morrow, M.J. Garland, Y.K. Demir, K. Migalska, E. Ryan, D. Gillen, C.J. Scott, Pharm. Res. 28 (2011) 41–57.

[46] E.M. Cahill, E.D. O'Cearbhaill, Bioconjug. Chem. 26 (2015) 1289–1296.

[47] J.H. Park, M.G. Allen, M.R. Prausnitz, J. Control. Release 104 (2005) 51–66.

[48] R.E.M. Lutton, J. Moore, E. Larrañeta, S. Ligett, A.D. Woolfson, R.F. Donnelly, Drug Deliv. Transl. Res. 5 (2015) 313–331.

[49] X.-M. Wu, H. Todo, K. Sugibayashi, J. Control. Release 118 (2007) 189–195.

[50] M.R. Prausnitz, Adv. Drug Deliv. Rev. 56 (2004) 581–587.

[51] L. Niu, L.Y. Chu, S.A. Burton, K.J. Hansen, J. Panyam, J. Control. Release 294 (2019) 268–278.

[52] G. Du, R.M. Hathout, M. Nasr, M.R. Nejadnik, J. Tu, R.I. Koning, A.J. Koster, B. Slütter, A. Kros, W. Jiskoot, J. Control. Release 266 (2017) 109–118.

[53] G. Du, M. Leone, S. Romeijn, G. Kersten, W. Jiskoot, J.A. Bouwstra, Int. J. Pharm. 547 (2018) 250–257.

[54] P.C. DeMuth, A. V Li, P. Abbink, J. Liu, H. Li, K.A. Stanley, K.M. Smith, C.L. Lavine, M.S. Seaman, J.A. Kramer, Nat. Biotechnol. 31 (2013) 1082–1085.

[55] Q. Zeng, J.M. Gammon, L.H. Tostanoski, Y.-C. Chiu, C.M. Jewell, ACS Biomater. Sci. Eng. 3 (2017) 195–205.

[56] J.W. Lee, S. Choi, E.I. Felner, M.R. Prausnitz, Small 7 (2011) 531–539.

[57] S.P. Sullivan, D.G. Koutsonanos, M. del Pilar Martin, J.W. Lee, V. Zarnitsyn, S.-O. Choi, N. Murthy, R.W. Compans, I. Skountzou, M.R. Prausnitz, Nat. Med. 16 (2010) 915.

[58] N.G. Rouphael, M. Paine, R. Mosley, S. Henry, D. V McAllister, H. Kalluri, W. Pewin, P.M. Frew, T. Yu, N.J. Thornburg, Lancet 390 (2017) 649–658.

[59] M.H. Ling, M.C. Chen, Acta Biomater. (2013).

[60] E. Cohen-Sela, M. Chorny, N. Koroukhov, H.D. Danenberg, G. Golomb, J. Control. Release 133 (2009) 90–95.

[61] A.A. Walters, S. Somavarapu, V. Riitho, G.R. Stewart, B. Charleston, F. Steinbach, S.P. Graham, Vaccine 33 (2015) 6588–6595.

[62] P.C. DeMuth, W.F. Garcia-Beltran, M.L. Ai-Ling, P.T. Hammond, D.J. Irvine, Adv. Funct. Mater. 23 (2013) 161–172.

[63] P.C. DeMuth, Y. Min, D.J. Irvine, P.T. Hammond, Adv. Healthc. Mater. 3 (2014) 47–58.

[64] X. Hong, Z. Wu, L. Chen, F. Wu, L. Wei, W. Yuan, Nano-Micro Lett. 6 (2014) 191–199.

[65] S. Jiang, S. Liu, W. Feng, J. Mech. Behav. Biomed. Mater. 4 (2011) 1228–1233.

[66] K.-Y. Seong, M.-S. Seo, D.Y. Hwang, E.D. O'Cearbhaill, S. Sreenan, J.M. Karp, S.Y. Yang, J. Control. Release 265 (2017) 48–56.

[67] A.J. Courtenay, M.T.C. McCrudden, K.J. McAvoy, H.O. McCarthy, R.F. Donnelly, Mol. Pharm. 15 (2018) 3545–3556.

[68] S. Yang, F. Wu, J. Liu, G. Fan, W. Welsh, H. Zhu, T. Jin, Adv. Funct. Mater. 25 (2015) 4633–4641.

[69] J. Wang, Z. Wang, J. Yu, A.R. Kahkoska, J.B. Buse, Z. Gu, Adv. Mater. (2019) 1902004.

[70] J. Wang, Y. Ye, J. Yu, A.R. Kahkoska, X. Zhang, C. Wang, W. Sun, R.D. Corder, Z. Chen, S.A. Khan, ACS Nano 12 (2018) 2466–2473.

[71] C. Li, X. Liu, Y. Liu, F. Huang, G. Wu, Y. Liu, Z. Zhang, Y. Ding, J. Lv, R. Ma, Nanoscale 11 (2019) 9163–9175.

[72] S. Chen, H. Matsumoto, Y. Moro-oka, M. Tanaka, Yuji Miyahara, T. Suganami, A. Matsumoto, ACS Biomater. Sci. Eng. 5 (2019) 5781–5789.

[73] G. Jiang, B. Xu, J. Zhu, Y. Zhang, T. Liu, G. Song, Biomed. Phys. Eng. Express 5 (2019) 45038.

[74] B. Xu, Q. Cao, Y. Zhang, W. Yu, J. Zhu, D. Liu, G. Jiang, ACS Biomater. Sci. Eng. (2018).

[75] Y. Ye, J. Yu, C. Wang, N. Nguyen, G.M. Walker, J.B. Buse, Z. Gu, Adv. Mater. 28 (2016) 3115–3121.

[76] Y. Hiraishi, T. Nakagawa, Y.-S. Quan, F. Kamiyama, S. Hirobe, N. Okada, S. Nakagawa, Int. J. Pharm. 441 (2013) 570–579.

[77] C. Kolluru, Y. Gomaa, M.R. Prausnitz, Drug Deliv. Transl. Res. 9 (2019) 192–203.

[78] R. Jamaledin, R. Sartorius, C. Di Natale, R. Vecchione, P. De Berardinis, P.A. Netti, Microorganisms (2020).

[79] G. Del Pozzo, D. Mascolo, R. Sartorius, A. Citro, P. Barba, L. D'Apice, P. De Berardinis, J. Biomed. Biotechnol. 2010 (2010).

[80] R. Sartorius, L. D'Apice, P. Barba, D. Cipria, L. Grauso, A. Cutignano, P. De Berardinis,

Front. Immunol. 9 (2018) 1496.

[81] C. Di Natale, V. Onesto, E. Lagreca, R. Vecchione, P.A. Netti, Materials (Basel). 13 (2020) 1807.

[82] Y. Yang, N. Bajaj, P. Xu, K. Ohn, M.D. Tsifansky, Y. Yeo, Biomaterials 30 (2009) 1947–1953.

[83] M. Odonchimeg, S.C. Kim, Y.K. Shim, W.K. Lee, Mong. J. Chem. 18 (2017) 41–47.

[84] R. Agarwal, C.T. Johnson, B.R. Imhoff, R.M. Donlan, N.A. McCarty, A.J. García, Nat. Biomed. Eng. 2 (2018) 841–849.

[85] J. Sambrook, E.F. Fritsch, T. Maniatis, Molecular Cloning: A Laboratory Manual., Cold spring harbor laboratory press, 1989.

[86] L. D'Apice, R. Sartorius, A. Caivano, D. Mascolo, G. Del Pozzo, D.S. Di Mase, E. Ricca, G.L. Pira, F. Manca, D. Malanga, Vaccine 25 (2007) 1993–2000.

[87] F. Niesler, M. Hermatschweiler, Laser Tech. J. 12 (2015) 44–47.

[88] P. Makvandi, M. Kirkby, A.R.J. Hutton, M. Shabani, C.K.Y. Yiu, Z. Baghbantaraghdari, R. Jamaledin, M. Carlotti, B. Mazzolai, V. Mattoli, Nano-Micro Lett. 13 (2021) 1–41.

[89] E. Larraneta, J. Moore, E.M. Vicente-Perez, P. Gonzalez-Vazquez, R. Lutton, A.D. Woolfson, R.F. Donnelly, Int. J. Pharm. 472 (2014) 65–73.

[90] C. Mircioiu, V. Voicu, V. Anuta, A. Tudose, C. Celia, D. Paolino, M. Fresta, R. Sandulovici, I. Mircioiu, Pharmaceutics 11 (2019) 140.

[91] J.H. Lee, Y. Yeo, Chem. Eng. Sci. 125 (2015) 75–84.

[92] M. Allahyari, E. Mohit, Hum. Vaccin. Immunother. 12 (2016) 806–828.

[93] A.L. Silva, P.C. Soema, B. Slütter, F. Ossendorp, W. Jiskoot, Hum. Vaccin. Immunother. 12 (2016) 1056–1069.

[94] M. Yoshida, J. Mata, J.E. Babensee, J. Biomed. Mater. Res. Part A An Off. J. Soc. Biomater. Japanese Soc. Biomater. Aust. Soc. Biomater. Korean Soc. Biomater. 80 (2007) 7–12.

Chapter 2

Materials and

Methods

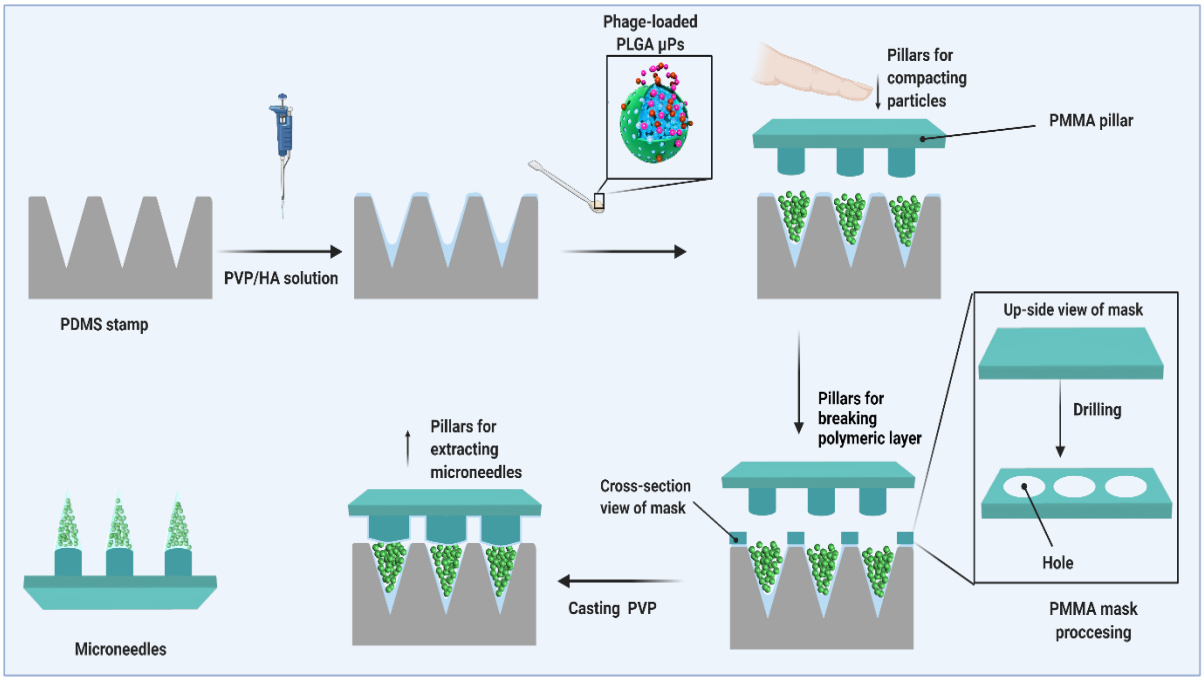

Part of this chapter is based on these research papers:

"**Non-invasive Production of Multi-Compartmental Biodegradable Polymer Microneedles for Controlled Intradermal Drug Release of Labile Molecules"** M. Battisti, R. Vecchione, C. Casale, F. A. Pennacchio, V. Lettera, R. Jamaledin, M. Profeta, C. Di Natale, G. Imparato, F. Urciuolo, Front. Bioeng. Biotechnol. **2019**, 7, 296.

"**Design of biodegradable bi-compartmental microneedles for the stabilization and the controlled release of the labile molecule collagenase for skin healthcare"** C. Di Natale, D. De Rosa, M. Profeta, R. Jamaledin, A. Attanasio, E. Lagreca, P. L. Scognamiglio, P. A. Netti and R. Vecchione, J. M. Ch. B. **2020**, 9, 392.

2. Materials and Methods

2.1 Materials

Poly(lactic-co-glycolic acid) 50:50 (PLGA RESOMER RG 504H, 38–54 kDa), was purchased from Ivonik industries. Dichloromethane (DCM) sodium acetate anhydrous, Ammonium bicarbonate (ABC), fluorescein isothiocyanate isomer I (FITC), Poly(vinylpyrrolidone) (PVP, Mw 55 kDa), Cesium Chloride gradient, Isopropyl-beta–d-thiogalactopyranoside, Sodium chloride (NaCl), Poly(vinyl alcohol) (PVA, MW 27–32 kDa), Tween 20, Polyethylene glycol 6000 (PEG) were bought from Sigma Aldrich. Poly(dimethylsiloxane) (PDMS) was provided by Sylgard R (184 Silicone Elastomer Kit, Dow Corning). Poly(methylmethacrylate) (PMMA) was purchased from GoodFellow. Hyaluronic acid (HA, Mw 200 kDa) was provided by Fidia. IP-S negative tone photoresist and ITO-coated glass substrate were purchased from Nanoscribe GmbH. NOA 61 glue was purchased from Norland Optical Adhesive. Developer mr-Dev 600 was purchased from Micro Resist Technology GmbH.

2.2 Bacteriophage Purification

Recombinant hybrid bacteriophage fdOVA (expressing ovalbumin peptide SIINFEKL (residues 257–264)-pVIII proteins) was generated as described elsewhere [78,79]. Briefly, DNA oligos encoding the OVA (257–264) MHC H-2b-restricted peptide (5′-CCGCGGAGGGTTCCATCATCAACTTCGAAAAACTGGACGATCCCGCCAAGG-3′) were cloned into SacII-StyI-digested fdAMPLAY88 phage genome containing two copies of pVIII proteins: one wild-type and one with the SacII-StyI restriction sites. This second copy was under the control of the isopropyl-beta–d-thiogalactopyranoside (IPTG)-inducible promoter pTac. *E. coli* TG1 *recO* cells, transformed with recombinant bacteriophages fdOVA DNA release hybrid phages

in the supernatant. Hybrid fdOVA filamentous bacteriophages were purified from the supernatant of *E. coli* TG1*recO* cells previously transformed with the phage DNA, according to [80]. Briefly, bacteria transformed with the phage DNA were grown in 2XTY medium (16 g/L Tryptone, 10 g/L Yeast Extract, 5.0 g/L NaCl) for 16 h in the presence of 100μg/mL Ampicillin. The expression of the recombinant OVA-pVIII proteins was induced by adding 0.1 mM IPTG to the growing cultures (at Absorbance A600 = 0.25 optical density (OD)). The supernatant containing bacteriophages was harvested from *E. coli* cultures by centrifugation, and phages were subjected to double precipitation by adding 20% polyethylene glycol 6000 (PEG) and 2.5M NaCl to the supernatant. Phages were collected by centrifugation (16,000g), the pellet was resuspended in 10mMTris/1mM EDTA pH8.0 buffer (TE) and phages were purified by ultracentrifugation (240,500g) on cesium chloride gradient (0.5 g/mL). The resulting virions were dialyzed against phosphate-buffered saline (PBS) 1X and the concentration of bacteriophage was determined using a spectrophotometer. The spectrum of filamentous fd phages typically exhibits a broad plateau at 260–280 nm with a shallow maximum around 269 nm. Concentration is calculated according to the formula:

$$\text{mg of phages/mL} = (A269 - A320)/3.84, \quad (1)$$

assuming that an OD of 1 is equivalent to a concentration of 3.8 mg/mL.

fdOVA is a hybrid bacteriophage in which recombinant copies of the major coat protein pVIII are interspersed with wild-type pVIII copies on the coat surface of each single virion. The number of copies of pVIII displaying the OVA $_{(257–264)}$ peptide was estimated based on the relative yields of the various N terminal sequences obtained by N-terminal sequence analysis of the purified virions, which resulted in 15–20% for each bacteriophage preparation.

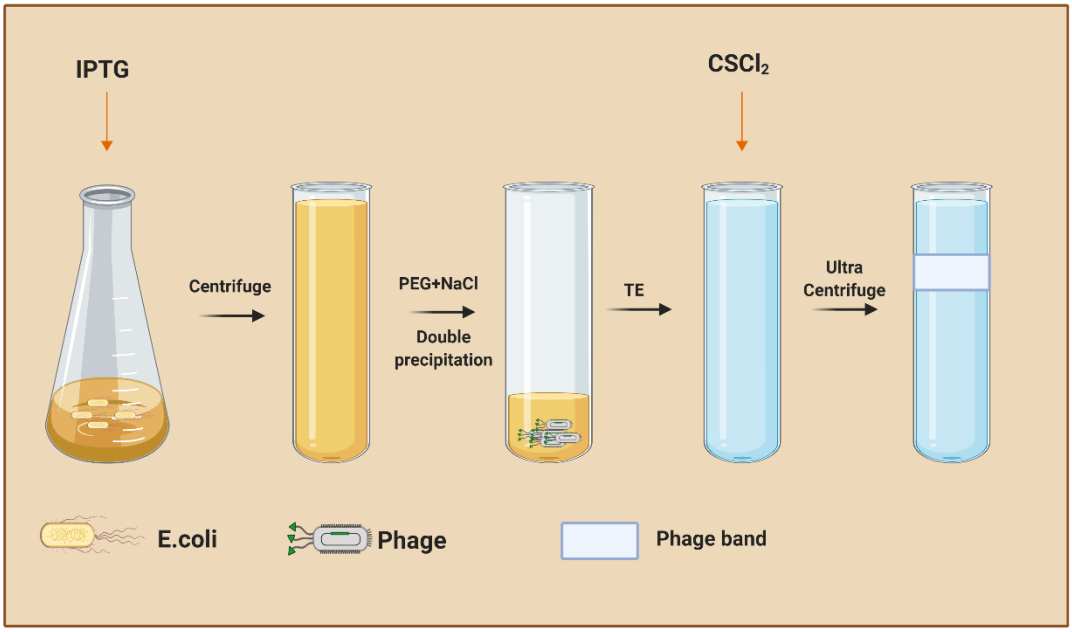

Figure 2.1. Hybrid fdOVA filamentous bacteriophages were purified from the supernatant of E. coli TG1recO cells previously transformed with the fdOVA phage DNA. Briefly, bacteria transformed with the phage DNA were grown in 2XTY medium in the presence of Ampicillin. The expression of the recombinant OVA-pVIII proteins was induced by adding IPTG to the growing cultures. The supernatant containing bacteriophages was harvested from E. coli cultures by centrifugation, and phages were subjected to double precipitation by adding polyethylene glycol and NaCl to the supernatant. Phages were collected by centrifugation; the pellet was resuspended in Tris/1mM EDTA buffer (TE) and phages were purified by ultracentrifugation on cesium chloride gradient. Cesium Chloride: CsCl, Isopropyl-beta–d-thiogalactopyranoside: IPTG, Polyethylene glycol: PEG.

2.3 Fluorescent Labeling of Bacteriophage Virion

Hybrid fdOVA (100 µL) virions (7 µg/µL) in PBS buffer pH 8.2 were treated with a 20-fold molar excess of Fluorescein isothiocyanate (FITC) and stirred gently for 2 h at room temperature **Figure 2.2** [78]. The unreacted FITC was removed with five washes using a 3-kDa MWCO Vivaspin system and the bacteriophage was re-equilibrated in PBS 1X pH 7.2. The concentration of bacteriophage after conjugation was evaluated by UV.

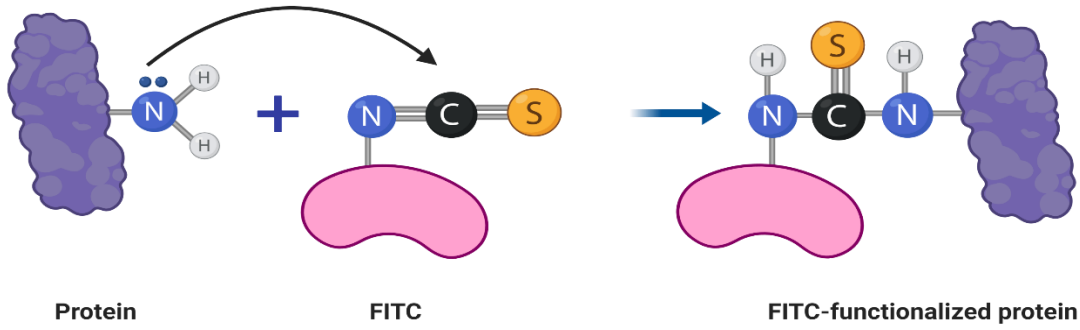

Figure 2.2. FITC conjugation occurs through the free amino groups of proteins or peptides of the phage scaffold, forming a stable thiourea bond. Fluorescein isothiocyanate: FITC. Reprinted with permission from [78].

2.4 Bone Marrow Derived-Dendritic Cells Generation

Female C57BL/6 mice were purchased from Charles River (Lecco, Italy) and housed in IGB "A. Buzzati-Traverso" Animal House Facility under standard pathogen-free conditions abiding by institutional guidelines. Bone marrow-derived dendritic cells (BM-DCs) were produced from precursors isolated from tibiae of euthanized C57BL/6 mice. Both ends of tibiae were cut and bone marrow was flushed with a needle of a syringe filled with ice-cold RPMI 1640 medium. Clusters of cells were dissolved by pipetting, cells were washed twice with medium, plated, and cultured

with 200 U/mL recombinant murine granulocyte/macrophage colony-stimulating factor (GM-CSF) in RPMI 1640 medium supplemented with 10% fetal calf serum (FCS), 100 U/mL penicillin, 100 µg/mL streptomycin, 1 mM sodium pyruvate and 50 µM 2-mercaptoethanol. Immature DCs were collected at day 7 of culture and were assayed for dendritic cell phenotype by staining with the monoclonal antibody anti-CD11c-PE-Cy7 (HL3, BD Biosciences) and FACS analysis.

2.5 Fabrication of PLGA Microparticles

PLGA MPs were prepared by the double-emulsion ($W_1/O/W_2$) solvent evaporation technique as already described [21,28,78,81,82]. Briefly, for direct encapsulation, 100 mg PLGA was dissolved in 1 mL dichloromethane. Next, 100 µL (7 mg/mL) bacteriophage was added to PLGA solution. 100 µL ammonium bicarbonate (7.5mg/mL water) as porogen agent were added and homogenized at 20,000 rpm for 30 s, then mixed with 10 mL of 2% PVA and homogenized at 25,000 rpm for 1 min. The final emulsion was added to 40 mL water and stirred to evaporate all the DCM for 3 h. MPs were washed with deionized water three times to remove the PVA then exposed to the lyophilization process overnight.

For post encapsulation [83,84], 100 mg PLGA was dissolved in 1 mL DCM. Next, 100 µL ABC (7.5mg/mL water) were added and homogenized at 20,000 rpm for 30 s, then mixed with 10 mL of 2% PVA and homogenized at 25,000 rpm for 1 min. The final emulsion was added to 40 mL water and stirred to evaporate all the DCM for 3 h. MPs were washed with deionized water three times to remove the PVA **Figure 2.3**. Empty MPs (5 mg) were suspended in a solution of purified fdOVA bacteriophage (0.1 µg/µL) in PBS and incubated overnight with mild shaking at 4 °C. MPs were then washed three times with PBS 1X and then lyophilized.

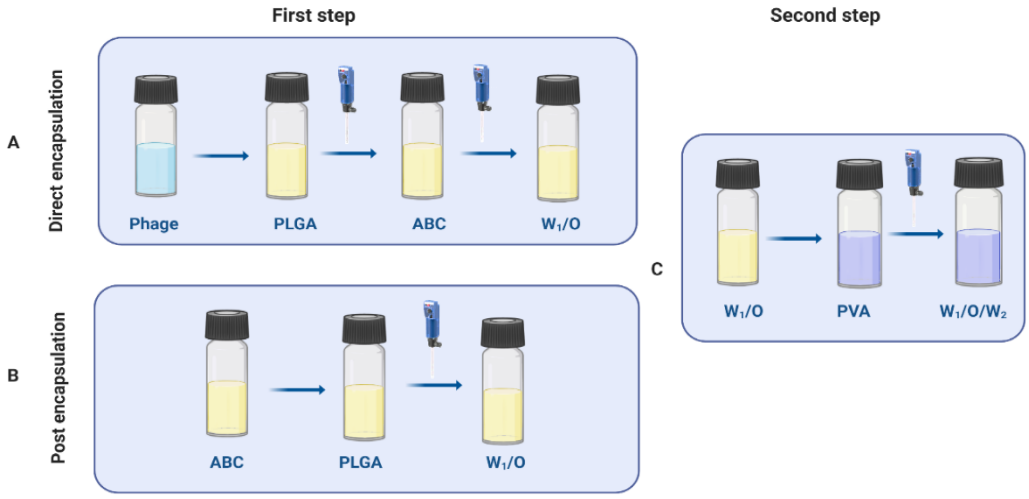

Figure 2.3. Microparticle production by double emulsion method. A) Direct encapsulation; bacteriophage was added in the water phase. B). Fabrication of empty MPs for post encapsulation. C) Double emulsion final step. Ammonium bicarbonate: ABC, Poly(lactic-co-glycolic acid): PLGA, Poly(vinyl alcohol): PVA.

2.6 Characterization of Microparticles

After the fabrication process, the MPs were analyzed by SEM and Confocal microscopy to investigate the morphology of microparticles.

2.6.1 Size Distribution

The size distribution of the MPs was evaluated using a laser diffraction instrument (Mastersizer2000, Malvern Instruments, Malvern, UK) using a concentration of 2 mg of PLGA particles in water [28,78]. Mastersizer 2000 consists of a 2-mW He–Ne laser (λ = 632.8 nm) as a light source, an optic lens, and photo-sensitive detectors. Lyophilized MPs (3 mg) were suspended in water and added to the tank to measure the particle size distribution.

2.6.2 Scanning Electron Microscopy

For scanning electron microscopy (LEO1550), MPs were positioned on a scanning electron microscopy stub, then the samples were gold-sputtered (10 nm thickness) with a HR208 Cressington sputter coater and analyzed by FESEM ULTRA-PLUS (Zeiss) at 5 kV with the SE2 detector [28,78].

2.6.3 Confocal Microscopy

Confocal analysis was performed using a Leica SP5 confocal microscope [28,78]. Fluorescence analysis was achieved using the λ_{exc} at 550 nm, λ_{em} 600–700 for a rhodamine signal and λ_{exc} 488 and λ_{em} 500–600 for the FITC channel. Images were acquired using a HCX IRAPO L 40×/0.95 water objective, a resolution of 1024 × 1024 pixels, zoom 1, and 2.33AU at a maximum pinhole, as already described.

2.6.4 Bacteriophage Release from Particles and Encapsulation Efficacy

Freeze-dried phage-loaded MPs (5 mg) were placed in a 2mL microcentrifuge tube and suspended in 1 mL of PBS pH 7.4. This mixture was kept under stirring at 50 rpm in a shaker at 37°C. At defined time points, samples were collected and centrifuged at 3468 g (MICROCL 21R Centrifuge, Thermoscientific, USA) for 5 min. Aliquots of 1 mL supernatant containing phages were taken and replaced with an equal volume of fresh PBS. The supernatants were centrifuged at 9632 g for 10 min. The amount of bacteriophages in the collected supernatant was measured by UV at 269 nm, which is the typical UV signal of phages. All release tests were performed in triplicate over 8 h for post encapsulation and over 3 days for direct encapsulation. The percentage of released phages were related to the total amount of encapsulated phages inside MPs, and the cumulative release was obtained by adding the quantity of phages released at different times.

The release experiments for (75% post+25% direct), (50% post+50% direct), and (25% post+75% direct) were repeated.

For encapsulation efficiency, freeze-dried PLGA MPs (5 mg) were placed in a 2-mL microcentrifuge tube and dissolved in 375 µL DMSO, then kept in a shaker for 1 h. Next, 150 µL NaOH, 375 µL SDS and 600 µL H_2O were added. Bacteriophage content was read by UV spectroscopy. Encapsulation efficiency was calculated using the following formula.

$$\text{Encapsulation efficiency (\%)} = \frac{\text{Amount of phage entrapped}}{\text{The initial amount of phage}} \times 100 \quad (2)$$

2.6.5 Circular Dichroism

CD spectra were recorded on a Jasco J-1000 spectropolarimeter (JASCO Corp, Milan, Italy), as already reported [78]. Spectra were obtained in phosphate buffer pH 7.4, standard bacteriophages were analyzed at 0.22 mg/mL while post and direct phage were encapsulated at 0.14 mg/mL (spectra recorded after 6 hours of release).

2.6.6 Colony-forming Unit determination

Infective bacteriophages were counted with the Colony Forming Unit (CFU) assay using the plating method [85,86]. Serial dilutions of the bacteriophage were made in PBS and 10 µl of each dilution was added to 200 µl of 0.6 OD TG1 *recO* bacterial culture. Each mixture was incubated for 20 min at 37 °C and plated on top of selective LB-agar plates containing 100 µg/ml Ampicillin. A bacterial culture without bacteriophage and a bacterial culture with a known concentration of purified fdOVA bacteriophage were prepared in the same manner as negative and positive controls. Following overnight incubation at 37 °C, the number of the colony was counted for each dilution and was used to calculate the number of CFU/ml. Each measurement was performed in triplicate and each experiment was repeated at least three times.

2.6.7 Analysis of IL-6 production

To analyze IL-6 production, BM-DCs ($1x10^6$/mL) were incubated with PLGA-MPs resuspended in PBS at a concentration from 0.1 to 1 mg/mL. After overnight incubation, cells were centrifuged and IL-6 production was measured in supernatants of cultures (0.1 mL/well), according to the manufacturer's instructions, using a commercially available ELISA kit (mouse IL-6 ELISA MAX™ Standard (Biolegend)).

2.6.8 BM-DC Presentation Assay

$1x10^6$/mL BM-DCs were incubated overnight with different concentrations (0.06 and 0.6 ug/mL) of fdOVA released from MPs and encapsulated by post or direct method [78].

In another set of experiments, BM-DC ($1x10^6$/mL) was left to adhere to multiwell plates. Phage-loaded MPs were resuspended in PBS and immediately added (from 0.01 to 2 mg/mL) to adherent BM-DCs **Figure 2.4**.

After the overnight incubation, cells were washed twice to remove the excess of bacteriophages and were co-cultured (100,000/well) with the OTI hybridoma cell line B3Z (50,000/well) for 40 h. B3Z OTI hybridoma cell line, recognizing the OVA(257–264) SIINFEKL determinant, was grown in complete RPMI1640 (10% fetal calf serum (FCS), 100 U/mL penicillin, 100 µg/mL streptomycin 1% Glutamine, 1% NEM, 1% Sodium Pyruvate, 50 µM 2-Mercaptoethanol) Recognition of the major histocompatibility complex (MHC I)-presented-OVA peptide 257-264 (SIINFEKL) by B3Z T cell receptor leads to transcriptional activation of the IL-2 promoter element, resulting in the production of IL-2 that correlates with uptake and processing of the fdOVA and presentation of OVA (257-264) peptide on MHC I. The amount of IL-2 released into

cell co-culture supernatants was measured by ELISA. Supernatants of co-cultures (0.1 mL/well) were assayed in duplicate using mouse IL-2 ELISA MAX™ Standard (Biolegend), according to the manufacturer's instructions.

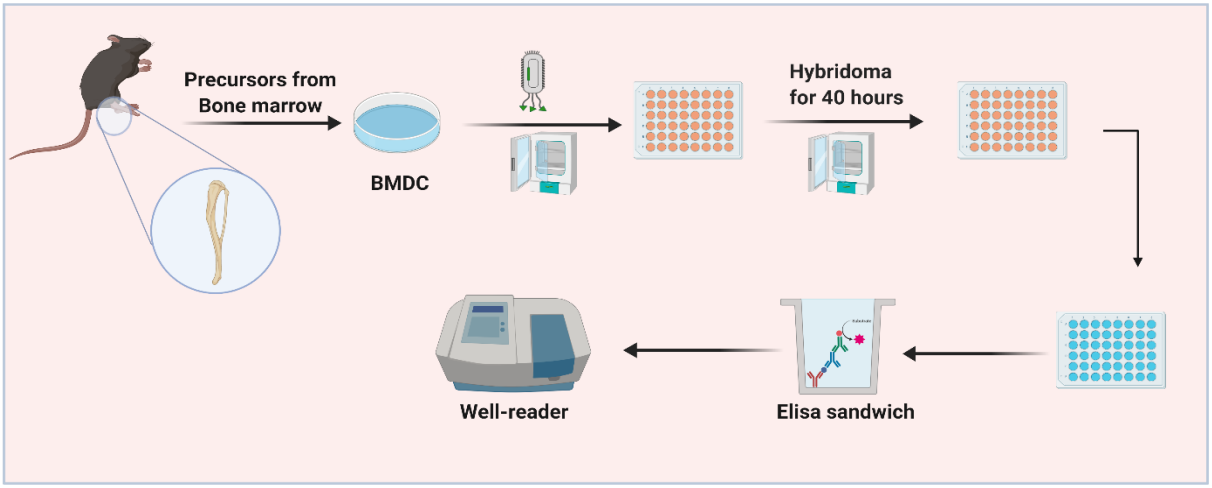

Figure 2.4. Bone-marrow derived dendritic cells were obtained by culturing bone-marrow precursors isolated from C57/BL6 mice in presence of GM-CSF. BMDC were incubated with fdOVA bacteriophages or fdOVA PLGA-MPs overnight. Later, cells were washed, B3Z hybridoma cells were added and cells were co-cultured for 40 h. Sandwich ELISA was conducted to evaluated Interleukin-2 released in the supernatant by B3Z cells in response to OVA antigen. Bone-marrow derived dendritic cells: BMDC, Enzyme Linked Immunosorbent Assay: ELISA.

2.6.9 In silico Release Study

A mathematical model describing and predicting bacteriophage direct and post encapsulation releases was developed as described in [81]. First, experimental data were normalized to extract releases for 1mg of MPs. Then, these data were fitted with an exponential growth model, using Matlab® (v.R2019a). In particular, the bacteriophage release B_r was described by:

$$B_r = \boldsymbol{a}(1 - e^{-\boldsymbol{b}t}) \qquad \text{Eq.1}$$

Where a and b are the fitting model parameters. $y = 0$ at $t = 0$ was assumed as the initial condition. In the case of MPs with bacteriophage entrapped by post-encapsulation method, Eq.1 is considered valid for a time t in the interval $0 \leq t \leq 6h$, being data for $t > 6h$ unavailable having the bacteriophage already been completely released.

Starting from Eq. 1, a simple release kinetics prediction under the non-linear first-order assumption was developed:

$$B_r = \frac{\sum_1^n B_n a_n (1 - e^{-b_n t})}{\sum_1^n B_n} \qquad \text{Eq.2}$$

with $\sum_1^n B_n = B_1 + B_2 + ... + B_n = 100$

where a_n and b_n are the fitting model parameters, B_n is the percentage of weighted bacteriophage MPs, n is the number of different MP formulations considered; in this specific case we fabricated two MPs encapsulating bacteriophage either directly or with a post-process, then $n = 2$.

2.7 Fabrication of Microneedles

Pillar-based microneedles have been fabricated as follow.

2.7.1 Master of Microneedles, Stamp and Pillars

The microcone master was manufactured by means of 2- photon polymerization (2PP) using the Nanoscribe Photonic Professional GT system (Nanoscribe GmbH) [87]. The Nanoscribe system uses a 780 nm Ti-Sapphire laser emitting ≈100 fs pulses at 80 MHz with a maximum power of 150 mW and equipped with the 25 × 0.8 NA oil-immersion objective of a Nanoscribe system to reduce the fabrication time of the master up to 15 times as compared to the 63 × 1.4 NA objective. The substrate was placed in a holder that fitted into a piezoelectric x/y/z stage. A galvo scanner determined the laser trajectories. The master was fabricated by processing the IP-DIP negative

tone photoresist (Nanoscribe GmbH). The basic master was fabricated with a conical shape and with a MN height of 600 µm and base diameter of 300µm. A layer of IP-DIP was spin-coated onto the glass substrate (5,500 rpm for 30 s) and photo-polymerized by UV lamp exposure (16 mW/cm2 for 4 h). A drop of photoresist was then dispensed onto the glass substrate and fabricated with the Nanoscribe to directly produce the microcone master. The master produced by 2PP was put under a UV lamp (3 h) to induce microcone hardening before use. The master structure was then replicated by pouring a solution of liquid PDMS precursor and its curing agent (10:1 w/w) onto it. This was then put under vacuum to remove entrapped air bubbles and cured in an oven at 70◦C for 1 h. After curing, the PDMS was peeled off and attached to double-sided adhesive tape on a glass slide; then, NOA 60 was poured onto it and put under vacuum to remove the bubbles for about 1 h. NOA 60 is a clear, colorless, liquid photosensitive polymer that is cured when exposed to ultraviolet light in the wavelength range of 350–380 nm (www.norlandprod.com). The curing time depends on the thickness and the energy of the ultraviolet light. In our case, the wavelength light was 365 nm and the optimized exposure time was 3 h. Finally, the PDMS negative stamp was removed and the NOA positive mold was obtained. The NOA positive mold was attached to a petri dish or glass slide with double-sided adhesive tape. Finally, the PDMS precursor was poured onto the NOA positive mold, cured at 70◦C for 1 h, and then peeled off from the NOA to obtain PDMS stamps. The master produced can thus be used many times without being damaged.

PMMA pillars to compact MPs, break the polymeric layer on the PDMS mold, supporting arrays, and mask were prepared by micro milling machine (CNC micromill, Minitech MiniMill 3/Pro, Minitech Machinery Corporation, Georgia, USA). Briefly, Computer-Aided Design (CAD) file was prepared and the “dxf” format was imported to deskam software and converted to G code file. Afterward, the micromilling process was initiated on the PMMA sheet.

2.7.2 Preparing the Microneedle Matrix

To make microneedles matrix, the previously reported method was used [21]. In brief, 150µl solution containing 6.3% Polyvinylpyrrolidone (PVP) and 1.54 % Hyaluronic acid (HA) was poured onto the mold. After being dried for 2 hours under a chemical hood, PLGA MPs were incorporated into the cavities with the aid of a spatula under an optical stereomicroscope (Olympus, SZX16). The fabricated PMMA pillars were used to sufficiently compress the microparticles into the mold cavities.

2.7.3 Integration of the Microneedles and Pillars

To integrate the supporting array and MNs, the mask was positioned on the mold then pillars were forced to break the polymeric layer on the mold. 40 µL of 25% (w/v) PVP aqueous solution was poured onto the pillars **Figure 2.5**. The pillars was aligned into the filled MN cavities (still in the mold) under a stereomicroscope (Olympus, SZX16) to elevate the height of the microneedles [22–24]. This assembly was placed under the hood for 1 hour to form the MN patch. Patches were then demolded and freeze-dried overnight. Afterward, patches were kept into an aluminium-laminated sachet containing sieves and stored in a desiccator at room temperature (25 °).

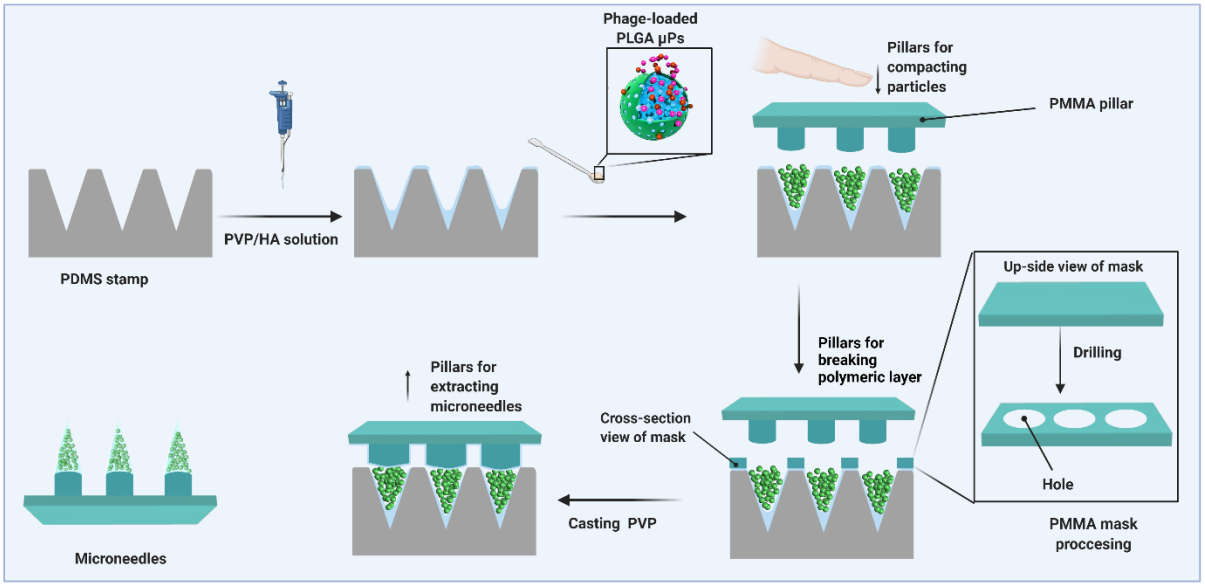

Figure 2.5. Schematic illustrations of the fabrication process for microneedle (MN) patch. Step 1, depositing PVP/HA polymeric solution; step 2, incorporating microparticle and pressing process by PMMA pillars; step 3, breaking the polymeric layer on the mold using PMMA pillar; step 4, applying the PMMA pillars to extract microneedles. HA: Hyaluronic acid. PDMS: polydimethylsiloxane; PVP: Polyvinylpyrrolidone.

2.8 Characterization of Microneedles

After fabrication, the microneedles were analyzed by a stereomicroscope (Olympus, SZX16 double objective) and Confocal microscopy to investigate the sharpness of the tips and the pattern distribution.

2.8.1 Optical Stereomicroscopy

Microneedle masters fabricated by the Nanoscribe system were analyzed by a stereomicroscope (Olympus, SZX16 double objective) to ensure the good quality of the fabrication and integrity of

the tips. After extraction, each microneedle patch was analyzed by the stereomicroscope to investigate the sharpness of the tips and the pattern distribution.

2.8.2 Scanning Electron Microscopy

Microneedle morphology was investigated through a scanning electron microscope (SEM) [28]. SEM samples were prepared by attaching the microneedle patch onto a cover slip mounted on a standard SEM pin stub. The samples were gold-sputtered with a sputter coater (15 nm thickness) and analyzed by FESEM ULTRA-PLUS (Zeiss) at 10–20 kV with the SE2 detector.

2.8.3 Fluorescent Microscopy

Fluorescent microscopy analyses were performed using Sulforhodamin-loaded tips [78]. Sample morphology was investigated using a confocal microscope (Leica Microsystems TCS SP5 II, Germany) with a 20× air objective. Images were acquired with a resolution of 1,024 × 1,024 pixels.

2.8.4 Parafilm Test

A commercial polymeric film (Parafilm M®, a blend of a hydrocarbon wax and a polyolefin) was used as a model membrane for microneedle (MN) insertion studies [88,89]. Parafilm M® was folded before the insertions as skin simulant for insertion studies. A sheet of Parafilm was folded to get an eight-layer film (≈1 mm thickness) and a poly(urethane) needle testing film (Deka®) was used as received (0.4 mm thickness).

References

[1] H. Suh, J. Shin, Y.-C. Kim, Clin. Exp. Vaccine Res. 3 (2014) 42–49.

[2] R. Donnelly, D. Douroumis, Drug Deliv Transl Res 5 (2015) 311–312.

[3] J.M. Mazzara, L.J. Ochyl, J.K.Y. Hong, J.J. Moon, M.R. Prausnitz, S.P. Schwendeman, Bioeng. Transl. Med. 4 (2019) 116–128.

[4] K.T.M. Tran, T.D. Gavitt, N.J. Farrell, E.J. Curry, A.B. Mara, A. Patel, L. Brown, S. Kilpatrick, R. Piotrowska, N. Mishra, Nat. Biomed. Eng. (2020) 1–10.

[5] S. Bobbala, S. Hook, Pharm. Res. 33 (2016) 2078–2097.

[6] I. Jones, P. Roy, Lancet (2021).

[7] K. Modjarrad, C.C. Roberts, K.T. Mills, A.R. Castellano, K. Paolino, K. Muthumani, E.L. Reuschel, M.L. Robb, T. Racine, M. Oh, Lancet Infect. Dis. 19 (2019) 1013–1022.

[8] T.R.F. Smith, A. Patel, S. Ramos, D. Elwood, X. Zhu, J. Yan, E.N. Gary, S.N. Walker, K. Schultheis, M. Purwar, Nat. Commun. 11 (2020) 1–13.

[9] S. Shi, H. Zhu, X. Xia, Z. Liang, X. Ma, B. Sun, Vaccine 37 (2019) 3167–3178.

[10] M.D. Knoll, C. Wonodi, Lancet 397 (2021) 72–74.

[11] Z. Cui, Adv. Genet. 54 (2005) 257–289.

[12] E.H. Livingston, JAMA 325 (2021) 898.

[13] R. Sartorius, D. Russo, L. D'Apice, P. De Berardinis, in: Innov. Vaccinol., Springer, 2012, pp. 123–134.

[14] R. Sartorius, P. Pisu, L. D'Apice, L. Pizzella, C. Romano, G. Cortese, A. Giorgini, A. Santoni, F. Velotti, P. De Berardinis, J. Immunol. 180 (2008) 3719–3728.

[15] R. Sartorius, L. D'Apice, A. Prisco, P. De Berardinis, Pharmaceutics 11 (2019) 437.

[16] J. Fang, G. Wang, Q. Yang, J. Song, Y. Wang, L. Wang, Vaccine 23 (2005) 4860–4866.

[17] N. Bastien, M. Trudel, C. Simard, Virology 234 (1997) 118–122.

[18] L.J. Cruz, P.J. Tacken, R. Fokkink, B. Joosten, M.C. Stuart, F. Albericio, R. Torensma, C.G. Figdor, J. Control. Release 144 (2010) 118–126.

[19] R. Jamaledin, C. Di Natale, V. Onesto, Z.B. Taraghdari, E.N. Zare, P. Makvandi, R. Vecchione, P.A. Netti, J. Clin. Med. 9 (2020) 542.

[20] M. Battisti, R. Vecchione, C. Casale, F.A. Pennacchio, V. Lettera, R. Jamaledin, M. Profeta, C. Di Natale, G. Imparato, F. Urciuolo, P.A. Netti, Front. Bioeng. Biotechnol. 7 (2019).

[21] C. Di Natale, D. De Rosa, M. Profeta, R. Jamaledin, A. Attanasio, E. Lagreca, P.L. Scognamiglio, P.A. Netti, R. Vecchione, J. Mater. Chem. B 9 (2021) 392–403.

[22] S. Lee, S. Fakhraei Lahiji, J. Jang, M. Jang, H. Jung, Pharmaceutics 11 (2019) 402.

[23] M.C. Chen, K.Y. Lai, M.H. Ling, C.W. Lin, Acta Biomater. (2018).

[24] M.-C. Chen, S.-F. Huang, K.-Y. Lai, M.-H. Ling, Biomaterials 34 (2013) 3077–3086.

[25] H. Jun, M.H. Ahn, I.J. Choi, S.K. Baek, J.H. Park, S.O. Choi, RSC Adv. 8 (2018) 17786–17796.

[26] K. Sahil, M. Akanksha, S. Premjeet, A. Bilandi, B. Kapoor, Int. J. Res. Pharm. Chem 1 (2011) 1184–1198.

[27] R. Jamaledin, P. Makvandi, C.K.Y. Yiu, T. Agarwal, R. Vecchione, W. Sun, T.K. Maiti, F.R. Tay, P.A. Netti, Adv. Ther. (n.d.) 2000171.

[28] M. Battisti, R. Vecchione, C. Casale, F.A. Pennacchio, V. Lettera, R. Jamaledin, M. Profeta, C. Di Natale, G. Imparato, F. Urciuolo, Front. Bioeng. Biotechnol. 7 (2019).

[29] X. He, J. Sun, J. Zhuang, H. Xu, Y. Liu, D. Wu, Dose-Response 17 (2019) 1559325819878585.

[30] H. Juster, B. van der Aar, H. de Brouwer, Polym. Eng. Sci. 59 (2019) 877–890.

[31] S.P. Sullivan, N. Murthy, M.R. Prausnitz, Adv. Mater. 20 (2008) 933–938.

[32] H.R. Nejad, A. Sadeqi, G. Kiaee, S. Sonkusale, Microsystems Nanoeng. 4 (2018) 1–7.

[33] Y.K. Demir, Z. Akan, O. Kerimoglu, PLoS One 8 (2013) e77289.

[34] K.J. Krieger, N. Bertollo, M. Dangol, J.T. Sheridan, M.M. Lowery, E.D. O'Cearbhaill, Microsystems Nanoeng. 5 (2019) 1–14.

[35] T.E. Andersen, A.J. Andersen, R.S. Petersen, L.H. Nielsen, S.S. Keller, Microelectron. Eng. 195 (2018) 57–61.

[36] A. Ono, H. Azukizawa, S. Ito, Y. Nakamura, H. Asada, Y.-S. Quan, F. Kamiyama, I. Katayama, S. Hirobe, N. Okada, Int. J. Pharm. 532 (2017) 374–383.

[37] R. Jamaledin, C. Di Natale, V. Onesto, Z.B. Taraghdari, E.N. Zare, P. Makvandi, R. Vecchione, P.A. Netti, J. Clin. Med. 9 (2020) 542.

[38] K. Lee, J.D. Kim, C.Y. Lee, S. Her, H. Jung, Biomaterials 32 (2011) 7705–7710.

[39] J.D. Kim, M. Kim, H. Yang, K. Lee, H. Jung, J. Control. Release 170 (2013) 430–436.

[40] S. Henry, D. V McAllister, M.G. Allen, M.R. Prausnitz, J. Pharm. Sci. 87 (1998) 922–925.

[41] M.W. Zhu, H.W. Li, X.L. Chen, Y.F. Tang, M.H. Lu, Y.F. Chen, J. Micromechanics Microengineering 19 (2009) 115010.

[42] S. Aoyagi, H. Izumi, Y. Isono, M. Fukuda, H. Ogawa, Sensors Actuators A Phys. 139 (2007) 293–302.

[43] F. Perennes, B. Marmiroli, M. Matteucci, M. Tormen, L. Vaccari, E. Di Fabrizio, J. Micromechanics Microengineering 16 (2006) 473.

[44] S. Yang, Y. Feng, L. Zhang, N. Chen, W. Yuan, T. Jin, Int. J. Nanomedicine 7 (2012) 1415.

[45] R.F. Donnelly, R. Majithiya, T.R.R. Singh, D.I.J. Morrow, M.J. Garland, Y.K. Demir, K. Migalska, E. Ryan, D. Gillen, C.J. Scott, Pharm. Res. 28 (2011) 41–57.

[46] E.M. Cahill, E.D. O'Cearbhaill, Bioconjug. Chem. 26 (2015) 1289–1296.

[47] J.H. Park, M.G. Allen, M.R. Prausnitz, J. Control. Release 104 (2005) 51–66.

[48] R.E.M. Lutton, J. Moore, E. Larrañeta, S. Ligett, A.D. Woolfson, R.F. Donnelly, Drug Deliv. Transl. Res. 5 (2015) 313–331.

[49] X.-M. Wu, H. Todo, K. Sugibayashi, J. Control. Release 118 (2007) 189–195.

[50] M.R. Prausnitz, Adv. Drug Deliv. Rev. 56 (2004) 581–587.

[51] L. Niu, L.Y. Chu, S.A. Burton, K.J. Hansen, J. Panyam, J. Control. Release 294 (2019) 268–278.

[52] G. Du, R.M. Hathout, M. Nasr, M.R. Nejadnik, J. Tu, R.I. Koning, A.J. Koster, B. Slütter, A. Kros, W. Jiskoot, J. Control. Release 266 (2017) 109–118.

[53] G. Du, M. Leone, S. Romeijn, G. Kersten, W. Jiskoot, J.A. Bouwstra, Int. J. Pharm. 547 (2018) 250–257.

[54] P.C. DeMuth, A. V Li, P. Abbink, J. Liu, H. Li, K.A. Stanley, K.M. Smith, C.L. Lavine, M.S. Seaman, J.A. Kramer, Nat. Biotechnol. 31 (2013) 1082–1085.

[55] Q. Zeng, J.M. Gammon, L.H. Tostanoski, Y.-C. Chiu, C.M. Jewell, ACS Biomater. Sci. Eng. 3 (2017) 195–205.

[56] J.W. Lee, S. Choi, E.I. Felner, M.R. Prausnitz, Small 7 (2011) 531–539.

[57] S.P. Sullivan, D.G. Koutsonanos, M. del Pilar Martin, J.W. Lee, V. Zarnitsyn, S.-O. Choi, N. Murthy, R.W. Compans, I. Skountzou, M.R. Prausnitz, Nat. Med. 16 (2010) 915.

[58] N.G. Rouphael, M. Paine, R. Mosley, S. Henry, D. V McAllister, H. Kalluri, W. Pewin, P.M. Frew, T. Yu, N.J. Thornburg, Lancet 390 (2017) 649–658.

[59] M.H. Ling, M.C. Chen, Acta Biomater. (2013).

[60] E. Cohen-Sela, M. Chorny, N. Koroukhov, H.D. Danenberg, G. Golomb, J. Control. Release 133 (2009) 90–95.

[61] A.A. Walters, S. Somavarapu, V. Riitho, G.R. Stewart, B. Charleston, F. Steinbach, S.P. Graham, Vaccine 33 (2015) 6588–6595.

[62] P.C. DeMuth, W.F. Garcia-Beltran, M.L. Ai-Ling, P.T. Hammond, D.J. Irvine, Adv. Funct. Mater. 23 (2013) 161–172.

[63] P.C. DeMuth, Y. Min, D.J. Irvine, P.T. Hammond, Adv. Healthc. Mater. 3 (2014) 47–58.

[64] X. Hong, Z. Wu, L. Chen, F. Wu, L. Wei, W. Yuan, Nano-Micro Lett. 6 (2014) 191–199.

[65] S. Jiang, S. Liu, W. Feng, J. Mech. Behav. Biomed. Mater. 4 (2011) 1228–1233.

[66] K.-Y. Seong, M.-S. Seo, D.Y. Hwang, E.D. O'Cearbhaill, S. Sreenan, J.M. Karp, S.Y. Yang, J. Control. Release 265 (2017) 48–56.

[67] A.J. Courtenay, M.T.C. McCrudden, K.J. McAvoy, H.O. McCarthy, R.F. Donnelly, Mol. Pharm. 15 (2018) 3545–3556.

[68] S. Yang, F. Wu, J. Liu, G. Fan, W. Welsh, H. Zhu, T. Jin, Adv. Funct. Mater. 25 (2015) 4633–4641.

[69] J. Wang, Z. Wang, J. Yu, A.R. Kahkoska, J.B. Buse, Z. Gu, Adv. Mater. (2019) 1902004.

[70] J. Wang, Y. Ye, J. Yu, A.R. Kahkoska, X. Zhang, C. Wang, W. Sun, R.D. Corder, Z. Chen, S.A. Khan, ACS Nano 12 (2018) 2466–2473.

[71] C. Li, X. Liu, Y. Liu, F. Huang, G. Wu, Y. Liu, Z. Zhang, Y. Ding, J. Lv, R. Ma, Nanoscale 11 (2019) 9163–9175.

[72] S. Chen, H. Matsumoto, Y. Moro-oka, M. Tanaka, Yuji Miyahara, T. Suganami, A. Matsumoto, ACS Biomater. Sci. Eng. 5 (2019) 5781–5789.

[73] G. Jiang, B. Xu, J. Zhu, Y. Zhang, T. Liu, G. Song, Biomed. Phys. Eng. Express 5 (2019) 45038.

[74] B. Xu, Q. Cao, Y. Zhang, W. Yu, J. Zhu, D. Liu, G. Jiang, ACS Biomater. Sci. Eng. (2018).

[75] Y. Ye, J. Yu, C. Wang, N. Nguyen, G.M. Walker, J.B. Buse, Z. Gu, Adv. Mater. 28 (2016) 3115–3121.

[76] Y. Hiraishi, T. Nakagawa, Y.-S. Quan, F. Kamiyama, S. Hirobe, N. Okada, S. Nakagawa, Int. J. Pharm. 441 (2013) 570–579.

[77] C. Kolluru, Y. Gomaa, M.R. Prausnitz, Drug Deliv. Transl. Res. 9 (2019) 192–203.

[78] R. Jamaledin, R. Sartorius, C. Di Natale, R. Vecchione, P. De Berardinis, P.A. Netti, Microorganisms (2020).

[79] G. Del Pozzo, D. Mascolo, R. Sartorius, A. Citro, P. Barba, L. D'Apice, P. De Berardinis, J. Biomed. Biotechnol. 2010 (2010).

[80] R. Sartorius, L. D'Apice, P. Barba, D. Cipria, L. Grauso, A. Cutignano, P. De Berardinis, Front. Immunol. 9 (2018) 1496.

[81] C. Di Natale, V. Onesto, E. Lagreca, R. Vecchione, P.A. Netti, Materials (Basel). 13 (2020) 1807.

[82] Y. Yang, N. Bajaj, P. Xu, K. Ohn, M.D. Tsifansky, Y. Yeo, Biomaterials 30 (2009) 1947–1953.

[83] M. Odonchimeg, S.C. Kim, Y.K. Shim, W.K. Lee, Mong. J. Chem. 18 (2017) 41–47.

[84] R. Agarwal, C.T. Johnson, B.R. Imhoff, R.M. Donlan, N.A. McCarty, A.J. García, Nat. Biomed. Eng. 2 (2018) 841–849.

[85] J. Sambrook, E.F. Fritsch, T. Maniatis, Molecular Cloning: A Laboratory Manual., Cold spring harbor laboratory press, 1989.

[86] L. D'Apice, R. Sartorius, A. Caivano, D. Mascolo, G. Del Pozzo, D.S. Di Mase, E. Ricca, G.L. Pira, F. Manca, D. Malanga, Vaccine 25 (2007) 1993–2000.

[87] F. Niesler, M. Hermatschweiler, Laser Tech. J. 12 (2015) 44–47.

[88] P. Makvandi, M. Kirkby, A.R.J. Hutton, M. Shabani, C.K.Y. Yiu, Z. Baghbantaraghdari, R. Jamaledin, M. Carlotti, B. Mazzolai, V. Mattoli, Nano-Micro Lett. 13 (2021) 1–41.

[89] E. Larraneta, J. Moore, E.M. Vicente-Perez, P. Gonzalez-Vazquez, R. Lutton, A.D. Woolfson, R.F. Donnelly, Int. J. Pharm. 472 (2014) 65–73.

[90] C. Mircioiu, V. Voicu, V. Anuta, A. Tudose, C. Celia, D. Paolino, M. Fresta, R. Sandulovici, I. Mircioiu, Pharmaceutics 11 (2019) 140.

[91] J.H. Lee, Y. Yeo, Chem. Eng. Sci. 125 (2015) 75–84.

[92] M. Allahyari, E. Mohit, Hum. Vaccin. Immunother. 12 (2016) 806–828.

[93] A.L. Silva, P.C. Soema, B. Slütter, F. Ossendorp, W. Jiskoot, Hum. Vaccin. Immunother. 12 (2016) 1056–1069.

[94] M. Yoshida, J. Mata, J.E. Babensee, J. Biomed. Mater. Res. Part A An Off. J. Soc. Biomater. Japanese Soc. Biomater. Aust. Soc. Biomater. Korean Soc. Biomater. 80 (2007) 7–12.

Chapter 3

Results and Discussion

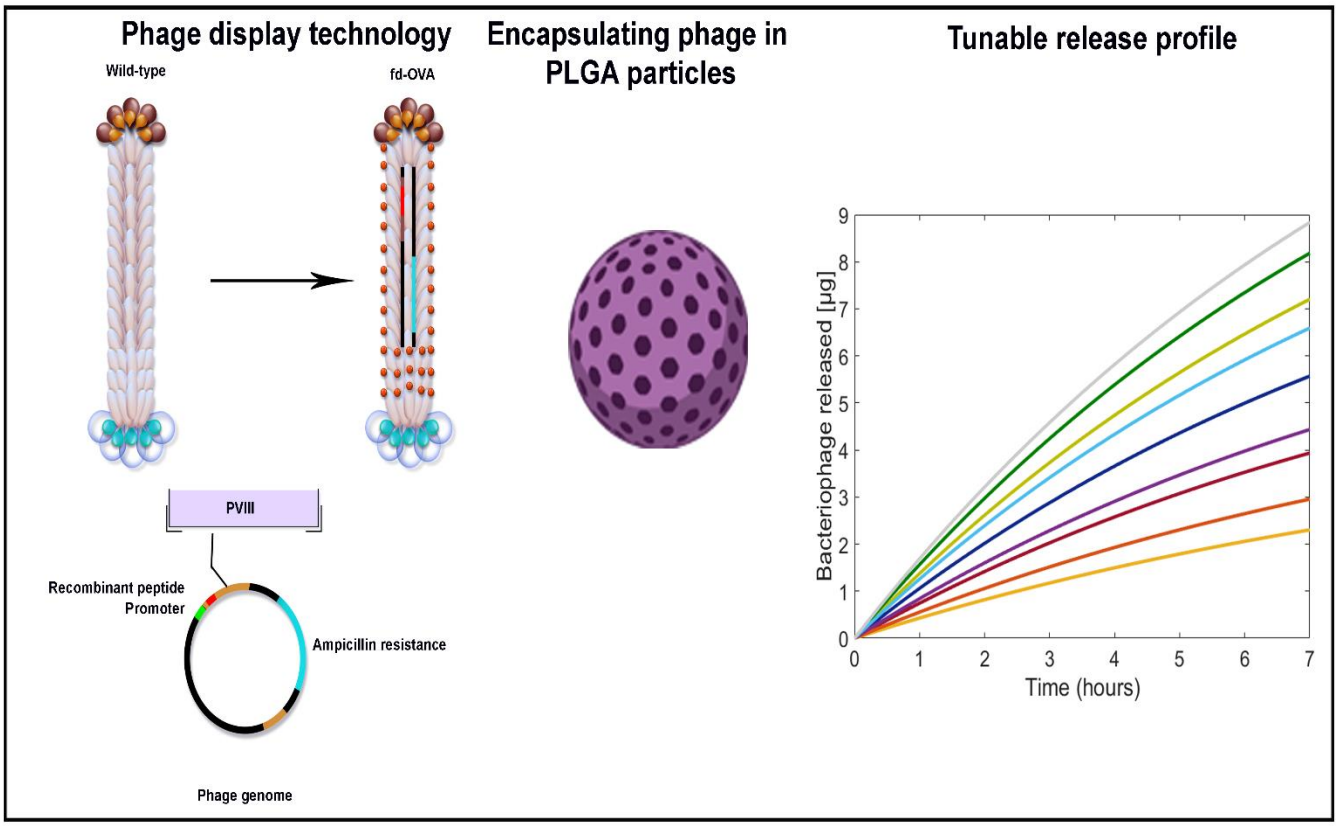

Part of this chapter is based on these papers:

"**Recombinant Filamentous Bacteriophages Encapsulated in Biodegradable Polymeric Microparticles for Stimulation of Innate and Adaptive Immune Responses"** R. Jamaledin, R. Sartorius, C. Di Natale, R.Vecchione, P. De Berardinis, and P. A. Netti, Microorganism. **2020,** *8*, 650.

"A comparative study on the release of filamentous bacteriophage through PLGA particles to induce immune responses: in vitro and in silico-supported approach" R. Jamaledin, R. Sartorius, C. Di Natale, R. Manco, V. Onestso, R. Vecchione, P. De Berardinis, P. A. Netti, **Under Submission**

3. Results and Discussion

3.1 Fluorescent Labeling of Bacteriophage Virions

To study the morphological characteristics of the bacteriophages, we functionalized them with the FITC dye. UV spectrum of protein fd bacteriophage before and after conjugation with FITC shown in **Figure 3.1**. The red line is the UV absorbance spectrum before chemical conjugation with a maximum at 269 nm. The blue line is the UV spectrum of bacteriophage after conjugation which shows the presence of two shoulders at characteristic peaks of the bacteriophage and FITC at 269 nm and 500 nm respectively.

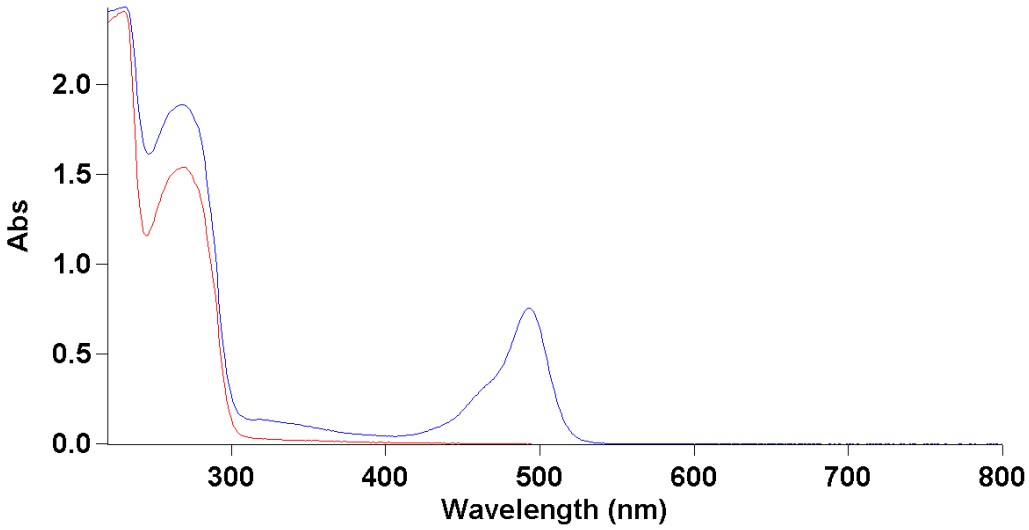

Figure 3.1. UV spectrum of protein fd bacteriophage before and after conjugation with FITC. The red line is the UV spectrum of bacteriophage before conjugating with FITC. The blue line is the UV spectrum of bacteriophage after conjugation with FITC.

3.2 Characterization of Microparticles

The morphological features of the MPs were investigated by using Scanning electron microscopy, and confocal microscopy.

3.2.1 Scanning Electron Microscopy and Size Distribution

PLGA MPs were prepared using a water-in-oil-in-water (W/O/W) double emulsion method with ammonium bicarbonate as a porogen. To study the morphological differences between MPs, their morphology was evaluated using SEM microscopy. The size of MPs was also confirmed by analyzing their size with a Malvern Mastersizer. The obtained results showed that phage-encapsulated MPs have a uniform distribution with a mean diameter of 10 µm for post encapsulated bacteriophage-MPs and 12 µm for direct encapsulated bacteriophage-MPs **Figure 3.2**.

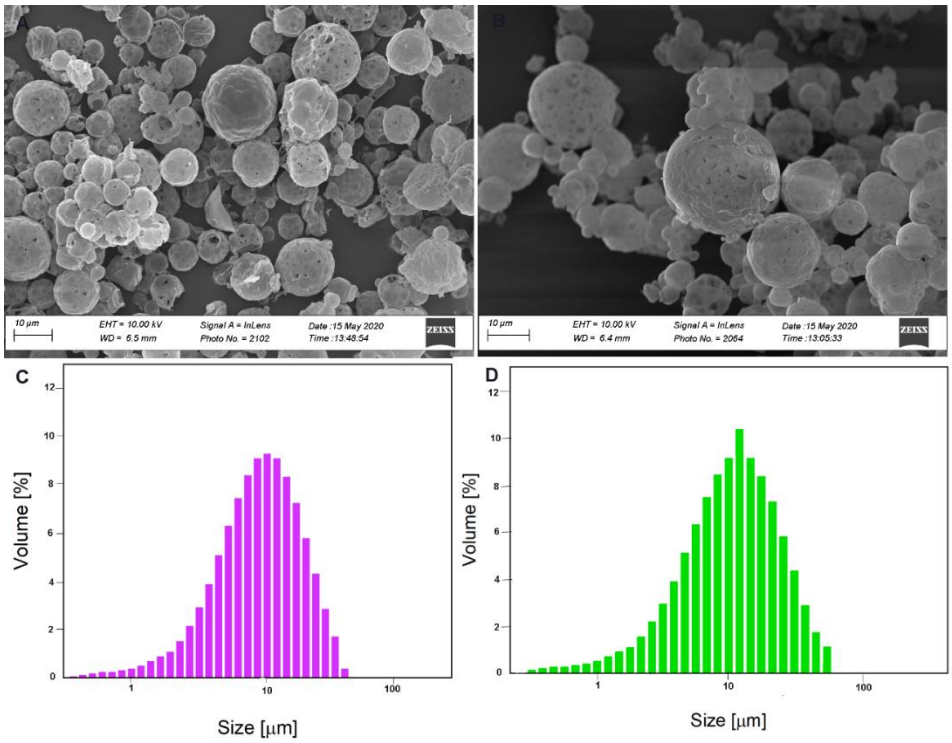

Figure 3.2. Scanning electron microscopy and size distribution of direct and post encapsulated phage-MPs. (A), (B) SEM of post encapsulated and direct encapsulated phage-MPs. (C), (D) Mean diameter of the post-encapsulated phage is 10 µm and for direct encapsulation is 12 µm. Scale bar represents 10 µm**.**

3.2.2 Confocal Microscopy

We performed a deeper morphological characterization of bacteriophage-loaded MPs by confocal microscopy. In detail, FITC-conjugated bacteriophage encapsulated PLGA MPs were analyzed

using a λ_{exc} of 488 nm and a λ_{emiss} between 500 and 600 nm while the DAPI range was used to analyzed the porous structure of the particles by exploiting the autofluorescence of PLGA. As shown in **Figure 3.3**, the correct loading of bacteriophage-FITC particles through adsorption (panel A-C) or encapsulation (panel D-F) in PLGA MPs was assessed, and in particular, in the first case, it was possible to observe bacteriophage on the external structure of the MPs, while in direct encapsulation, they were found inside the porous structures.

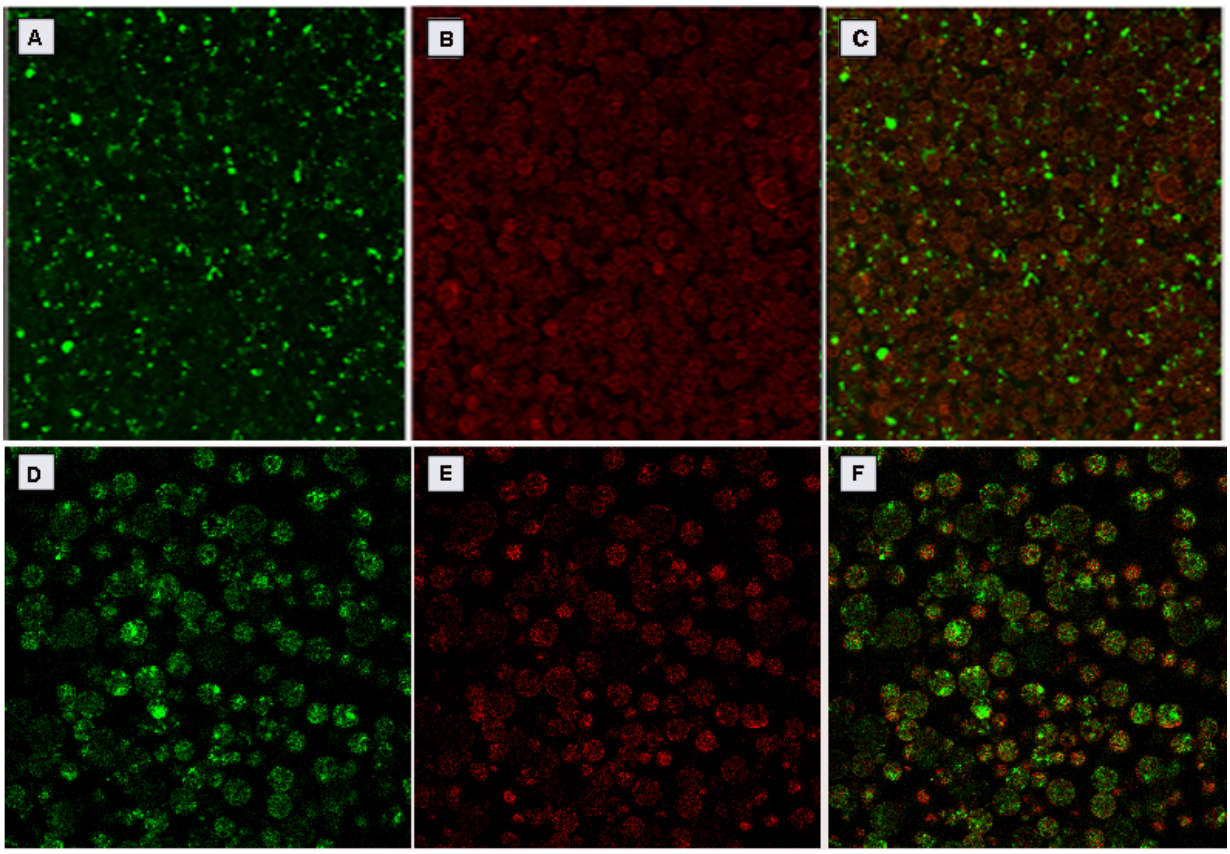

Figure 3.3. Confocal microscopy for post (A-C) and direct (D-F) encapsulation. Fluorescence images were acquired using a λ_{exc} of 488 nm and a λ_{emiss} between 500 and 600 nm. Red channel is related to PLGA acquired in DAPI range.

3.2.3 *In vitro* Controlled Release and Encapsulation Efficiency

The release kinetic of bacteriophages over time was evaluated for PLGA MPs. The release of bacteriophage was evaluated by UV-Vis spectroscopy following its characteristic peak at 269 nm, and concentration was evaluated by the Beer-Lambert law.

Both kind of MP formulations showed a sustained-release *in vitro*, with an initial burst release followed by a relatively slow-release **Figure 3.4**. The phage-loaded MPs by post encapsulation method showed faster-releasing speed compared with direct encapsulated Phage-MPs. All the bacteriophage particles by post encapsulation method after 6h were released, while the direct-encapsulated bacteriophages were completely released after 72 hours. Encapsulation efficacy of bacteriophage into PLGA MPs for post and direct encapsulation were calculated 40 % and 78 % respectively.

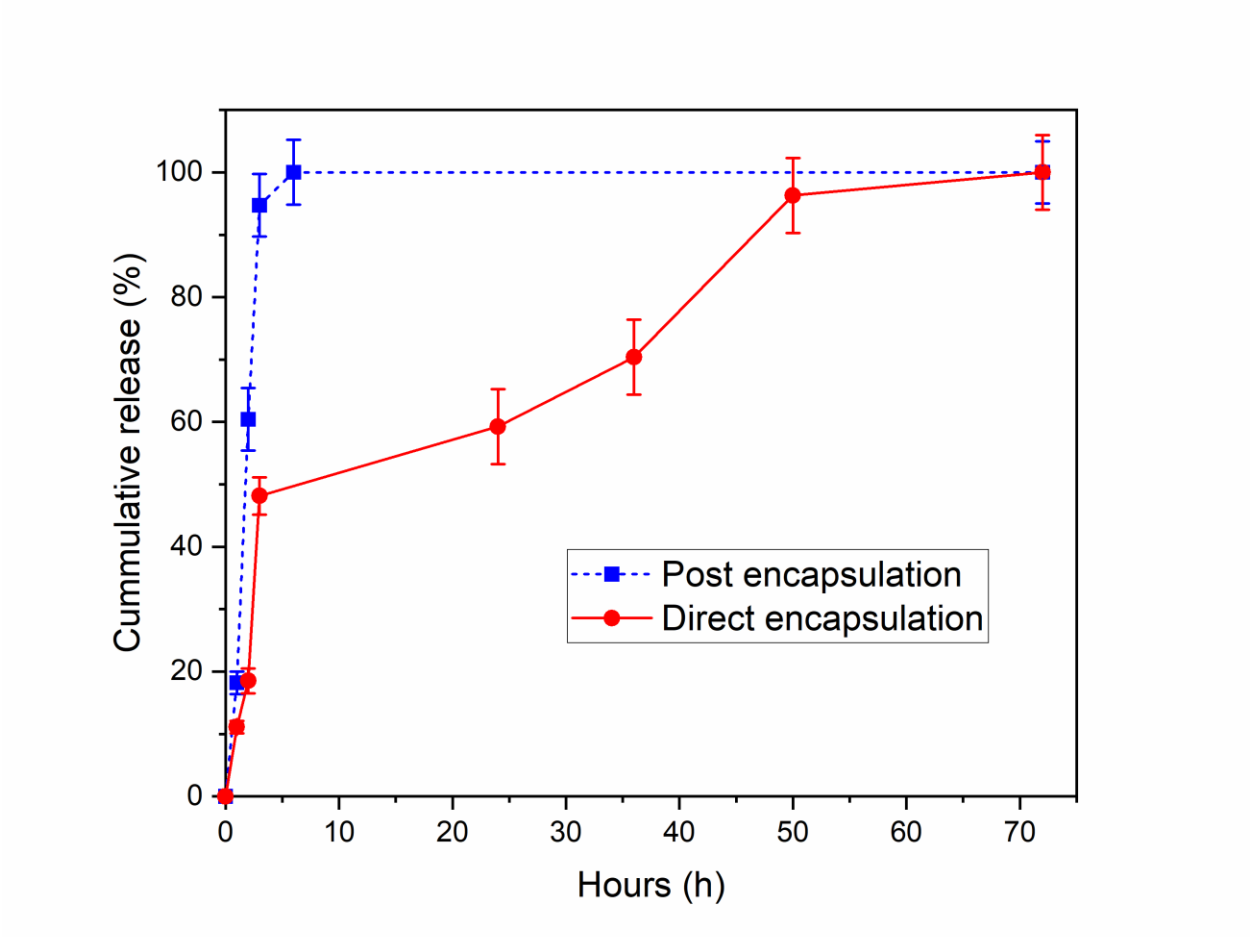

Figure 3.4 In vitro release study of the two bacteriophage-MPs formulations. The phage release versus the time is shown. Cumulative bacteriophage release for direct encapsulation (red), all the bacteriophages after 72 hours were released. Cumulative release for post encapsulation (blue), after 6 hours, all the bacteriophages were released (n=3).

3.2.4 Circular Dichroism

Circular dichroism (CD) analysis of direct encapsulated bacteriophage was compared to the free and post encapsulated one. Experiments were conducted in 10 mM phosphate buffer at pH 7.4 at a concentration of 0.14 mg/mL for both encapsulated phages and concentration of 0.35 mg/mL for free phages as already reported in our previous work [78]. As shown in **Figure 3.5**, the direct encapsulated bacteriophage (blue spectrum) retained the mixed α-helix–β-sheet conformation (shown by the free (blue spectrum) and post encapsulated (green spectrum) ones), with a minimum centered at 222 nm (typical of the β structures) and another at 205 nm, together with a positive shoulder at 190 nm, which are characteristic signs of ellipticity. Moreover, a slight decrease in the Cotton Effect, at the same concentration of the post encapsulated method, is evident for the direct encapsulated phages, this can probably be due to phenomena of protein aggregation during the production of MPs. Despite this, the presence of the helical content mixed with beta-sheet conformation, underlined as our method does not affect the secondary structure of proteins.

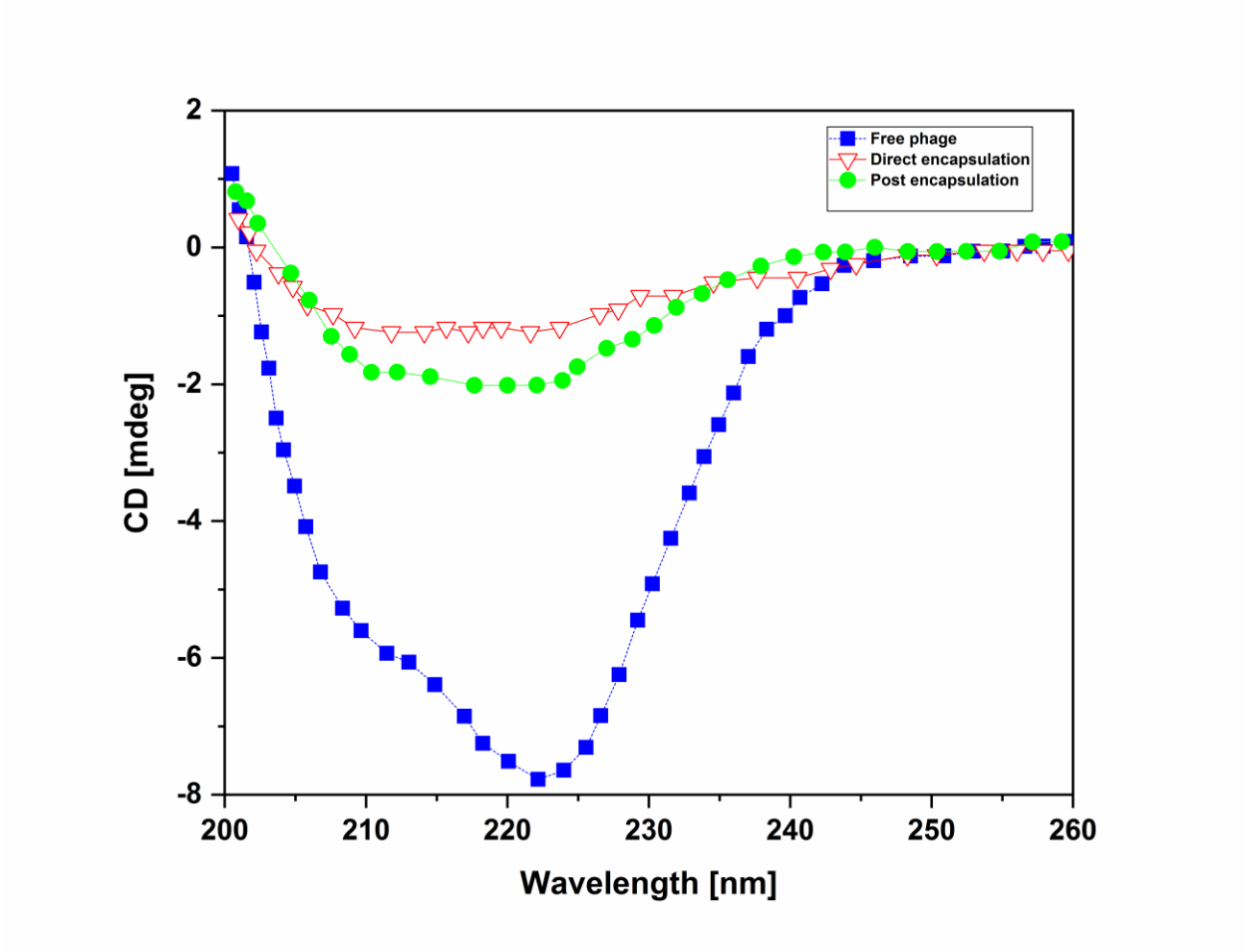

Figure 3.5 A Circular dichroism (CD) spectrum of free bacteriophage (blue spectrum), bacteriophage released from post-encapsulated MPs (green spectrum), and bacteriophage released from direct-encapsulated MPs (red spectrum).

3.2.5 Biological Activity of Filamentous Bacteriophage after Encapsulation

Starting from good results obtained by CD analysis, we assessed the biological activity of filamentous bacteriophages embedded in the MPs using both direct and post encapsulation methods. Freeze-dried MPs were reconstituted in PBS and phages were allowed to be released. The capability of released bacteriophage after 6 h to infect bacteria cells by CFU assay demonstrated the good retention of activity of the bacteriophages for both methods of encapsulation **Figure 3.6**. A more significant reduction in phage titer was observed for direct encapsulation method. This difference may be due to a greater degree of stress due to the exposure of the bacteriophages to the water-dichloromethane interface in case of direct-encapsulated

bacteriophage during the first emulsion. Overall, these results demonstrate that the lyophilization step following bacteriophage encapsulation does not significantly affect the infectivity of the virions.

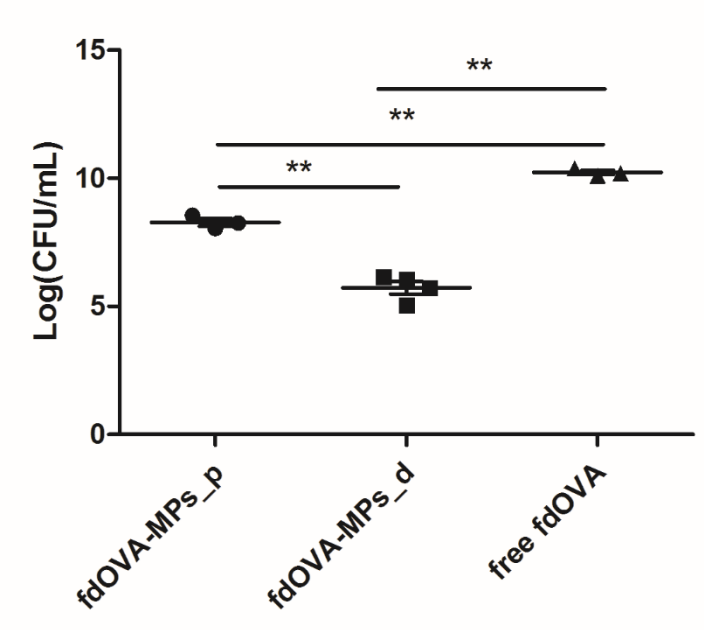

Figure 3.6 Effect of the encapsulation process on the biological activity of the bacteriophage. Infectivity of free filamentous bacteriophage fdOVA or fdOVA released from MPs prepared with the two different methods (direct encapsulation, fdOVA-MPs_direct, and post encapsulation fdOVA-MPs_post). The infectivity was expressed as the number of colony-forming units of TG1 E. coli bacterial cells infected with bacteriophage that were able to grow on Ampicillin plates. As a negative control, we used the release of empty MPs. Each measurement was performed in triplicate, and the median and SEM of three different experiments is reported (black line). Differences are significant by Student't test ($p<0.05$).

3.2.6 Effect of Lyophilization on Stability and Activity of MPs Encapsulated Bacteriophage.

We analyzed the stability of the phage particles inside lyophilized MPs. Lyophilized phage-containing MPs were stored at 4 °C and 22 °C at different times, particles were resuspended in PBS and the released phages were assayed by Colony-forming Unit Determination. As shown in **Figure 3.7**, the encapsulation of bacteriophages into PLGA MPs was able to successfully protect phage particles. In fact, we observed that the titer of the phages released from MPs remains the same after the different times, without any significant difference ($p>0.05$ by one-way ANOVA)

Figure 3.7.A. Previous works have demonstrated that PLGA MPs can provide a protective and stable environment to encapsulate drugs and pharmaceutics. Bacteriophage particles encapsulated with the two different methods (direct encapsulation, and post encapsulation) retained the same activity following MPs reconstitution and virion release. The stability of the bacteriophage in the lyophilized MPs was followed over 60 days. We can conclude that both the MPs formulations are capable to preserve intact the infectivity of encapsulated phage over time when stored at 4 °C.

A

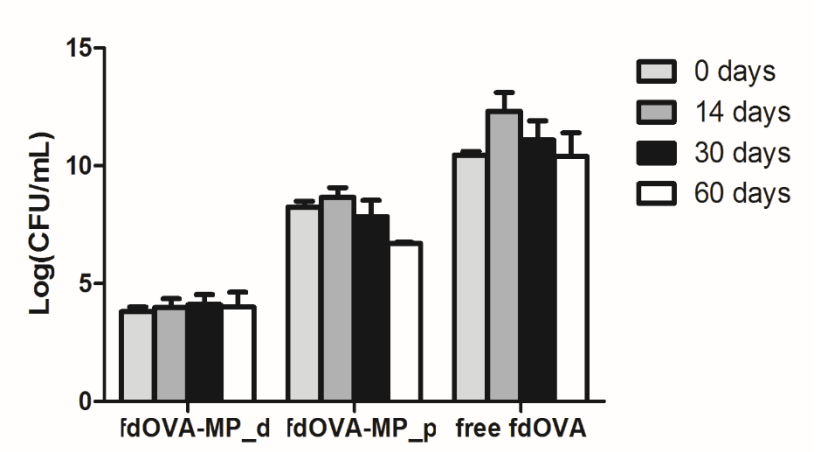

B

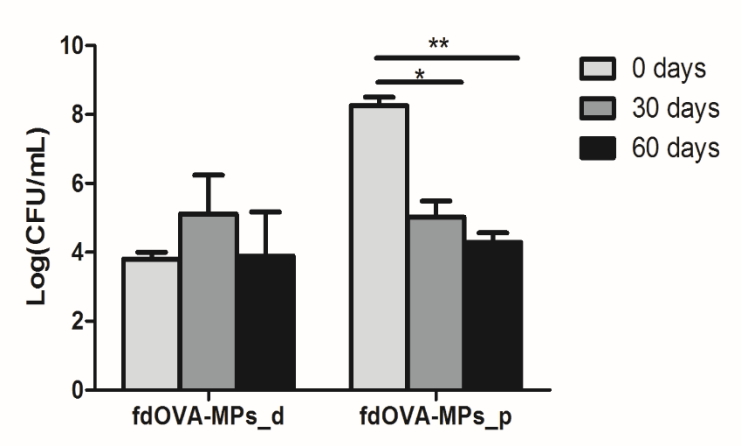

Figure 3.7 Stability of filamentous bacteriophages encapsulated in PLGA MPs using both direct encapsulations, and post encapsulation methods, with free fdOVA bacteriophages as a control.

MPs were stored at 4 °C (A) or at 22°C (B) and the titre of encapsulated bacteriophages was measured at the reported time points. Each measurement was performed in triplicate, and the mean + SEM is reported. Differences are significant by one-way ANOVA (*=$p<0.05$; **=$p<0.01$).

Moreover, we assessed the capability of MPs to store phage activity when kept at room temperature (22 °C). fdOVA encapsulated both by post or direct method were stored at 22 °C and the phages released from MPs were analyzed at different times by Colony-forming Unit Determination.

As shown in **Figure 3.7.B**, we found that direct encapsulation formulation is able to guarantee the same phage activity also after 60 days at 22°C, while the phage released by post encapsulation method showed a significant loss of the 39% of active particles after 30 days of storage at room temperature; after other 30 days the bacteriophage titre remains almost the same ($p>0.05$).

3.2.7 PLGA-MPs Induction of IL-6 Production by DCs

Activation of antigen-presenting cells is crucial for the induction of an effective adaptive immune response, so we analyze if PLGA MPs can directly activate DCs. The effect of PLGA MPs on the production of IL-6 by DCs was then assayed. BM-DCs were incubated in the absence or presence of empty PLGA MPs at 0.1 or 1mg/ml for 24 h, and IL-6 concentrations in the supernatants were measured by ELISA. PLGA MPs were able to induce the production of IL-6 by bone marrow-derived DCs in a dose-dependent manner **Figure 3.8**, demonstrating the adjuvant proprieties of PLGA MPs. Filamentous bacteriophage is able by itself to induce the production of proinflammatory cytokines by BMDCs (1-2). So, this effect exerted by PLGA MPs is further boosted by the encapsulation of phage particles in MPs (data not shown).

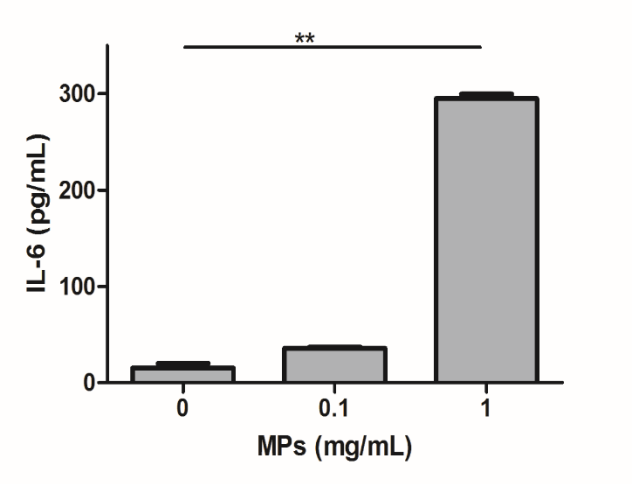

Figure 3.8. IL-6 release of BMDC pulsed with empty PLGA MPs. Bone marrow-derived dendritic cells (BMDCs) were incubated with different doses of PLGA MPs for 24 hours and supernatants were assayed by ELISA in duplicate. Mean + SEM is reported, one representative experiment of two is shown. Differences are significant by one-way ANOVA(**=$p<0.01$).

3.2.8 Antigen-Specific Immune Response to Encapsulated fdOVA Bacteriophage

In previous work, we have shown that fdOVA bacteriophage post-encapsulated in PLGA MPs was able to be released, internalized, and processed by dendritic cells, resulting in activation of the OVA-specific hybridoma cell line B3Z [78]. We then compared whether the recombinant fdOVA phages encapsulated in the MPs by the direct method were able to activate an OVA-specific T response in the same way. As showed in **Figure 3.9 A**, we found that both fdOVA encapsulated in PLGA MPs using both direct encapsulations, and post encapsulation methods were able to stimulate OVA-specific T cells, inducing a similar response in terms of IL-2 release.

We then analyzed the induction of an antigen-specific response by directly adding fdOVA-MPs obtained by the two different encapsulation methods in the BM-DC cultures and allowing phage particles to be released during BM-DC incubation. We found that both the fdOVA-MPs preparations are able to stimulate IL-2 release by B3Z cells in a dose-response manner, without significant differences between the two different methods of encapsulation **Figure 3.9 B**. In many works, it has been described the superiority of using peptide delivery by phage over the use of free

peptide. Especially in vivo, the use of peptides alone is not recommended, as they are poorly immunogenic.

A

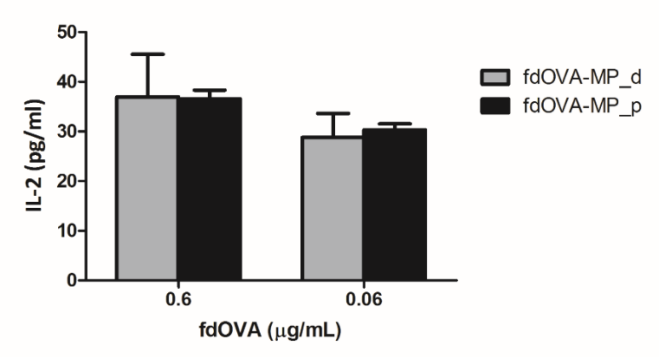

B

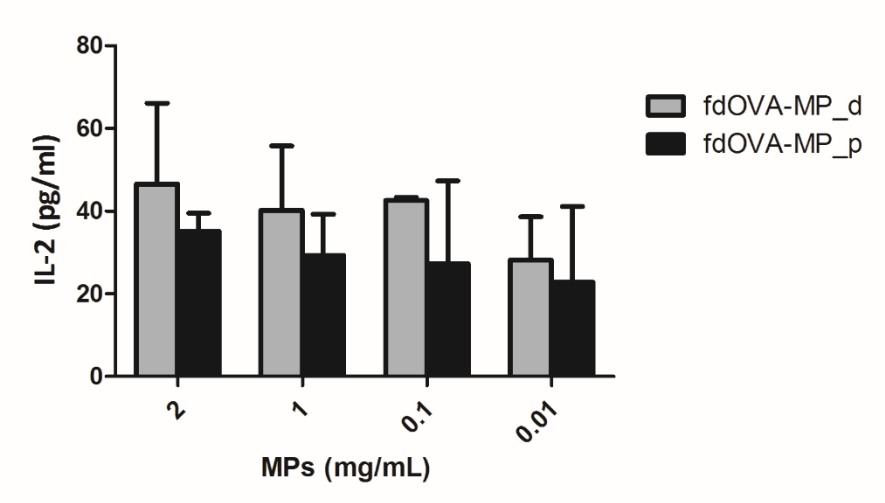

Figure 3.9. IL-2 release of B3Z hybridoma cell line in response to fdOVA delivering OVA257–264 SIINFEKL peptide. Bone marrow-derived dendritic cells (BMDCs) were incubated with graded doses of fdOVA released phage particles (A) or fdOVA-MPs encapsulated using both direct encapsulations, and post encapsulation methods (B). BMDCs were co-cultured with B3Z hybridoma cells for 40 hours and supernatants were assayed in duplicate. Mean + SEM of two different experiments is shown. Differences among the two groups are not significant by one-way ANOVA ($p>0.05$).

3.2.9 Mathematical Prediction of Bacteriophage Releases

Mathematical modeling is a valuable instrument to provide quantitative information about the mechanisms of release [90] and can be used to control, measure, and adjust the drug dose during therapy [91].

To extract bacteriophage release kinetics, the experimental data of the two kinds of MPs embedding bacteriophage were fitted by a non-linear first-order equation. In **Figure 3.10** are showed the data fittings and the corresponding model parameters a and b. The mathematical model showed to adequately reproduce experimental data, as demonstrated from the correlation coefficient R^2 and adjusted R^2 values, indicating the feasibility of the non-linear first-order kinetics equation in describing these release rates.

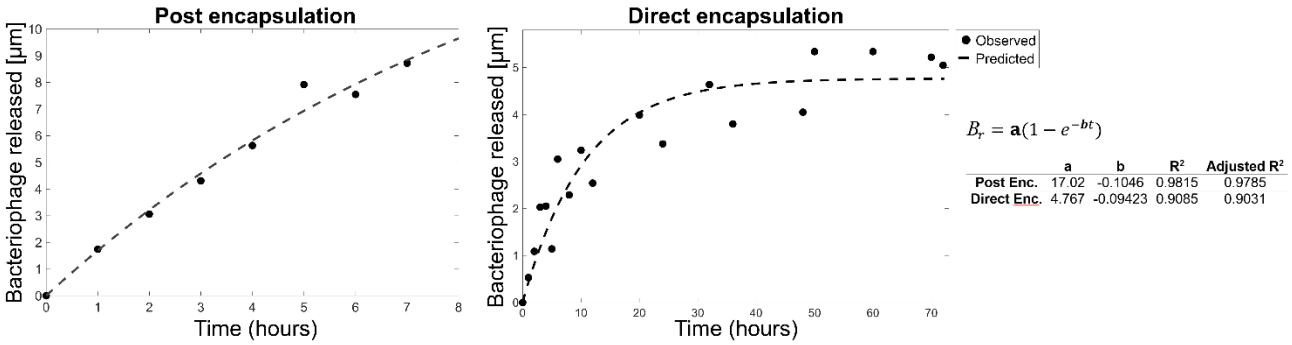

Figure 3.10 Bacteriophage releases obtained from experiments were fitted with non-linear first-order equations (dashed lines). In the table are shown the model parameters a and b and R2 and adjusted R2 values, expressing the goodness of the fitting.

Once described the dependence of the two MP releases as a function of time, a quantitative combination of these non-linear first-order models **Equation 2** was used to simulate further releases of the encapsulated bacteriophage. In particular, mathematical modeling has been used to design controlled MP-based vaccine delivery systems that release, with the desired timing, a specific concentration of phage in the target tissues. Examples of some of such possible MP combinations are shown in **Figure 3.11**. This method can very useful to design MPs formulations with specific releases without the necessity of realizing experiments.

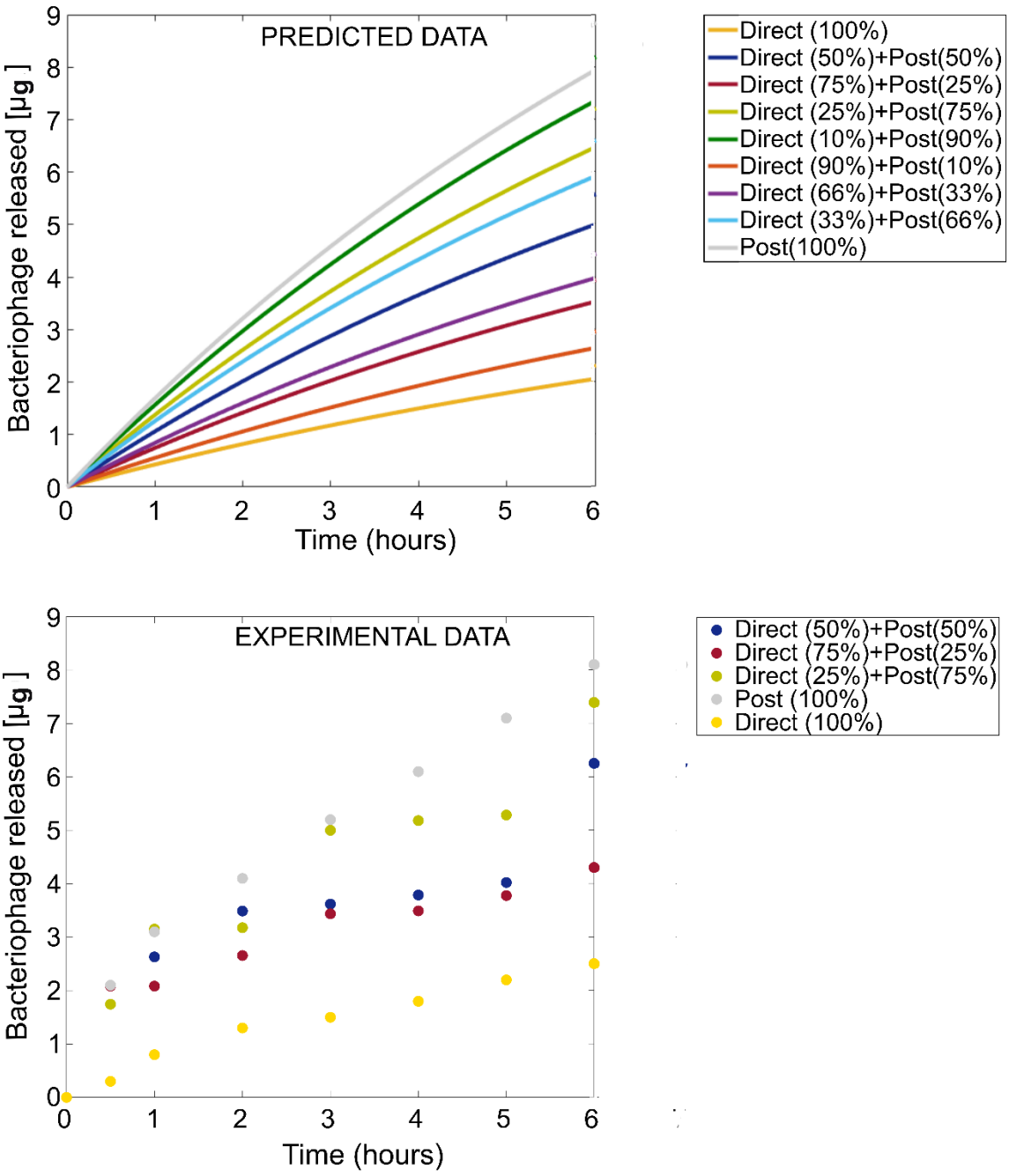

Figure 3.11. Correlation of bacteriophage released from different MP combinations. (A) In silico predictions. (B) In vitro predictions. Data are normalized for 1 mg of MPs.

To validate the accuracy of our mathematical studies, experimental *in vitro* release profiles of bacteriophage were performed **Figure 3.11.B**. Particularly, three different combinations were

compared with our theoretical studies: (75% post+25% direct), (50% post+50% direct), and (25% post+75% direct) **Figure 3.11**. In addition, the release of bacteriophage from the single MP formulations was also evaluated as a control. As shown in the **table 2**, a good correlation between experimental and hypothetical results was obtained underlying as the *in silico* models they can be of great help in the prediction and subsequent formulation of drug delivery systems. The amounts of bacteriophage released coming from *in silico* and *in vitro* experiments after 6 h, are summarized in **Table 2**.

MPs	**µg of Bacteriophage released *in silico* (6 h)**	**µg of Bacteriophage released *in vitro* (6 h)**
Direct (D)	2.06	2.50 ± 0.41
Post (P)	7.93	8.20 ± 0.22
50% P +50% D	4.99	6.21 ± 0.40
75% P +25% D	6.46	7.41 ± 0.11
25% P+75% D	3.53	4.37 ± 0.20

*normalized data

3.3 Morphological Microneedle Characterization

The morphological features of the microneedles were investigated by using optical, scanning electron microscopy, and confocal microscopy.

3.3.1 Optical Microscopy of Master and Molds

The microcones of the master were individually prepared in a serial production by 2PP onto a glass substrate. In order to improve the material-substrate adhesion of the microcones, the substrate was first treated with oxygen plasma and then a thin layer of photoresist was spin-coated and cured on it. Finally, another layer of uncured photoresist was dispensed and processed by 2PP according to

the defined 3D layout. In order to optimize the master fabrication time, only the external shell of the microcones was photopolymerized by 2PP, whereas their body was one-shot cured under a UV lamp. A master of the microcones was produced with 300 µm base diameter and 600 µm height extended onto an area of 1 cm^2. A maximum density of 256 microneedles *per* cm^2 was chosen to avoid any "bed-of-nails" effect. In fact, if the tips bend when designing arrays of microneedles, this has a negative impact on the microneedles' ability to penetrate the skin as the insertion force would be distributed among too many microneedles so that none would be able to penetrate the skin. Because of the fragility of the master material, the polydimethylsiloxane (PDMS) stamp was not used directly. In fact, in order to avoid master breakage, a less fragile master was fabricated using Norland Optical Adhesive (NOA) 60. Therefore, starting from the original positive master, a negative PDMS stamp was replicated on it first and then a positive replica was obtained using NOA. This stamp was then used as a final master, according to the procedure reported in the Materials and Methods section. Optical images of the master produced by 2PP, the PDMS replica, the NOA master, and the final PDMS stamp are shown **Figure 3.12**. The high quality of the PDMS stamps, achieved through replication from the starting master and from the NOA master, is highlighted in **Figure 3.12. D**, which show sections of the tips belonging to the PDMS stamps.

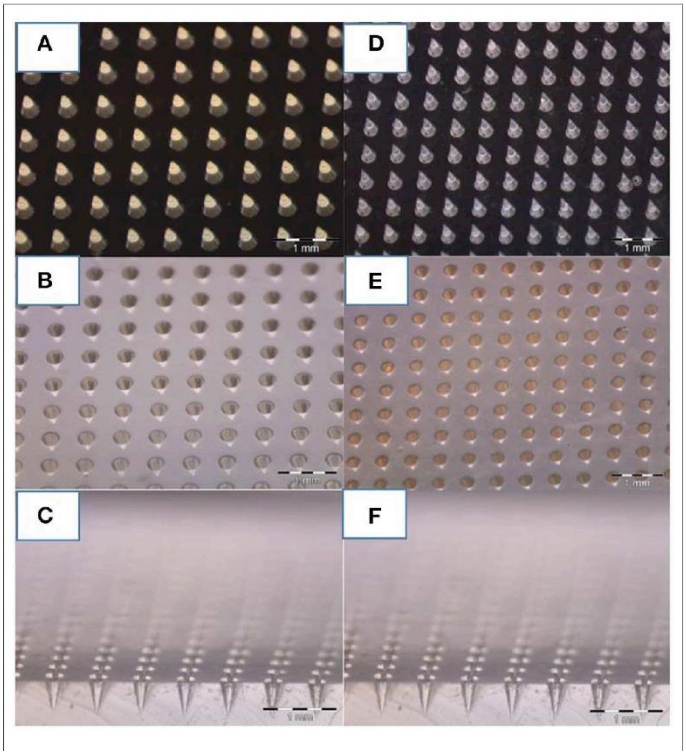

Figure 3.12. Optical image of microneedles molded at various steps. (A) Master of 600 µm of height and 300 µm of bases of microneedles fabricated by 2PP, (B) PDMS stamp replicated on the master, and (C) cross-section of the PDMS mold. (D) NOA master replicated on the PDMS stamp, and (E) final PDMS stamp replicated on it (F) including a cross-section. A comparison between photos (C, F) reveals how, despite the various stages of replication, the needles geometry is very well kept.

3.3.2 Optical Microscopy of Mask and Pillars

To break the polymeric layer on the mold, the mask and pillars were fabricated using micromilling (CNC micromill, Minitech MiniMill 3/Pro, Minitech Machinery Corporation, Georgia, USA) process. The diameter of mask, the height of the pillar for breaking the polymeric layer, and pillars for extraction were 320 µm, 600 µm, and 600 µm respectively **Figure 3.13.**

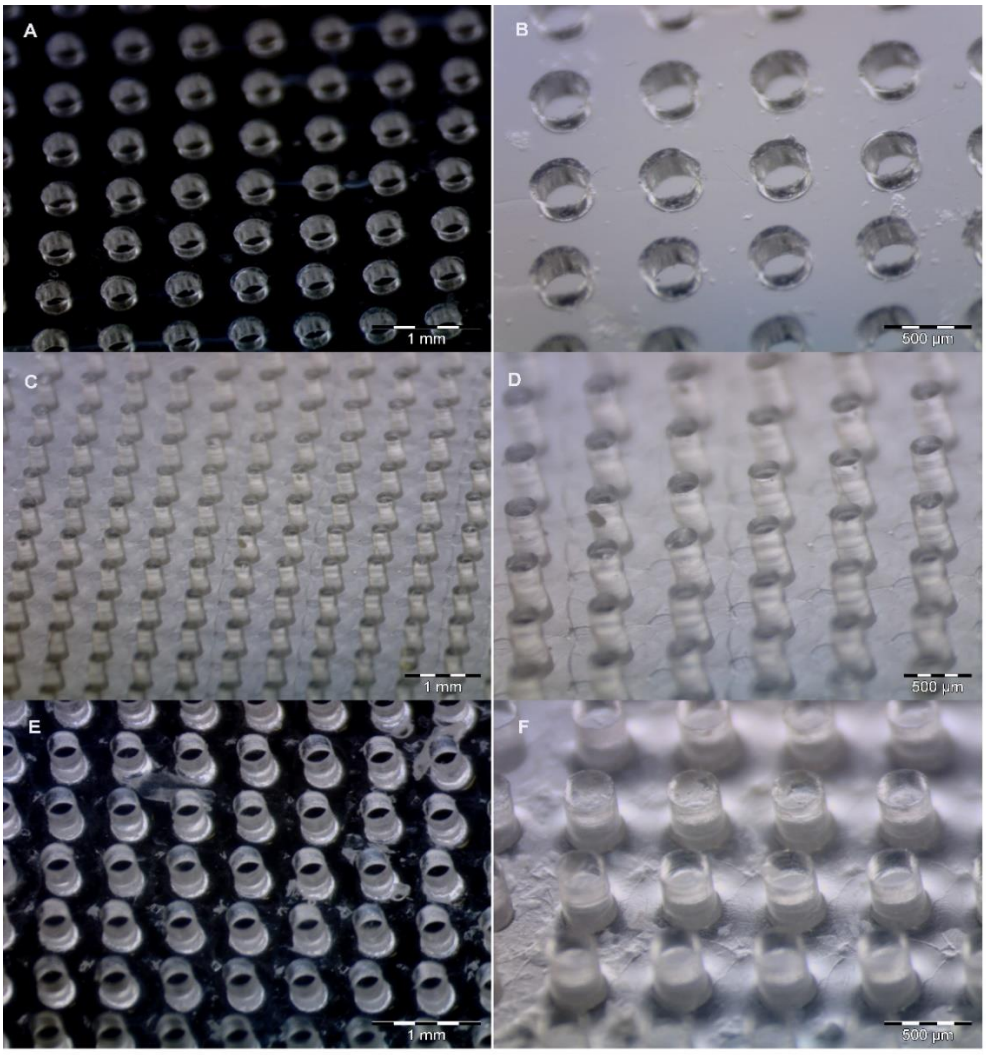

Figure 3.13. Optical image of mask and pillars. (A, B) Mask to cover the stamp. (C, D) Pillars for breaking the polymeric layer on the mold. (E, F) Pillars for extracting the microneedles.

3.3.3 Optical and Fluorescent Microscopy of Microneedles

A picture of a complete array of pillar-based microneedles is reported in Figure 3.14A. A stereomicroscope image of the microneedles including an inset with magnification is represented in the Figure 3.14B. Then, by exploiting the presence of sulphorhodamine B encapsulated in the fast dissolvable PVP/HA phase, which represent the tip and the wall of the microneedles it was possible to reconstruct the microneedles by performing a zeta-stack under a confocal microscope,

Figure 3.14C-D. Finally, a confocal analysis was carried out in order to show the ability to embed bacteriophages loaded PLGA MPs within the proposed microneedles. For this purpose, PLGA MPs encapsulating FITC labeled bacteriophages were used and a match of the two colors coming from sulphorhodamine and FITC was carried out, Figure 3.14E,F,G. In order to visualize the body of the microneedle, the tip was partially scrubbed. In this way it was possible to clearly show the fluorescence of sulphorhodamine B coming from the tip and wall residue and FITC coming from the bacteriophages located in the body of the microneedles, as well as their match.

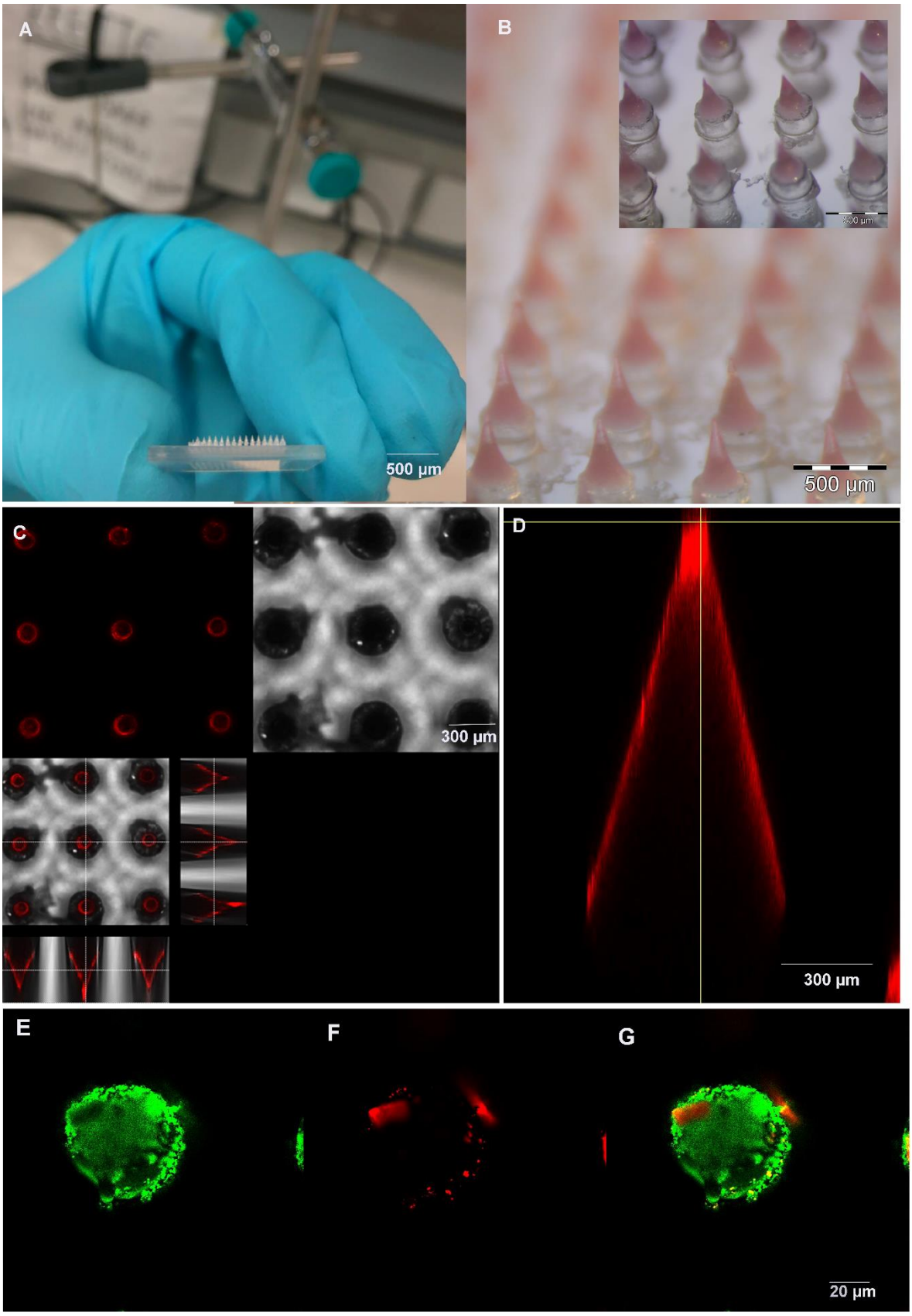
A
500 µm
B
500 µm
C
300 µm
D
300 µm
E
F
G
20 µm

Figure 3.14. Stereomicroscope and confocal microscopy of microneedles. **A.** Photograph of fabricated microneedles. Scale bar 500 µm **B.** Stereomicroscope image of pillar-based microneedles. Scale bar 500µm **C.** Confocal microscopy of microneedles. **D.** Excitation of sulphorhodamine from the intact microneedles. Scale bar 300 µm **E, F and G**. Partially scrubbed microneedles shows: **E.** FITC labeled bacteriophage encapsulated into PLGA microparticles and incorporated into the microneedles body. **F.** Sulphorhodamine-loaded into the tip and wall of the microneedles. **G.** Merging the green fluorescent of bacteriophage and red fluorescent of sulphorhodamine.

3.3.5 Parafilm Test

It is fundamental that microneedles are able to pierce the stratum corneum of the skin. To assess this aspect, a commercial polymeric film (Parafilm M®, a blend of a hydrocarbon wax and a polyolefin) was used as a model membrane for MN insertion studies. All the microneedles were successfully implanted into the parafilm layers thanks to the implementation of the pillars at the base of the MNs.

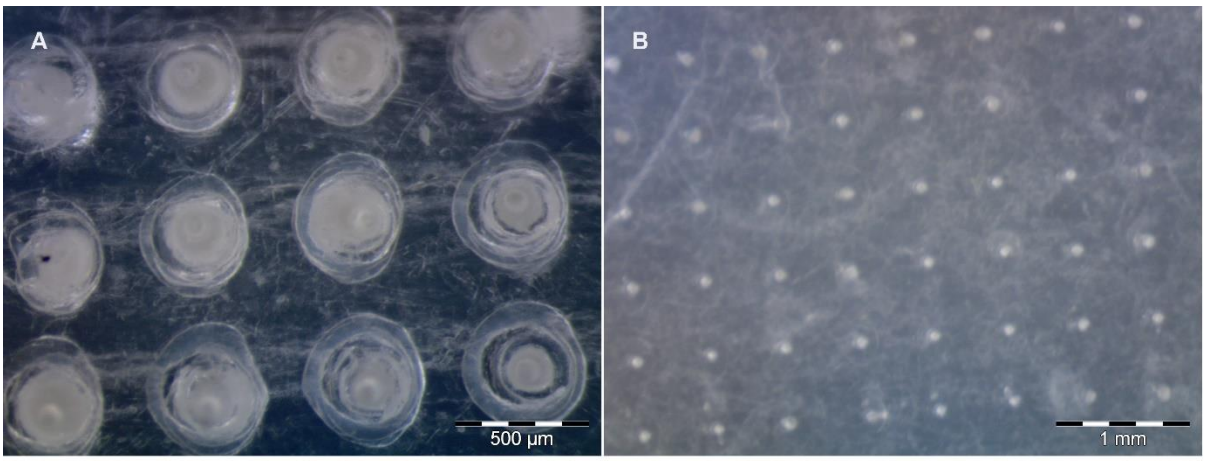

Figure 3.15. Photograph of 600 mm arrays after insertion in parafilm. The pillar-based microneedles were successfully implanted into the parafilm layers.

4. Discussion

The vaccine delivery vehicle developed here combines some major components to form a new platform that has several priorities over traditional vaccine delivery. First, it utilizes PLGA

microparticles to have prolonged release which is vital to achieve effective immune responses. Elimination of multiple injections is one of the largest obstacles to improving worldwide vaccination coverage, and therefore is an essential component of the system developed here.

PLGA-based particles can be used as protein carriers by encapsulation, chemical binding, or simply adsorption of proteins [92,93]. In this work, we have encapsulated fdOVA bacteriophages, a particulate immunogenic carrier delivering the OVA immunogenic peptide, in PLGA-MPs using both post and direct encapsulation methods. The adsorption of proteins or drugs within the MPs by post encapsulation was meant for the minimization of the degradation of the proteins caused by the use of organic solvents in the majority of MPs encapsulation techniques.

Actually, both fabrication methods demonstrated to be effective in encapsulating phage particles and the availability of these two kinds of bacteriophage encapsulated PLGA MPs allowed to the final release by combining them in different ratio. Indeed, by *in vitro* release studies we observed that, although post-encapsulated-bacteriophages displayed a sustained release profile as that of the direct encapsulated fdOVA MPs, release kinetics was faster. In addition, both methods of production of fdOVA-MPs have been shown to ensure correct conservation of active phages when stored at 4 degrees, without loss of phage titre over time. The stability study conducted at room temperature has instead shown that fdOVA-MPs constructed with the direct encapsulation method are superior in keeping the phage titer active up to 60 days at 22°C. PLGA MPs can exert several adjuvant effects. According to the previously reported observations [94], PLGA MP can activate dendritic cells as stated by the release of the proinflammatory cytokine IL-6, hallmark of DC maturation. The adjuvant effect of PLGA-MPs by post and direct encapsulation of phage particles in the development of an adaptive immune response was evaluated. Both formulations were able to induce activation of T cell-specific for the antigen displayed on bacteriophage carrier. The differences between direct and post encapsulation were not significant, suggesting that phage released from post encapsulating MPs can induce similar immune responses as fdOVA directly encapsulated in MPs. Our results demonstrated that PLGA MPs can retain the structural integrity of the bacteriophage after the encapsulation and lyophilization process, allowing a gradual release after resuspension in PBS and effective delivery of the payload to DCs. Accordingly, the bacteriophage is highly appropriate for peptide delivery, due to the low-cost production method, safety, and potent adjuvant capacities. Additionally, the possibility to retain the integrity of

bacteriophages in MPs in a lyophilized form could extend the storage time of the encapsulated vaccine. Overall, this characteristic may represent a drastic practical and economic superiority for the storage and administration of phage particles in underdeveloped countries where healthcare is poor. Additionally, in silico approach can be easily applied to other drugs besides vaccine and it will be a promising method to predict the release of drugs to the targeted sites with a controlled timing and quantitative amount.

To the aim of transferring the bacteriophage loaded MPs within the derma where they can encounter immune-cells such MPs have been effectively encapsulated within microneedles as assessed by confocal analysis. Additionally, in this work, the procedure to prepare microneedles has been modified as compared to previous works in order to build them on rigid pillars. This strategy is meant to overcome the elasticity of the skin to obtain complete insertion ability and guaranty the complete delivery of the microneedles and thus of the bacteriophages into the dermis.

5. Conclusion

To conclude, we present two methods for entrapping fd filamentous bacteriophage into PLGA polymeric MPs that guarantees bacteriophage integrity and infectivity, as well as the immunogenicity of the OVA peptide displayed on bacteriophage and incorporating them into polymeric microneedles that can make their transfer in the derma. Considering the pillar-based configuration of the prepared MNs, we expect that when inserted into the skin, PVP/HA MNs detach from the base of the pillars (as observed in the case of the parafilm test) and are then completely implanted within the tissues, allowing prolonged antigen release without keeping a patch on the skin for a long time. The embeddable MNs will extend antigen exposure at the insertion site for longer time induce a robust antibody response. The results pave the way fora prolonged intradermal delivery system for vaccines or other biomolecules. Additionally, mathematical modeling successfully predicts the release of bacteriophage from PLGA MPs and it can be tuned by combining MPs with different kinetic release (i.e direct and post encapsulated) to maximize efficiency and decreasing the side effects.

Future direction

At the moment, *in vivo* intradermal delivery from MPs and MNs encapsulated bacteriophages are under investigation. Comparing commercial microinjector and our pillar-based polymeric

microneedles will be thoroughly discussed. Beside OVA peptide, expressing multiple copies of foreign antigens for different types of cancers e.g., melanoma cancer by means of microneedles will be performed.

Current treatment of cancer with monotherapy is not satisfying. For instance, photodynamic therapy is a promising treatment modality in cancer management, which refers to the preferential destruction of tumor cells by combination of photosensitizer, light, and oxygen. To enhance the therapeutic efficacy, for instance, microneedle-assisted co-administration platform will be integrated with photosensitizer and immunotherapy drug for photothermal-immunotherapy combination of focal antitumor treatment. Such co-delivery system may be a promising tool for focal cancer and systematic treatment.

Acknowledgments

A huge thank you to Pooyan, for his love, his patience, and above all, whenever I feel tired and discouraged it was enough to talk to him and I got the strength to face every difficulty. I also want to thank my parents, brother, my niece for all their love and support. Special thanks to my sister Donya who has always had a high opinion of me, which is a daily motivation and incitation.

I would like to express my special appreciation and thanks to my advisor Dr. Vecchione for accepting me and giving me the opportunity to join his group committing me to a challenging and outstanding project in the field of drug delivery and for the support and patience along the years of the doctoral course. I take also the occasion to thank my supervisor Prof. Netti. Special thanks go to him and to all the other guys of the brilliant research group, Conny, Valentina and Elena which have been a source of friendship.

Many thanks to Rosella who sincerely helped me to understand immunology and vaccination concepts during the years of my PhD course.

16 May 2021

References

[1] H. Suh, J. Shin, Y.-C. Kim, Clin. Exp. Vaccine Res. 3 (2014) 42–49.

[2] R. Donnelly, D. Douroumis, Drug Deliv Transl Res 5 (2015) 311–312.

[3] J.M. Mazzara, L.J. Ochyl, J.K.Y. Hong, J.J. Moon, M.R. Prausnitz, S.P. Schwendeman, Bioeng. Transl. Med. 4 (2019) 116–128.

[4] K.T.M. Tran, T.D. Gavitt, N.J. Farrell, E.J. Curry, A.B. Mara, A. Patel, L. Brown, S. Kilpatrick, R. Piotrowska, N. Mishra, Nat. Biomed. Eng. (2020) 1–10.

[5] S. Bobbala, S. Hook, Pharm. Res. 33 (2016) 2078–2097.

[6] I. Jones, P. Roy, Lancet (2021).

[7] K. Modjarrad, C.C. Roberts, K.T. Mills, A.R. Castellano, K. Paolino, K. Muthumani, E.L. Reuschel, M.L. Robb, T. Racine, M. Oh, Lancet Infect. Dis. 19 (2019) 1013–1022.

[8] T.R.F. Smith, A. Patel, S. Ramos, D. Elwood, X. Zhu, J. Yan, E.N. Gary, S.N. Walker, K. Schultheis, M. Purwar, Nat. Commun. 11 (2020) 1–13.

[9] S. Shi, H. Zhu, X. Xia, Z. Liang, X. Ma, B. Sun, Vaccine 37 (2019) 3167–3178.

[10] M.D. Knoll, C. Wonodi, Lancet 397 (2021) 72–74.

[11] Z. Cui, Adv. Genet. 54 (2005) 257–289.

[12] E.H. Livingston, JAMA 325 (2021) 898.

[13] R. Sartorius, D. Russo, L. D'Apice, P. De Berardinis, in: Innov. Vaccinol., Springer, 2012, pp. 123–134.

[14] R. Sartorius, P. Pisu, L. D'Apice, L. Pizzella, C. Romano, G. Cortese, A. Giorgini, A. Santoni, F. Velotti, P. De Berardinis, J. Immunol. 180 (2008) 3719–3728.

[15] R. Sartorius, L. D'Apice, A. Prisco, P. De Berardinis, Pharmaceutics 11 (2019) 437.

[16] J. Fang, G. Wang, Q. Yang, J. Song, Y. Wang, L. Wang, Vaccine 23 (2005) 4860–4866.

[17] N. Bastien, M. Trudel, C. Simard, Virology 234 (1997) 118–122.

[18] L.J. Cruz, P.J. Tacken, R. Fokkink, B. Joosten, M.C. Stuart, F. Albericio, R. Torensma, C.G. Figdor, J. Control. Release 144 (2010) 118–126.

[19] R. Jamaledin, C. Di Natale, V. Onesto, Z.B. Taraghdari, E.N. Zare, P. Makvandi, R. Vecchione, P.A. Netti, J. Clin. Med. 9 (2020) 542.

[20] M. Battisti, R. Vecchione, C. Casale, F.A. Pennacchio, V. Lettera, R. Jamaledin, M. Profeta, C. Di Natale, G. Imparato, F. Urciuolo, P.A. Netti, Front. Bioeng. Biotechnol. 7 (2019).

[21] C. Di Natale, D. De Rosa, M. Profeta, R. Jamaledin, A. Attanasio, E. Lagreca, P.L. Scognamiglio, P.A. Netti, R. Vecchione, J. Mater. Chem. B 9 (2021) 392–403.

[22] S. Lee, S. Fakhraei Lahiji, J. Jang, M. Jang, H. Jung, Pharmaceutics 11 (2019) 402.

[23] M.C. Chen, K.Y. Lai, M.H. Ling, C.W. Lin, Acta Biomater. (2018).

[24] M.-C. Chen, S.-F. Huang, K.-Y. Lai, M.-H. Ling, Biomaterials 34 (2013) 3077–3086.

[25] H. Jun, M.H. Ahn, I.J. Choi, S.K. Baek, J.H. Park, S.O. Choi, RSC Adv. 8 (2018) 17786–17796.

[26] K. Sahil, M. Akanksha, S. Premjeet, A. Bilandi, B. Kapoor, Int. J. Res. Pharm. Chem 1 (2011) 1184–1198.

[27] R. Jamaledin, P. Makvandi, C.K.Y. Yiu, T. Agarwal, R. Vecchione, W. Sun, T.K. Maiti, F.R. Tay, P.A. Netti, Adv. Ther. (n.d.) 2000171.

[28] M. Battisti, R. Vecchione, C. Casale, F.A. Pennacchio, V. Lettera, R. Jamaledin, M. Profeta, C. Di Natale, G. Imparato, F. Urciuolo, Front. Bioeng. Biotechnol. 7 (2019).

[29] X. He, J. Sun, J. Zhuang, H. Xu, Y. Liu, D. Wu, Dose-Response 17 (2019) 1559325819878585.

[30] H. Juster, B. van der Aar, H. de Brouwer, Polym. Eng. Sci. 59 (2019) 877–890.

[31] S.P. Sullivan, N. Murthy, M.R. Prausnitz, Adv. Mater. 20 (2008) 933–938.

[32] H.R. Nejad, A. Sadeqi, G. Kiaee, S. Sonkusale, Microsystems Nanoeng. 4 (2018) 1–7.

[33] Y.K. Demir, Z. Akan, O. Kerimoglu, PLoS One 8 (2013) e77289.

[34] K.J. Krieger, N. Bertollo, M. Dangol, J.T. Sheridan, M.M. Lowery, E.D. O'Cearbhaill, Microsystems Nanoeng. 5 (2019) 1–14.

[35] T.E. Andersen, A.J. Andersen, R.S. Petersen, L.H. Nielsen, S.S. Keller, Microelectron. Eng. 195 (2018) 57–61.

[36] A. Ono, H. Azukizawa, S. Ito, Y. Nakamura, H. Asada, Y.-S. Quan, F. Kamiyama, I. Katayama, S. Hirobe, N. Okada, Int. J. Pharm. 532 (2017) 374–383.

[37] R. Jamaledin, C. Di Natale, V. Onesto, Z.B. Taraghdari, E.N. Zare, P. Makvandi, R. Vecchione, P.A. Netti, J. Clin. Med. 9 (2020) 542.

[38] K. Lee, J.D. Kim, C.Y. Lee, S. Her, H. Jung, Biomaterials 32 (2011) 7705–7710.

[39] J.D. Kim, M. Kim, H. Yang, K. Lee, H. Jung, J. Control. Release 170 (2013) 430–436.

[40] S. Henry, D. V McAllister, M.G. Allen, M.R. Prausnitz, J. Pharm. Sci. 87 (1998) 922–925.

[41] M.W. Zhu, H.W. Li, X.L. Chen, Y.F. Tang, M.H. Lu, Y.F. Chen, J. Micromechanics Microengineering 19 (2009) 115010.

[42] S. Aoyagi, H. Izumi, Y. Isono, M. Fukuda, H. Ogawa, Sensors Actuators A Phys. 139 (2007) 293–302.

[43] F. Perennes, B. Marmiroli, M. Matteucci, M. Tormen, L. Vaccari, E. Di Fabrizio, J. Micromechanics Microengineering 16 (2006) 473.

[44] S. Yang, Y. Feng, L. Zhang, N. Chen, W. Yuan, T. Jin, Int. J. Nanomedicine 7 (2012) 1415.

[45] R.F. Donnelly, R. Majithiya, T.R.R. Singh, D.I.J. Morrow, M.J. Garland, Y.K. Demir, K. Migalska, E. Ryan, D. Gillen, C.J. Scott, Pharm. Res. 28 (2011) 41–57.

[46] E.M. Cahill, E.D. O'Cearbhaill, Bioconjug. Chem. 26 (2015) 1289–1296.

[47] J.H. Park, M.G. Allen, M.R. Prausnitz, J. Control. Release 104 (2005) 51–66.

[48] R.E.M. Lutton, J. Moore, E. Larrañeta, S. Ligett, A.D. Woolfson, R.F. Donnelly, Drug Deliv. Transl. Res. 5 (2015) 313–331.

[49] X.-M. Wu, H. Todo, K. Sugibayashi, J. Control. Release 118 (2007) 189–195.

[50] M.R. Prausnitz, Adv. Drug Deliv. Rev. 56 (2004) 581–587.

[51] L. Niu, L.Y. Chu, S.A. Burton, K.J. Hansen, J. Panyam, J. Control. Release 294 (2019) 268–278.

[52] G. Du, R.M. Hathout, M. Nasr, M.R. Nejadnik, J. Tu, R.I. Koning, A.J. Koster, B. Slütter, A. Kros, W. Jiskoot, J. Control. Release 266 (2017) 109–118.

[53] G. Du, M. Leone, S. Romeijn, G. Kersten, W. Jiskoot, J.A. Bouwstra, Int. J. Pharm. 547 (2018) 250–257.

[54] P.C. DeMuth, A. V Li, P. Abbink, J. Liu, H. Li, K.A. Stanley, K.M. Smith, C.L. Lavine, M.S. Seaman, J.A. Kramer, Nat. Biotechnol. 31 (2013) 1082–1085.

[55] Q. Zeng, J.M. Gammon, L.H. Tostanoski, Y.-C. Chiu, C.M. Jewell, ACS Biomater. Sci. Eng. 3 (2017) 195–205.

[56] J.W. Lee, S. Choi, E.I. Felner, M.R. Prausnitz, Small 7 (2011) 531–539.

[57] S.P. Sullivan, D.G. Koutsonanos, M. del Pilar Martin, J.W. Lee, V. Zarnitsyn, S.-O. Choi, N. Murthy, R.W. Compans, I. Skountzou, M.R. Prausnitz, Nat. Med. 16 (2010) 915.

[58] N.G. Rouphael, M. Paine, R. Mosley, S. Henry, D. V McAllister, H. Kalluri, W. Pewin, P.M. Frew, T. Yu, N.J. Thornburg, Lancet 390 (2017) 649–658.

[59] M.H. Ling, M.C. Chen, Acta Biomater. (2013).

[60] E. Cohen-Sela, M. Chorny, N. Koroukhov, H.D. Danenberg, G. Golomb, J. Control. Release 133 (2009) 90–95.

[61] A.A. Walters, S. Somavarapu, V. Riitho, G.R. Stewart, B. Charleston, F. Steinbach, S.P. Graham, Vaccine 33 (2015) 6588–6595.

[62] P.C. DeMuth, W.F. Garcia-Beltran, M.L. Ai-Ling, P.T. Hammond, D.J. Irvine, Adv. Funct. Mater. 23 (2013) 161–172.

[63] P.C. DeMuth, Y. Min, D.J. Irvine, P.T. Hammond, Adv. Healthc. Mater. 3 (2014) 47–58.

[64] X. Hong, Z. Wu, L. Chen, F. Wu, L. Wei, W. Yuan, Nano-Micro Lett. 6 (2014) 191–199.

[65] S. Jiang, S. Liu, W. Feng, J. Mech. Behav. Biomed. Mater. 4 (2011) 1228–1233.

[66] K.-Y. Seong, M.-S. Seo, D.Y. Hwang, E.D. O'Cearbhaill, S. Sreenan, J.M. Karp, S.Y. Yang, J. Control. Release 265 (2017) 48–56.

[67] A.J. Courtenay, M.T.C. McCrudden, K.J. McAvoy, H.O. McCarthy, R.F. Donnelly, Mol. Pharm. 15 (2018) 3545–3556.

[68] S. Yang, F. Wu, J. Liu, G. Fan, W. Welsh, H. Zhu, T. Jin, Adv. Funct. Mater. 25 (2015) 4633–4641.

[69] J. Wang, Z. Wang, J. Yu, A.R. Kahkoska, J.B. Buse, Z. Gu, Adv. Mater. (2019) 1902004.

[70] J. Wang, Y. Ye, J. Yu, A.R. Kahkoska, X. Zhang, C. Wang, W. Sun, R.D. Corder, Z. Chen, S.A. Khan, ACS Nano 12 (2018) 2466–2473.

[71] C. Li, X. Liu, Y. Liu, F. Huang, G. Wu, Y. Liu, Z. Zhang, Y. Ding, J. Lv, R. Ma, Nanoscale 11 (2019) 9163–9175.

[72] S. Chen, H. Matsumoto, Y. Moro-oka, M. Tanaka, Yuji Miyahara, T. Suganami, A. Matsumoto, ACS Biomater. Sci. Eng. 5 (2019) 5781–5789.

[73] G. Jiang, B. Xu, J. Zhu, Y. Zhang, T. Liu, G. Song, Biomed. Phys. Eng. Express 5 (2019) 45038.

[74] B. Xu, Q. Cao, Y. Zhang, W. Yu, J. Zhu, D. Liu, G. Jiang, ACS Biomater. Sci. Eng. (2018).

[75] Y. Ye, J. Yu, C. Wang, N. Nguyen, G.M. Walker, J.B. Buse, Z. Gu, Adv. Mater. 28 (2016) 3115–3121.

[76] Y. Hiraishi, T. Nakagawa, Y.-S. Quan, F. Kamiyama, S. Hirobe, N. Okada, S. Nakagawa, Int. J. Pharm. 441 (2013) 570–579.

[77] C. Kolluru, Y. Gomaa, M.R. Prausnitz, Drug Deliv. Transl. Res. 9 (2019) 192–203.

[78] R. Jamaledin, R. Sartorius, C. Di Natale, R. Vecchione, P. De Berardinis, P.A. Netti, Microorganisms (2020).

[79] G. Del Pozzo, D. Mascolo, R. Sartorius, A. Citro, P. Barba, L. D'Apice, P. De Berardinis, J. Biomed. Biotechnol. 2010 (2010).

[80] R. Sartorius, L. D'Apice, P. Barba, D. Cipria, L. Grauso, A. Cutignano, P. De Berardinis, Front. Immunol. 9 (2018) 1496.

[81] C. Di Natale, V. Onesto, E. Lagreca, R. Vecchione, P.A. Netti, Materials (Basel). 13 (2020) 1807.

[82] Y. Yang, N. Bajaj, P. Xu, K. Ohn, M.D. Tsifansky, Y. Yeo, Biomaterials 30 (2009) 1947–1953.

[83] M. Odonchimeg, S.C. Kim, Y.K. Shim, W.K. Lee, Mong. J. Chem. 18 (2017) 41–47.

[84] R. Agarwal, C.T. Johnson, B.R. Imhoff, R.M. Donlan, N.A. McCarty, A.J. García, Nat. Biomed. Eng. 2 (2018) 841–849.

[85] J. Sambrook, E.F. Fritsch, T. Maniatis, Molecular Cloning: A Laboratory Manual., Cold spring harbor laboratory press, 1989.

[86] L. D'Apice, R. Sartorius, A. Caivano, D. Mascolo, G. Del Pozzo, D.S. Di Mase, E. Ricca, G.L. Pira, F. Manca, D. Malanga, Vaccine 25 (2007) 1993–2000.

[87] F. Niesler, M. Hermatschweiler, Laser Tech. J. 12 (2015) 44–47.

[88] P. Makvandi, M. Kirkby, A.R.J. Hutton, M. Shabani, C.K.Y. Yiu, Z. Baghbantaraghdari, R. Jamaledin, M. Carlotti, B. Mazzolai, V. Mattoli, Nano-Micro Lett. 13 (2021) 1–41.

[89] E. Larraneta, J. Moore, E.M. Vicente-Perez, P. Gonzalez-Vazquez, R. Lutton, A.D. Woolfson, R.F. Donnelly, Int. J. Pharm. 472 (2014) 65–73.

[90] C. Mircioiu, V. Voicu, V. Anuta, A. Tudose, C. Celia, D. Paolino, M. Fresta, R. Sandulovici, I. Mircioiu, Pharmaceutics 11 (2019) 140.

[91] J.H. Lee, Y. Yeo, Chem. Eng. Sci. 125 (2015) 75–84.

[92] M. Allahyari, E. Mohit, Hum. Vaccin. Immunother. 12 (2016) 806–828.

[93] A.L. Silva, P.C. Soema, B. Slütter, F. Ossendorp, W. Jiskoot, Hum. Vaccin. Immunother. 12 (2016) 1056–1069.

[94] M. Yoshida, J. Mata, J.E. Babensee, J. Biomed. Mater. Res. Part A An Off. J. Soc. Biomater. Japanese Soc. Biomater. Aust. Soc. Biomater. Korean Soc. Biomater. 80 (2007) 7–12.